

# Advanced Carbon Electrode Materials for Molecular Electrochemistry

Richard L. McCreery\*

National Institute for Nanotechnology, Department of Chemistry, University of Alberta, Edmonton, Alberta T6G 2M9, Canada

Received October 26, 2007

## Contents

1. Introduction and Scope	2646
2. Materials Chemistry of Carbon Electrodes	2647
2.1. Carbon Allotropes	2647
2.1.1. Graphite and Related $sp^2$ Hybridized Carbon Materials	2647
2.1.2. Diamond	2648
2.1.3. Carbon Nanotubes	2649
2.2. Electronic Properties of Carbon Electrode Materials	2649
2.3. Spectroscopy and Optical Properties	2650
3. Electrochemical Properties of Carbon Materials	2653
3.1. Surface Structure of Carbon Electrode Materials	2654
3.1.1. Termination	2654
3.1.2. Surface Oxides	2655
3.2. Electronic Structure and Conductivity	2656
3.3. Adsorption	2658
3.4. Electrocatalysis	2658
3.5. Classes of Redox Systems on Carbon Electrodes	2660
3.5.1. Outer-Sphere Redox Systems	2660
3.5.2. "Surface-Sensitive" and Electrocatalytic Redox Systems	2661
3.6.1. Polishing and Cleaning	2663
3.6.2. Vacuum and Heat Treatments	2664
3.6.3. Carbon Electrode Activation	2665
3.7. Summary and Generalizations	2666
4. Advanced Carbon Electrode Materials	2666
4.1. Microfabricated Carbon Thin Films	2666
4.2. Boron-Doped Diamond for Electrochemistry	2668
4.3. Fibers and Nanotubes	2669
4.4. Carbon Composite Electrodes	2674
5. Carbon Surface Modification	2675
5.1. Diazonium Ion Reduction	2675
5.2. Thermal and Photochemical Modifications	2679
5.3. Amine and Carboxylate Oxidation	2680
5.4. Modification by "Click" Chemistry	2681
6. Synopsis and Outlook	2681
7. Acknowledgments	2682
8. References	2682

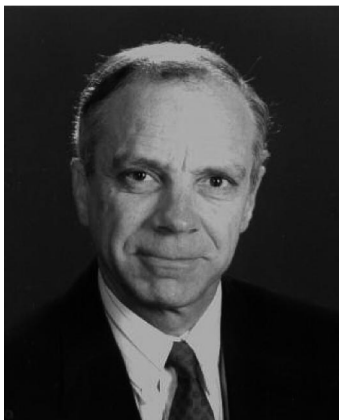
## 1. Introduction and Scope

Since the historical application by Sir Humphrey Davy of graphite electrodes for electrochemical production of alkali metals, carbon materials have been widely used in both

analytical and industrial electrochemistry. The often-cited advantages of carbon electrodes include low cost, wide potential window, relatively inert electrochemistry, and electrocatalytic activity for a variety of redox reactions. Of particular relevance to the current review are oxidations and reductions of organic and biological molecules in both aqueous and nonaqueous media, for which the electrochemical properties of carbon electrodes are often superior to those of noble metals. In addition, the well-known applications of carbon electrodes to metals production, energy storage in batteries and supercapacitors, and catalyst supports has resulted in a rich literature on both carbon materials and their interactions with electrolytes and redox systems. Of general interest are several reviews and monographs on carbon electrode materials, notably the "classical" carbon materials based on graphite, glassy carbon, and carbon black.<sup>1–4</sup>

Despite extensive past investigations of carbon materials for electrochemistry, recent years have brought fundamental innovations that add significantly to the utility of this venerable material in organic and biological electrochemistry. Boron-doped diamond, fullerenes, vapor deposited carbon films, and microfabricated carbon structures offer distinct properties compared with the graphitic carbon electrodes in common use in the early 1990s and also enable novel applications in sensing, electrocatalysis, and electronics. The diversity of carbon as an electrode material stems largely from its structural polymorphism, chemical stability, rich surface chemistry, and strong carbon–carbon bonds present both internally and often between the carbon material and a surface modifier. A comprehensive review of all of the electrochemical properties and applications of carbon materials would require several volumes, even if limited to the past 15 years. Hence, the scope of the current review is limited to physical and analytical electrochemistry using carbon electrode materials, with an emphasis on the electronic and chemical properties of carbon that determine its electrochemical performance. Of particular interest are the relationships between carbon surface and bulk structure, which affect electrode kinetics and interactions with molecules in solution. While it is not practical to write a comprehensive review of all electrochemical applications of carbon electrodes, it is useful to consider those aspects of the materials chemistry of carbon that dictate its electrochemical utility. Borrowing an analogy from Richard Feynman, it is possible to understand the rules of a chess game without also knowing all possible outcomes that arise from those rules. As much as possible, this review will attempt to understand which aspects of bulk and surface chemistry of carbon electrode materials determine their utility for physical and analytical electrochemistry, particularly involving organic and biological redox systems.

\* E-mail: mcreery@ualberta.ca.



Richard L. McCreery is currently Professor of Chemistry at the University of Alberta, with a joint appointment as a Senior Research Officer at the National Institute for Nanotechnology. Until 2006, he was Dow Professor of Chemistry at The Ohio State University. He received his B.S. in chemistry from the University of California, Riverside, in 1970, and Ph.D. under Ralph Adams at the University of Kansas in 1974. His research involves spectroscopic probes of electrochemical processes, the electronic and electrochemical properties of carbon materials, and carbon-based molecular electronics. Much of the research involves collaborations with materials scientists and engineers, as well as surface scientists and electrochemists. He leads an effort at NINT and UofA to investigate hybrid devices for molecular electronics, which combine existing CMOS technology with new electronic and optoelectronic devices containing active molecular components.

This review will start with some of the “rules” associated with carbon electrodes, that is, the electronic and materials properties that partially determine electrochemical behavior. These include band structure, polymorphism, and optical properties. The next section deals with how these materials properties relate to electrochemical properties, including electrode kinetics, adsorption, and electrocatalysis. The third major section deals with the fabrication and novel aspects of new carbon materials developed in the past 15 years, including boron-doped diamond, carbon nanotubes, vapor-deposited carbon films, and various composite electrodes. Finally, the several approaches to surface modification of carbon electrodes are reviewed, emphasizing those developed since the early 1990s. Throughout the discussion of carbon electrode materials, examples related to organic and biological redox reactions are cited.

## 2. Materials Chemistry of Carbon Electrodes

It is convenient to broadly separate the materials properties of carbon electrodes into two subdivisions: bulk properties derived from the interior structure and surface effects such as termination and surface modification. Bulk properties include electronic conductivity, hardness, band structure, and optical absorption and will be discussed first, after an initial overview of carbon structures relevant to electrochemistry. Surface properties are of obvious importance to electrochemistry and are discussed together with carbon electrochemical properties in section 3.

### 2.1. Carbon Allotropes

Although carbon materials used in electrochemistry share some of the electronic properties of metals, their structures and chemistry differ dramatically from all metallic electrodes. The well-known allotropes of carbon include graphite, diamond, and fullerenes, each of which can exist in a variety of materials with differing electrochemical properties. The

most common are based on the graphite structure, consisting of ideally infinite sheets of “graphene” stacked like parallel sheets of chicken wire. The carbon atoms in graphite are all  $sp^2$  hybridized, with an intraplanar C–C bond length of 1.42 Å and interplanar spacing of 3.354 Å. Diamond is entirely  $sp^3$  hybridized and tetrahedral, with a C–C bond length of 1.54 Å, and usually contains dopants to provide sufficient conductivity for electrochemistry, as described in sections 2.1.2 and 4.2. The most common fullerenes used as an electrode material are carbon nanotubes, which amount to single or multiple layers of graphite sheets “rolled up” to form tubes of varying diameter, length, and termination. The physical properties of these carbon materials relevant to electrochemistry are discussed below in turn.

#### 2.1.1. Graphite and Related $sp^2$ Hybridized Carbon Materials

Several structural and electronic properties of graphitic carbon materials are summarized in Table 1. The simplest graphite material is a two-dimensional graphene sheet, which is essentially a very large polyaromatic hydrocarbon. The synthesis and properties of a wide variety of graphene structures were recently reviewed.<sup>5</sup> The most ordered three-dimensional graphite materials are relatively uncommon and comprise highly oriented pyrolytic graphite (HOPG) and natural crystalline graphite. HOPG is made by high-temperature decomposition of gaseous hydrocarbons, often acetylene, followed by hot pressing at high pressure and temperature.<sup>3,6</sup> Graphite materials are often characterized by the dimensions of the crystallites,  $L_a$  for the in-plane crystallite size and  $L_c$  perpendicular to the graphene planes. X-ray diffraction and Raman spectroscopy are commonly used to determine these parameters, as has been discussed elsewhere.<sup>3,7–10</sup> The interplanar spacing in graphitic materials is often labeled “ $d_{002}$ ”, in reference to an X-ray diffraction peak. HOPG and natural single crystal graphite have  $L_a$  and  $L_c$  values exceeding 1  $\mu\text{m}$ , while polycrystalline graphite similar to pencil lead has values ranging from 10 to 100 nm, and carbon black has values in the range of 1–10 nm<sup>3</sup>. To provide some perspective, a single graphene square 1  $\mu\text{m}$  on a side contains about  $10^7$  carbon atoms and thus represents a quite large “molecule”. HOPG is “turbostratic”, meaning that the crystallites have their  $c$ -axes aligned parallel but are rotationally disordered relative to adjacent crystallites. Natural single crystal graphite shares the ABAB layer ordering of HOPG but has longer range rotational order. However, natural graphite contains various inorganic impurities (e.g., “ash”) and is rarely used for electrochemistry. The atomically ordered hexagonal plane containing the “ $a$ ” axis is commonly known as the “basal plane”, while the irregular surface parallel to the “ $c$ ” axis is known as “edge plane”. Edge plane graphite contains a variety of sites, often called “armchair” or “zig-zag”, as well as various oxygen-containing functional groups. As will be discussed in detail later, the edge and basal planes differ greatly in chemical and electrochemical reactivity, and are fundamental to the behavior of graphitic electrodes.

Carbon fibers have been used extensively for electrochemistry, particularly in applications requiring a small “footprint” such as in vivo monitoring in living tissue.<sup>11–13</sup> They generally have diameters in the range of 5–50  $\mu\text{m}$  and are made from small hydrocarbons or polymers or by catalytic chemical vapor deposition. Since the most common industrial application of carbon fibers is in structural materials, the

**Table 1. Properties of Various Carbon Electrode Materials<sup>3</sup>**

	apparent density (g/cm <sup>3</sup> )	$d_{002}$ (Å)	$\rho$ ( $\Omega \cdot \text{cm}$ )	$L_a$ (Å)	$L_c$ (Å)
HOPG, <i>a</i> -axis	2.26	3.354	$4 \times 10^{-5}$	>10000	
HOPG, <i>c</i> -axis			0.17		>100000
pyrolytic graphite	2.18	3.34		1000 (typ) <sup>a</sup>	1000 (typ)
randomly oriented graphite (ultracarbon UF-4s grade)	1.8	3.35	$1 \times 10^{-3}$	300 (typ)	500 (typ)
Tokai GC-10 <sup>b</sup>	1.5	3.49	$4.5 \times 10^{-3}$	20 (typ)	-10
Tokai GC-20 <sup>b</sup>	1.5	3.48	$4.2 \times 10^{-3}$	25 (typ)	12
Tokai GC-30 <sup>b</sup>	1.5	3.41	$3.7 \times 10^{-3}$	55	70
carbon fiber (typ)	1.8	3.4	$(5-20) \times 10^{-4}$	>100	40
carbon black (spheron 6)	(1.3-2.0) <sup>c</sup>	3.55	0.05	20	13
evaporated a-C	-2.0	>3.4	$\sim 10^3$	$\sim 10$	$\sim 10$
a-C:H	1.4-1.8		$10^7 - 10^{16}$		
pyrolyzed photoresist film (PFF)			0.006 <sup>149</sup>		
boron-doped diamond			0.05-0.5 <sup>d</sup>		
N-doped amorphous tetrahedral carbon			10-1000 <sup>e</sup>		

<sup>a</sup> Entries marked "typ" may vary significantly with sample or preparation procedures. <sup>b</sup> Number refers to heat treatment temperatures, for example, GC-20 was treated at 2000 °C. <sup>c</sup> Depends on technique used to measure density. <sup>d</sup> Depends strongly on doping level. See ref 30. <sup>e</sup> See ref 35.

fabrication process is designed to orient the graphitic *a*-axis along the length of the fiber to maximize tensile strength. Carbon fibers occur in a wide range of order and crystallite size and fall into three general types.<sup>14</sup> Radial fibers have graphene planes radiating out from the center of the fiber, "onion" fibers consist of concentric cylinders of graphene planes, and "random" fibers have a random orientation of graphitic planes. The degree of order and graphitization is often increased by heat treatment, and fiber manufacturers generally specify the thermal history in fiber specifications. The preparation and morphology of "onion" fibers is similar to those for carbon nanotubes (section 2.1.3), although nanotubes have much smaller diameters. The distinction between a small "onion" fiber and a multiwalled carbon nanotube is somewhat artificial, although as a practical matter carbon fibers are subject to manual manipulation while nanotubes are much less so.

An electrochemically important variant on the graphite structure is glassy carbon (GC), which is made by heat treating various polymers, often polyacrylonitrile. By heating the polymer under pressure in an inert atmosphere to 1000-3000 °C, the heteroatoms are evaporated until only carbon remains.<sup>15</sup> The C-C bonds in the polymer backbone do not break at these temperatures, so the carbon can form graphitic planes of only limited size, with  $L_a$  and  $L_c$  in the range of 30-70 Å. The interplanar spacing is larger than that of HOPG, about 3.6 Å, and the graphite structure cannot fully develop due to the unbroken C-C bonds. The structure is generally presented as randomly intertwined ribbons of graphitic planes, although the randomness results in significant uncertainty about the detailed microstructure.<sup>16,17</sup> It is known that GC is about 60% as dense as HOPG and must contain many voids, but its disordered nature makes structural characterization difficult at the atomic level. GC may also be made from a reactive polymeric precursor at relatively low temperature ( $\sim 700$  °C), which permits "doping" with various heteroatoms in the polymer, as well as the final product, including halogens, silicon, and metal catalysts.<sup>18-21</sup>

Glassy carbon should be distinguished from a variety of other disordered graphitic materials, such as "diamond-like carbon" (DLC),<sup>22</sup> amorphous carbon, polycrystalline graphite, and carbon black (see Table 1). While the properties of the materials vary greatly with preparation and pretreatment, some generalizations based on their origins are useful. As noted earlier, polycrystalline graphite has  $d_{002} = 3.35$  Å but

with randomly oriented crystallites much smaller than HOPG. It is made under conditions where the carbon is allowed to "graphitize", meaning allowed to form parallel planar sheets with the 3.35 Å layer spacing. Disordered carbon materials derived from polymers, such as GC and pyrolyzed photoresist, are unable to graphitize completely and have  $d_{002} > 3.35$  Å and  $L_a < 10$  nm (see Table 1). Amorphous carbon is made by vacuum deposition of carbon evaporated with an electron beam or by sputtering and is a very disordered combination of  $sp^2$  and  $sp^3$  hybridized carbon atoms and often small amounts of hydrogen.<sup>23,24</sup> Graphitization is prevented by the difficulty of breaking C-C bonds, and the ratio of  $sp^2$  to  $sp^3$  carbon atoms, as well as the hydrogen content, varies greatly with preparation conditions. DLC is a variant of amorphous carbon that is hard and wear resistant and is used widely for coating disk drive heads, while vapor-deposited amorphous carbon is used as a sample substrate for electron microscopy. Carbon black is made by several industrial processes, which result in materials of differing order and composition. "Graphitized" carbon black is used in electrochemistry and resembles polycrystalline graphite with quite small crystallites.<sup>3</sup> Although the list of graphitic materials is nearly endless and their properties range from soft, conductive lubricants to very hard, low conductivity solids, the parameters of crystallite size, long-range order, and anisotropy are critical factors toward determining electrochemical reactivity, as described in later sections.

Mesoporous carbon is a high surface area graphitic material made by "carbonization", or pyrolysis, of carbon-rich precursors such as sucrose, often using a silica template, which is later removed by etching.<sup>25,26</sup> Porosity is generally undesirable in electroanalytical applications; however mesoporous carbon has been used for the oxidation of cysteine,<sup>25</sup> as well as in supercapacitors<sup>26</sup> and electrocatalytic surfaces for methanol oxidation in fuel cells.<sup>27</sup> Mesoporous carbon supports for metal catalysts have been reported to be superior to more conventional carbon black materials, for example, Vulcan XC-72, in fuel cell applications.<sup>28,29</sup>

### 2.1.2. Diamond

The completely  $sp^3$  hybridized, tetrahedral bonding of diamond results in both its hardness and low electrical conductivity, with the latter property making single- or polycrystalline diamond uninteresting as an electrode mate-

rial. However, intentional introduction of impurities, for example, boron or nitrogen, into diamond during deposition can increase the conductivity of diamond sufficiently to make electrodes with distinct electrochemical properties. The most common of these is microcrystalline boron-doped diamond (BDD),<sup>30</sup> which is made by vapor deposition from a  $H_2$  plasma containing methane and a source of boron, often  $B_2H_6$ . Boron is electron-deficient relative to carbon and therefore a p-dopant, and the boron doping level is often quite high, often in the range of  $10^{18}$ – $10^{20}$  atoms/cm<sup>3</sup> or a B/C ratio of about  $10^{-5}$  to  $10^{-3}$ . Microcrystalline BDD has randomly oriented crystallites a few micrometers in size, with facets and grain boundaries characteristic of a polycrystalline material.

Nanocrystalline diamond is made from a  $CH_4/Ar$  plasma under conditions where nucleation is rapid, resulting in randomly oriented crystallites with dimensions of a few tens of nanometers.<sup>31–34</sup> Nitrogen gas or a boron source is often present during deposition, leading to nanocrystallites that are n-doped or p-doped, respectively. The crystallites have a much higher surface/volume ratio than microcrystalline diamond, and the surfaces have significant  $\pi$ -bonding and  $sp^2$  hybridization. The result is much higher electrical conductivity than undoped bulk diamond, even when the nanocrystalline diamond is itself undoped. As discussed in section 4.2, BDD and nanocrystalline diamond have useful electrochemical properties compared with graphitic materials and are chemically much more inert.

A significant variation on diamond electrodes is nitrogen-incorporated tetrahedral amorphous carbon, taC:N, which is made by deposition from beams of ionized carbon and nitrogen.<sup>35,36</sup> Although the resistivity of this material is relatively high,  $10$ – $10^3 \Omega \cdot cm$ , it is used in electrochemistry as thin films on conducting substrates so the ohmic potential losses are minimal. It has a high content of  $sp^3$  bonded carbon and may be deposited on unheated substrates. As will be described later, taC:N has low background current and active electrocatalysis relative to BDD.

### 2.1.3. Carbon Nanotubes

Carbon nanotubes (CNTs) are generally categorized into single-walled carbon nanotubes (SWNTs), which consist of a single graphene sheet “rolled” into a tube, or multiwalled carbon nanotubes (MWNTs), which contain several concentric tubes sharing a common axis. In addition, MWNTs can occur in various morphologies such as “hollow tube”, “bamboo” and “herringbone”, depending on their mode of preparation.<sup>37</sup> A recent review of CNT utility in analytical science discusses the various unusual properties, which hold promise for new applications, such as high aspect ratio, conductivity, thermal stability, flexibility, and reactivity.<sup>38</sup> Nanotubes are made either by the arc-discharge method, which also produces fullerenes such as  $C_{60}$  and  $C_{70}$ , or by chemical vapor deposition on metal particles, often Fe or Ni. Thousands of papers have appeared on CNT properties and applications, including reviews on their use as electrode materials.<sup>37,39</sup> The carbons are arranged hexagonally, like basal plane graphite, along the walls of the nanotubes, but the tube ends are terminated with a fullerene structure incorporating pentagons, or by functional groups similar to those on edge plane graphite. Individual nanotubes have metallic or semiconducting electronic properties, depending on the number of hexagons around the circumference of the tube, and these differences strongly affect certain nanotube

applications. However, the CNT materials used for electrochemistry are generally complex “ropes” consisting of bundles of nanotubes of various sizes. Some elegant experiments with single nanotube electrodes have been reported,<sup>40–42</sup> but the difficulty of isolating and mounting single nanotubes has impeded broad electrochemical application of individual SWNT or MWNT electrodes.

## 2.2. Electronic Properties of Carbon Electrode Materials

The resistivities of various carbon materials used in electrochemistry are listed in Table 1, with the caveat that some carbon materials show a wide range of resistivity depending on preparation conditions. Since the resistance for a carbon electrode equals the product of the resistivity and thickness divided by the cross sectional area of the carbon material, the observed resistance is a strong function of geometry. For example, a  $1 \times 1$  cm<sup>2</sup>, 100 nm thick carbon film with a resistivity of  $0.15 \Omega \cdot cm$  has a resistance of 15 k $\Omega$  for current passing parallel to the plane of the film and  $10^{-5} \Omega$  for current passing perpendicular to the plane. In addition, some carbon materials are anisotropic, particularly pyrolytic graphite with its much lower resistance parallel than perpendicular to the graphene layers.

An important consideration regarding electrode materials is the density of electronic states (DOS), which varies greatly for different forms of carbon. The high conductivity of metals results from the combination of a large number of atomic orbitals to form bands with a high density of electronic states. Electrons move freely without changing energy, and metallic conduction follows Ohm’s law. For example, gold has a DOS of 0.28 states atom<sup>-1</sup> eV<sup>-1</sup>, and this value is relatively constant with energy.<sup>43</sup> Conservation of energy dictates that electron transfer between an electrode and a redox system in solution or adsorbed on the electrode surface is fastest when the energy of the electron is equal in the metal and in the thermally activated redox system. A higher DOS in the electrode increases the likelihood that an electron of the correct energy is available for electron transfer to a redox system, so the heterogeneous electron transfer rate is expected to be dependent on the DOS of the electrode material.<sup>44,45</sup> Semiconductor electrodes represent the extreme opposite of a metallic DOS, in which there are no electronic states in the gap region, and electron transfer does not generally occur between a semiconductor electrode and redox systems with  $E^\circ$  values in the gap region.

Unlike the high and weakly energy-dependent DOS observed for metals, both the shape and magnitude of the DOS distribution for carbon materials vary greatly with carbon structure. The DOS distribution for HOPG is shown in Figure 1, with an expansion of the region near the Fermi energy as an inset.<sup>46,47</sup> The  $\sigma$  and  $\pi$  orbitals of the graphitic carbons combine to form the filled valence bands, which are shaded in the upper drawing, while antibonding orbitals comprise the conduction band. For an infinite graphene sheet and ideal crystalline graphite, there is a small overlap of the valence and conduction bands, leading to a low DOS at the Fermi level. Disorder in the graphite lattice results in many defect states with energies between the conduction and valence bands, effectively filling in the DOS near the Fermi level.<sup>48</sup> HOPG is considered a semimetal, while disordered graphite behaves electronically like a metal with a low DOS.

The minimum DOS for HOPG<sup>49</sup> is 0.0022 states atom<sup>-1</sup> eV<sup>-1</sup>, or about 0.8% that of Au. Even with disorder to

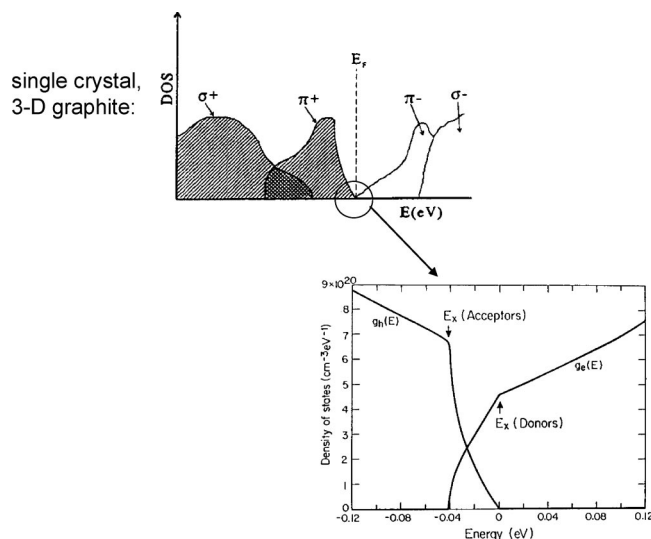


**Figure 1.** Calculated density of electronic states (DOS) for ideal single-crystal graphite. Reprinted with permission from refs 46 (<http://link.aps.org/abstract/PRB/v15/p3180>) and 47. Copyright 1977 American Physical Society and Copyright 1981 Marcel Dekker, respectively.

increase the DOS near the Fermi level, the lower conductivity of graphite materials compared with metals is at least partially a consequence of the low DOS. As will be noted in section 3.1, the low DOS of graphite also affects its electrochemical reactivity. An electrochemical manifestation of the unusual properties of ordered graphite is the low double layer capacitance of the basal plane of HOPG,  $<2 \mu\text{F}/\text{cm}^2$  in aqueous electrolytes, compared with  $\sim 60 \mu\text{F}/\text{cm}^2$  for edge plane HOPG,<sup>50</sup>  $24\text{--}36 \mu\text{F}/\text{cm}^2$  for glassy carbon,<sup>51</sup> and  $20 \mu\text{F}/\text{cm}^2$  for typical metal electrodes.<sup>52</sup>

Crystalline diamond is a wide bandgap semiconductor, with a gap of  $>6 \text{ eV}$  in a single crystal. However, the boron or nitrogen doping introduces a range of energy states in the gap region, as do defects present in microcrystalline and nanocrystalline diamond films. Nanocrystalline diamond has a sufficiently large number of defects that it is much more conductive than single crystal diamond even without doping. As discussed in section 3.1, the distribution of these energy levels is important to electron transfer to common redox systems at BDD electrodes,<sup>53</sup> although the details of the DOS will depend on electrode composition and preparation.

Carbon nanotubes have a variety of DOS distributions, which depend on tube diameter. Figure 2 shows an example,<sup>41</sup> plotted in the format developed by Gerischer for semiconductor electrochemistry.<sup>52</sup> The DOS of a semiconducting nanotube is shown in the left portion of Figure 2 and exhibits significantly more structure than that of graphite.<sup>40,41</sup> Semiconducting nanotubes have no electronic states in the gap region, while metallic nanotubes have a nonzero DOS both above and below the Fermi energy.

In the case shown in Figure 2, an oxidation occurs when the distribution of electron energies in the reduced material,  $W_{\text{red}}$ , overlaps with an unfilled level in the nanotube, as shown by the red arrow. As with semiconducting electrode materials, redox activity does not occur to redox levels of the molecule within the gap region.

To summarize the electronic properties of carbon materials relevant to electrochemistry, it is reasonably accurate to consider disordered  $\text{sp}^2$  carbon materials such as polycrystalline graphite and glassy carbon and  $\text{sp}^3$  carbon such as heavily boron-doped diamond to conduct electrons quali-

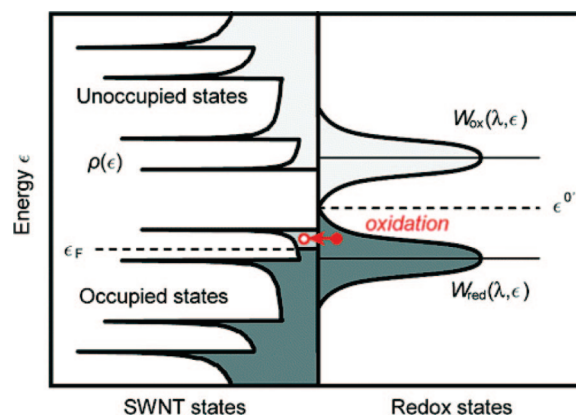


**Figure 2.** Density of electronic states for a semiconducting single-walled carbon nanotube plotted vs energy (left half) and the energy states of a redox system in solution (right half). Arrow indicates a favorable electron transfer from a reduced redox molecule to an empty level in the nanotube. Reprinted with permission from ref 41. Copyright 2006 American Chemical Society.

tatively similarly to metals. Although these materials do not exhibit gaps in the electronic DOS like semiconductors, the lower DOS leads to generally lower conductivity than metals. However, for ordered graphite, nanotubes, and lightly doped diamond, the generally lower and energy-dependent density of electronic states can have major effects on electron transfer behavior and cannot be ignored. Although many carbon materials used in electrochemistry are electronically similar to metals with no gaps in the DOS diagram, they differ greatly from metals in their surface chemistry, as will be discussed throughout this review, starting with section 3.

### 2.3. Spectroscopy and Optical Properties

Graphitic carbon materials such as graphite and GC absorb light over a wide energy range, at least from deep UV to radio frequencies.<sup>54,55</sup> Despite its black color as a bulk sample, thin films of disordered graphitic carbon are partially transparent in the visible wavelength range, with optically transparent carbon electrodes made from electron beam deposited carbon reported in 1975,<sup>56</sup> pyrolysis of an anhydride reagent from the gas phase in 1993,<sup>57</sup> and transparent thin films of pyrolyzed polymer on quartz in 2006.<sup>58</sup> Figure 3 shows the observed UV–vis spectrum of a  $\sim 6 \text{ nm}$  thick film of pyrolyzed photoresist on quartz, showing the broad absorption of the disordered graphitic structure.<sup>59</sup> Also included in Figure 3 are plots of the real and imaginary components of the refractive index,  $n$  and  $k$ , determined with spectroscopic ellipsometry. Crystalline diamond is optically transparent from its band gap at  $\sim 220 \text{ nm}$  into the infrared, but impurities and defects can result in weak absorption throughout the visible region.<sup>60</sup> Doping of diamond with boron decreases its optical transparency, but thin films of BDD have been used for both UV–vis and infrared spectroscopy.<sup>61–63</sup>

As one would expect for a technologically and scientifically important material, carbon has been examined with virtually all forms of analytical spectroscopy, for example, Raman and infrared spectroscopy, X-ray photoelectron spectroscopy (XPS), UV–vis, NMR, etc. Raman spectroscopy has proven particularly informative about all carbon materials used in electrochemistry and will be reviewed briefly here. Perfect graphite has two Raman active modes at  $47 \text{ cm}^{-1}$  ( $E_{2g}^{(1)}$ ) and  $1582 \text{ cm}^{-1}$  ( $E_{2g}^{(2)}$ ) plus two infrared active modes at  $868 \text{ cm}^{-1}$  ( $A_{2u}$ ) and  $1588 \text{ cm}^{-1}$  ( $E_{1u}$ ).<sup>64,65</sup>

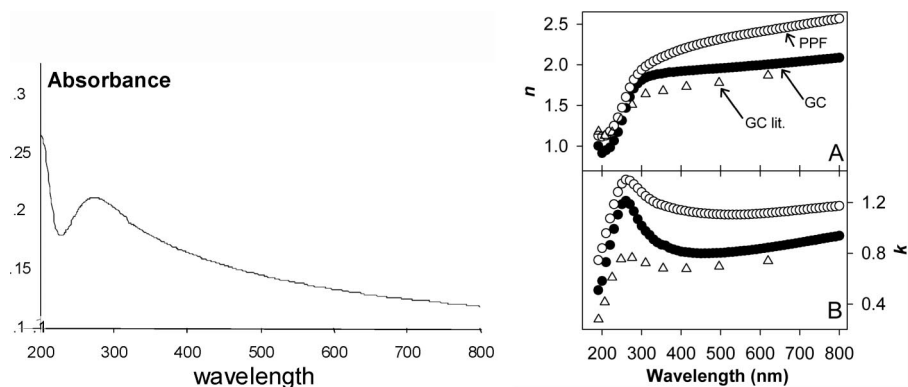


**Figure 3.** UV-vis absorption spectrum (left) of a 6 nm thick film of PPF on quartz and optical constants  $n$  and  $k$  (right) for GC (●) and PPF (○) determined by ellipsometry<sup>59</sup> and for GC from ref 10 (△). Right figure reprinted with permission from ref 59. Copyright 2007 American Chemical Society.

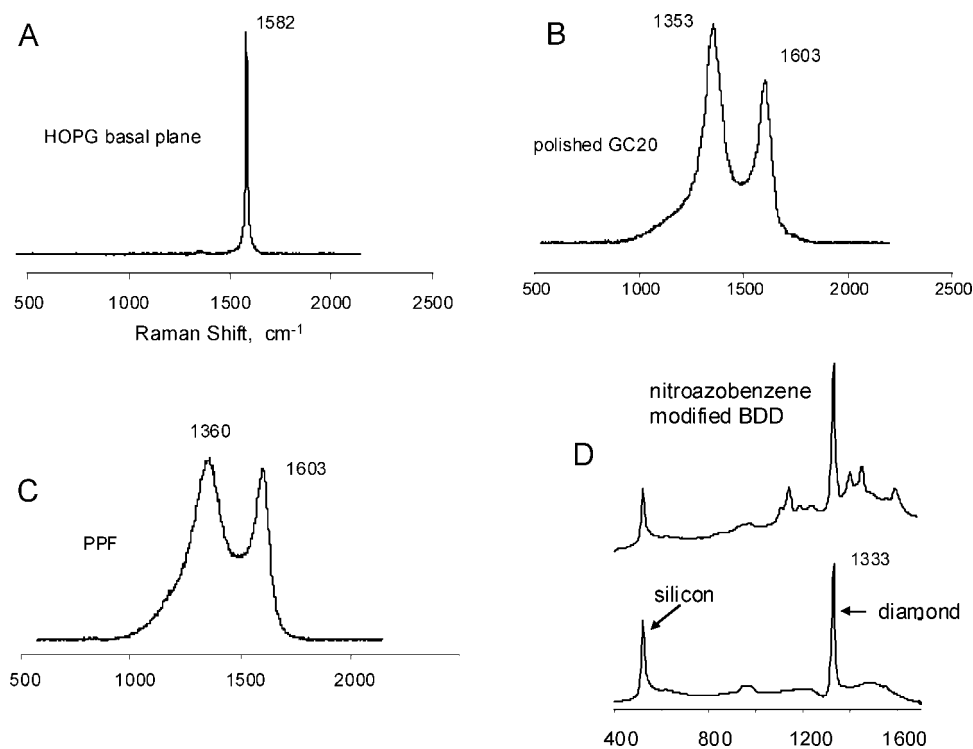


**Figure 4.** Raman spectra of carbon materials, obtained with 514.5 nm laser light. Intensity scales differ and are arbitrary: (A) HOPG basal plane; (B) polished GC; (C) pyrolyzed photoresist film; (D) boron-doped microcrystalline diamond, before (lower) and after (upper) modification with nitroazobenzene molecules. Panel D reproduced from ref 68 (Copyright 1999) by permission of The Electrochemical Society.

Since dipoles are weak or nonexistent in graphite, the IR modes are quite weak and have not been studied as extensively. However, graphite is very polarizable, and the Raman mode at 1582  $\text{cm}^{-1}$  is a prominent feature of Raman spectra of graphitic materials.<sup>7,10,66,67</sup> Although the mode itself is quite strong, the penetration and escape depths of the laser and Raman scattered photons are short in graphite ( $\sim 20$  nm);<sup>10</sup> hence the Raman signal of graphite is weaker than that of diamond. Figure 4A shows a Raman spectrum of HOPG basal plane obtained with a 514.5 nm laser. The sharp  $E_{2g}$  phonon vibration at 1582  $\text{cm}^{-1}$  is the only prominent feature in this region, although second-order transitions are observable above 2400  $\text{cm}^{-1}$ . If the graphite is disordered, a new band appears near 1360  $\text{cm}^{-1}$ , as shown for GC in Figure 4B. In addition, disorder causes broadening and slight upward frequency shifts of the 1582  $\text{cm}^{-1}$  band, as well as changes in the higher order features.<sup>10</sup> The  $\sim 1360$  and  $\sim 1582$   $\text{cm}^{-1}$  bands of disordered graphitic materials are

generally referred to as the “D” (disorder), and “G” (graphite) bands, since their origins are less clear in disordered materials. The D band was initially mistakenly attributed to vibrations along the edges of graphitic crystallites, since a smaller  $L_a$  yielded a larger D/G intensity ratio.<sup>64</sup> However, the D band is observed in HOPG substitutionally doped with boron atoms;<sup>10</sup> hence it is more correct to conclude that the D band results from breakdown of symmetry in the graphite lattice and the resulting effect on Raman selection rules.<sup>9,14,66</sup> The D band shows an unusual shift in frequency with laser wavelength,<sup>10</sup> a property that was explained only relatively recently.<sup>7</sup> In the context of electrochemistry, the D band has been useful for observing changes in electrode surface structure with various pretreatments, such as laser activation<sup>69,70</sup> and electrochemical oxidation.<sup>71–73</sup> Raman spectroscopy is also a good probe of intercalation, a process that is relevant to battery applications of graphite as well as to the effects of electrochemical pretreatment.<sup>14,74</sup> As the graphite layers

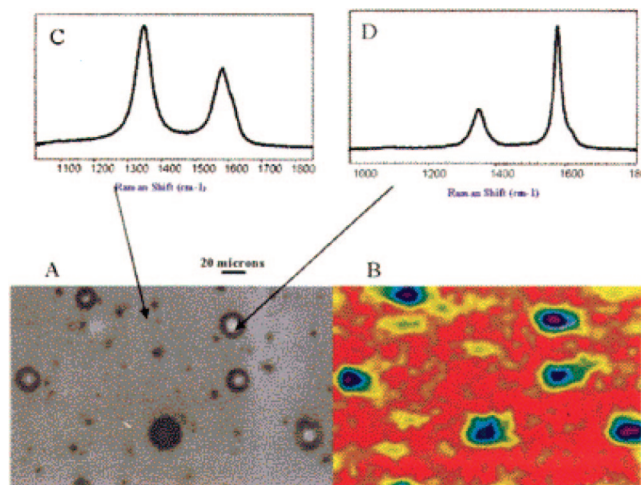


**Figure 5.** Raman imaging of polished glassy carbon (GC20): (A)  $100\times$  bright-field image; (B) Raman image of same area as panel A constructed by taking the ratio of the 1360/1580 peak area from 1200 points inside the sample area (red color indicates a high ratio; purple indicates a low ratio); (C) single spectrum acquired outside of pit; (D) single spectrum acquired inside of pit. Reprinted with permission from ref 76. Copyright 1997 American Chemical Society.

separate, the G band splits into two bands at 1582 and 1620  $\text{cm}^{-1}$ , with the relative intensities depending on the degree of intercalation.<sup>46</sup> As ions penetrate between graphite layers, the graphene sheets can fragment, leading to formation of the D band.<sup>74</sup> Raman spectra of both graphite oxide and modified graphene sheets have been reported recently.<sup>75</sup>

For graphitic materials more disordered than GC, the D and G bands broaden further and begin to merge. An example is pyrolyzed photoresist (Figure 4C). Significant effort has been expended toward relating the Raman features to the ratio of  $\text{sp}^2$  and  $\text{sp}^3$  bonding in the carbon material, in part because of the technological importance of hard carbon materials in wear resistance, particularly on disk drive read/write heads. Although the shape and relative magnitudes of the D and G bands, as well as related features in the second-order region, depend on carbon microstructure, their broad linewidths and overlap make interpretation difficult. Carbon fibers, carbon black, and polycrystalline graphite exhibit D and G bands that reflect their degrees of disorder as well as thermal history. The correlation of the D/G intensity ratio with disorder is illustrated graphically in Figure 5, which includes a Raman image of polished glassy carbon. GC often has “pits” derived from gas bubbles formed during fabrication. Raman microspectroscopy inside a pit shows a lower D/G ratio, implying a more ordered material, while the polished surface shows a higher D/G ratio. The red color of the Raman image indicates a high D/G ratio and is observed wherever the surface was disturbed by polishing.<sup>76</sup>

Microcrystalline diamond exhibits a prominent 1332  $\text{cm}^{-1}$  phonon band (Figure 4D and 6a), which occurs in single-crystal diamond. The line width of this band and changes in smaller features of the diamond Raman spectrum are good indicators of crystallinity and purity, providing a useful diagnostic for diamond film preparation.<sup>30,53,68,77</sup> Except for proximity, it bears no relation to the graphite D band, since it results from the first-order phonon associated with the  $\text{sp}^3$  diamond lattice rather than disorder in the  $\text{sp}^2$  structure of graphitic carbon. The 1332  $\text{cm}^{-1}$  diamond band is used extensively to evaluate the relative amounts of  $\text{sp}^3$  and  $\text{sp}^2$  hybridized carbon in diamond samples. The Raman cross

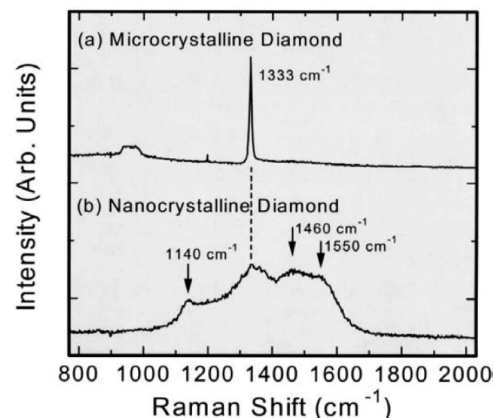


**Figure 6.** Raman spectra of microcrystalline and nanocrystalline boron-doped diamond, using visible laser light. Reprinted with permission from ref 30. Copyright 2004 Marcel Dekker.

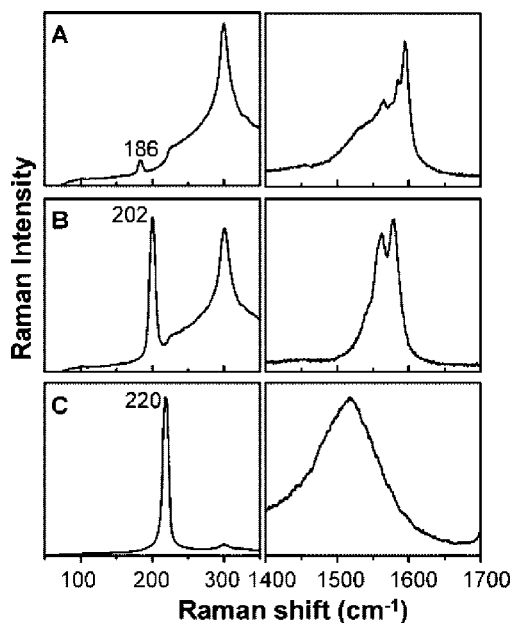


**Figure 7.** Raman spectra (632.8 nm laser) of metallic carbon nanotubes chosen from a mixture to indicate variations observed in the “G” band region (right) and “ring breathing mode” frequency region (left). Reprinted with permission from ref 85. Copyright 2007 American Chemical Society.

section for  $\text{sp}^2$  carbon is approximately 50 times that of  $\text{sp}^3$  carbon, so the 1360  $\text{cm}^{-1}$  intensity relative to the 1332  $\text{cm}^{-1}$  band is a sensitive indicator of  $\text{sp}^2$  impurities in natural or synthetic diamond. The line width of the 1332  $\text{cm}^{-1}$  band indicates the level defects,<sup>30</sup> with a single crystal having a line width of  $\sim 2 \text{ cm}^{-1}$  and microcrystalline diamond  $\sim 10 \text{ cm}^{-1}$ . Nanocrystalline diamond exhibits the severely broadened spectrum of Figure 6b, in which the 1332  $\text{cm}^{-1}$  band is part of a broad set of bands spanning the range from 1100 to 1600  $\text{cm}^{-1}$ . Boron doping at the high levels generally employed in electrochemically useful BDD results in observable changes in the symmetry of the 1332  $\text{cm}^{-1}$  Raman band, which can be used to infer doping level.<sup>53</sup>

Carbon nanotubes have quite interesting Raman spectra, due to resonance effects and electron–phonon interactions.<sup>78–81</sup> An example is shown in Figure 7 for the case of Raman microscopy of selected nanotubes in a complex mixture of metallic and semiconducting nanotubes. The “G” band in the region of 1600  $\text{cm}^{-1}$  has a similar origin to that observed in HOPG, but it obviously varies in position and shape for

different nanotubes. The low-frequency modes near  $300\text{ cm}^{-1}$  are commonly referred to as “ring breathing modes” and arise from vibrations of the circular cross section of the tube. Since there is no analogous vibration in graphite, the low-frequency modes are particularly useful for distinguishing nanotubes from the disordered graphitic materials which often accompany nanotubes as impurities.<sup>80,82–84</sup> Other than this quality control application of Raman spectroscopy, CNT Raman is not commonly used in electrochemical applications and will not be discussed in any detail.

An intriguing optical effect was reported recently for carbon “nanocrystals” made by electrochemical treatment of nanotubes to break the tubes into smaller particles, presumably at defects.<sup>86</sup> The nanocrystals exhibited a well-defined UV–vis absorption band at 270 nm and blue photoluminescence with a maximum at 410 nm. Although the mechanism for photoemission is not clear, it is likely to involve quantum size effects such as those observed for semiconductor nanoparticles.

The optical properties of carbon materials are relevant both to spectroelectrochemical applications involving transmission or reflection of light from carbon surfaces and to characterization techniques such as ellipsometry and Raman spectroscopy. For example, the sampling depth of Raman and the transmission of carbon optically transparent electrodes are directly related to the real and imaginary components of the refractive index, usually stated as  $n$  and  $k$ . Attenuation of light in a carbon material may be determined from  $k$  as  $\exp(-4\pi kz/\lambda)$ , where  $z$  is the path length into the material and  $\lambda$  is the wavelength. The two transparent  $\text{sp}^2$  hybridized carbon materials used in spectroelectrochemistry are thin films of disordered  $\text{sp}^2$  carbon made from electron beam deposition<sup>56,87,88</sup> and pyrolyzed photoresist,<sup>58,89</sup> usually deposited on quartz. The  $n$  and  $k$  values for pyrolyzed photoresist and glassy carbon are shown in Figure 3.

Pure diamond is transparent to visible wavelengths, of course, with a refractive index of 2.418. Diamond thin films are appreciably transparent over a wide wavelength range of 225 nm to  $\sim 100\ \mu\text{m}$ ,<sup>30</sup> making them useful for a wide variety of spectroelectrochemical applications. Boron doping, defects, and microcrystallite scattering can significantly reduce the transmission of diamond optically transparent electrodes (OTEs), as does the substrate employed during diamond deposition. Quartz is generally used as the substrate for UV–vis spectroelectrochemistry, while undoped silicon serves as a transparent substrate for the infrared region. Figure 8 shows transmission spectra for various diamond OTEs in both the visible and infrared regions. With comparison to  $\text{sp}^2$  carbon transmission shown in Figure 3, it is apparent that both BDD and graphitic thin films are sufficiently transparent in the visible region for spectroelectrochemical experiments. In addition, a recent report of a graphene–silica composite material demonstrates high transmission in the 400–1000 nm wavelength range as well as high electrical conductivity.<sup>90</sup>

### 3. Electrochemical Properties of Carbon Materials

In the context of the general review of carbon materials in section 2, we now turn to specific properties of carbon electrodes that affect electrochemical behavior. The choice of electrode material and surface preparation method are usually dictated by the suitability of the electrode for observing an electrochemical parameter, such as heterogeneous electron transfer rate, surface coverage, or redox

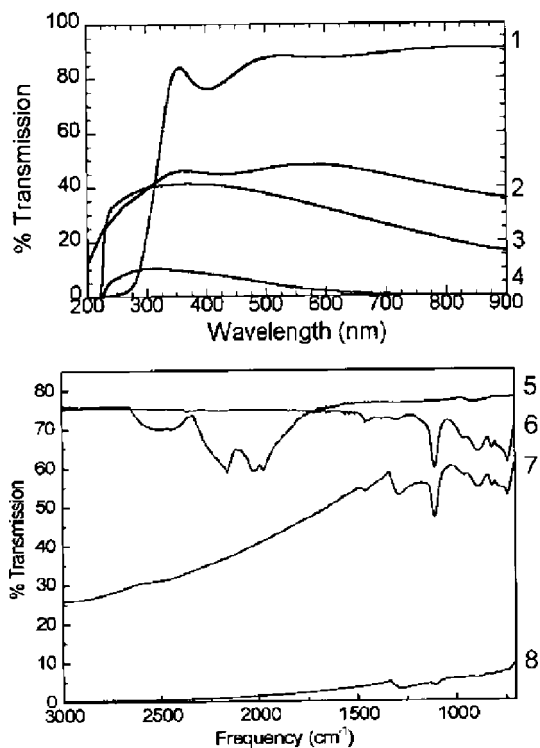


**Figure 8.** UV–vis (upper) and FTIR (lower) transmission spectra of several transparent electrode materials: (1) a thin film of indium–tin oxide on quartz, (2) boron-doped nanocrystalline diamond on quartz, (3) boron-doped diamond on a white diamond substrate, (4) a free-standing boron-doped polished diamond disk, (5) polished diamond disk, (6) undoped Si substrate, and (7, 8) moderately and heavily boron-doped microcrystalline diamond thin films on undoped Si. From: Stotter, J.; Haymond, S.; Zak, J. K.; Show, Y.; Cvackova, Z.; Swain, G. M. *Interface* 2003, 12, 33. Reproduced by permission of The Electrochemical Society.

potential. Carbon electrode properties that affect electrochemical behavior will be discussed in a series of sections on surface structure, electronic structure, adsorption, electrocatalysis, and surface preparation. Closing section 3 will be a brief discussion of how these properties can affect different redox systems to quite variable extents.

To aid comparison of various carbon electrodes for electron transfer reactivity to a simple outer-sphere redox system, the  $\text{Ru}(\text{NH}_3)_6^{3+/2+}$  redox system serves as a useful benchmark. As described in section 3.5,  $\text{Ru}(\text{NH}_3)_6^{3+/2+}$  is a nearly ideal outer-sphere redox system that is insensitive to most surface defects or impurities. Recent measurements of the electron transfer rate constant,  $k^0$ , for  $\text{Ru}(\text{NH}_3)_6^{3+/2+}$  in aqueous KCl electrolyte on a submicrometer diameter Pt ultramicroelectrode yielded a value of  $17.0 \pm 0.9\text{ cm/s}$ , based on the steady-state voltammogram.<sup>91</sup> While this high value may indeed be correct, more commonly reported values are in the range of 0.6–1.0 cm/s on metal electrodes, determined by fast scan voltammetry and impedance techniques.<sup>44,92</sup> Given the difficulty in measuring  $k^0$  values above 1 cm/s, suffice it to say that  $\text{Ru}(\text{NH}_3)_6^{3+/2+}$  is a fast redox system with nearly ideal behavior ( $k^0$  above 1 cm/s and transfer coefficient near 0.5), which can serve as a benchmark for comparing carbon electrodes. A selection of reported  $k^0$  values for  $\text{Ru}(\text{NH}_3)_6^{3+/2+}$  in aqueous KCl electrolyte is listed in Table 2, and the many entries for carbon electrodes will be used as examples in subsequent sections.

**Table 2. Electrode Kinetics<sup>a</sup> of Ru(NH<sub>3</sub>)<sub>6</sub><sup>+3/+2</sup> and Fe(CN)<sub>6</sub><sup>3-/4-</sup>**

electrode material	pretreatment	method	$k^\circ$ , Ru(NH <sub>3</sub> ) <sub>6</sub> <sup>+3/+2</sup> cm/s	$k^\circ$ , Fe(CN) <sub>6</sub> <sup>3-/4-</sup> cm/s	ref
Pt <sup>b</sup>		UME ss <sup>c</sup>	17.0 ± 0.9		91
Pt		UME fast CV <sup>e</sup>	0.8		408
Pt <sup>d</sup>	ultrasound	sampled voltammetry	0.6		92
Pt, Au, other metals			0.8–1.0		44
HOPG basal plane		CV	0.0014	<10 <sup>-7</sup>	50, 114
HOPG edge plane				0.06–0.1	50
GC 20 <sup>f</sup>	fractured	CV		0.5 ± 0.2	51
GC20	conventional polish <sup>g</sup>	CV		0.005 ± 0.003	51
GC20	ultraclean polish	CV	0.51	0.14	144, 146
GC20	polish + laser	CV	>0.4	0.46	51
GC20	IPA/AC <sup>h</sup>	CV	0.11	0.090	146
carbon fiber, 60 μm	polishing	UME CV	0.5 ± 0.06		166
carbon fiber, 60 μm	laser activation	UME CV	0.96 ± 0.07		166
carbon fiber, 7 μm	freshly cut	UME CV	1.22 ± 0.07		150
microcrystalline diamond, B-doped		CV	0.012–0.017	0.017–0.019	53
nanocrystalline diamond, B-doped		CV	<i>i</i>	<i>i</i>	225
nanocrystalline diamond, N-doped		CV	0.1		32
PPF	IPA/AC	CV	0.02		99
e-beam carbon	IPA/AC	CV	0.046		88
electron cyclotron resonance carbon film		CV	<i>i</i>	0.012	24

<sup>a</sup> 1 M KCl in water unless noted otherwise. <sup>b</sup> 0.5 M KCl. <sup>c</sup> Ultramicroelectrode, steady state current. <sup>d</sup> 0.1 M KCl. <sup>e</sup> Cyclic voltammetry. <sup>f</sup> Tokai glassy carbon, fabricated at 2000 °C. <sup>g</sup> Diamond followed by Al<sub>2</sub>O<sub>3</sub> slurries in water. <sup>h</sup> Isopropyl alcohol, activated carbon, ultrasound. <sup>i</sup> Close to the reversible limit using cyclic voltammetry.

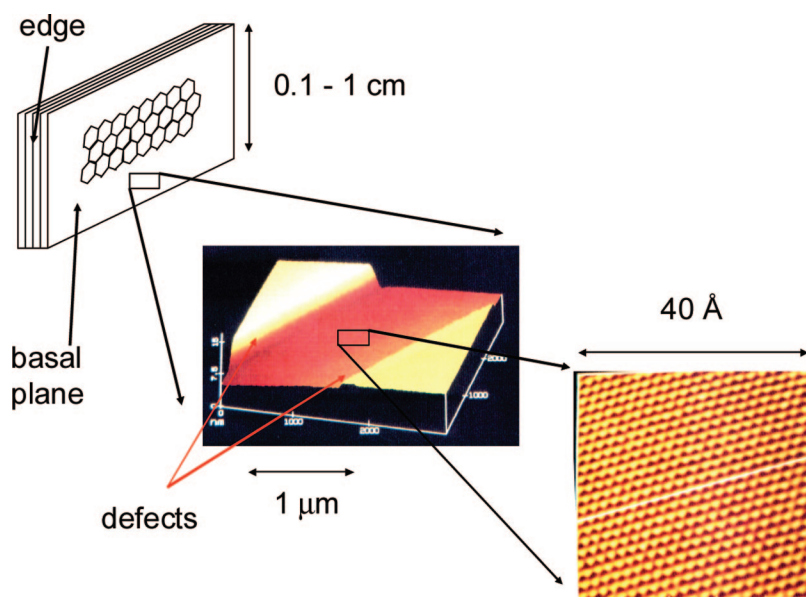


**Figure 9.** Scanning tunneling microscopy of HOPG basal plane, showing step edge defects (center) as well as an atomically smooth region between defects. Reprinted with permission from ref 16. Copyright 1993 American Chemical Society.

### 3.1. Surface Structure of Carbon Electrode Materials

Carbon materials have significantly more complex surface chemistry than metals, not only because the underlying microstructure varies with carbon type, but also because carbon forms a wider variety of surface bonds and functional groups. Since electrochemistry is based fundamentally on interfacial phenomena, the nature of the carbon electrode surface is of obvious importance. The discussion of carbon surface chemistry starts with the termination of the carbon electrode material at its surface, then continues with a brief discussion of a very common and electrochemically relevant termination, that is, surface oxides.

#### 3.1.1. Termination

When the bulk carbon microstructure is interrupted at a surface, reactions generally occur with ambient gases or

liquids to result in “termination”, whether intentional or adventitious. Considering HOPG initially, the basal plane parallel to the *a*-axis is atomically ordered and does not react with air except at elevated temperatures. Figure 9 shows a schematic of a HOPG sample with magnified images obtained using scanning tunneling microscopy. Although the HOPG sample may be centimeters in size, the basal plane contains step edge defects whose density depends on history and preparation. As shown in the lower right image, HOPG is atomically smooth over dimensions of a few tens of nanometers, but defects are difficult to avoid for areas greater than a few micrometers.<sup>16,93,94</sup> Thus for the much larger areas useful in electrochemistry, a basal plane electrode will certainly contain defects at step edges and grain boundaries. The “edge plane” of HOPG is rough and “ragged”, with features that cannot be imaged by STM due to multimicrometer variations in height. When the unsatisfied valences of the graphene edges are formed during cleavage or

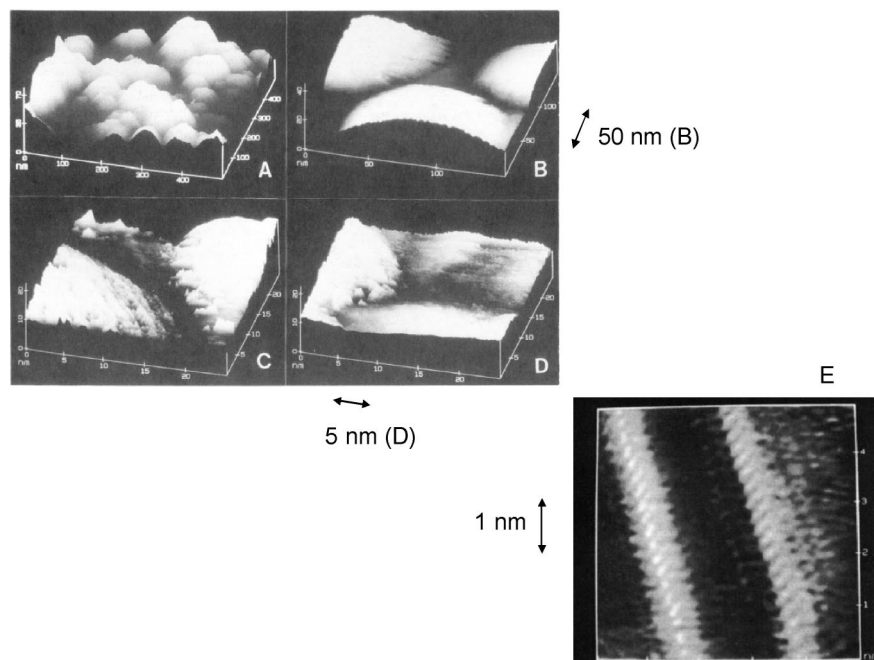


**Figure 10.** STM images of glassy carbon, after “fracturing” to avoid disturbance from polishing. Scale bars refer to the indicated panels. Reprinted with permission from refs 16 and 17. Copyright 1993 and 1994 American Chemical Society.

polishing, they react with oxygen and water to form various oxygen-containing functional groups, as discussed in the next section. The most common procedure for preparing carbon electrodes is polishing, usually with an abrasive such as diamond or alumina. Unfortunately, polishing results in a wide range of surface reactions with air and water, and the resulting surface is generally quite complex.<sup>3</sup> The hydrogen-terminated carbon surface is among the simplest structurally, but also one of the more difficult to prepare.<sup>95</sup> For now, suffice it to say that graphite basal and edge planes differ fundamentally in surface morphology and chemistry, and these differences are very apparent in electrochemical experiments, as described in section 3.5.

Given the origin of GC discussed in section 2.1.1, we expect that a GC surface would be a mixture of basal and edge plane, because the graphitic crystallites and “ribbons” are exposed at an electrode surface. A means to avoid disturbance of the GC structure induced by polishing involves “fracturing” a GC rod encased in epoxy such that the GC surface is exposed only to the electrolyte solution.<sup>96,97</sup> As noted in section 3.5, “fractured” GC surfaces show unusually high electrochemical reactivity, and relatively low oxide coverage. Figure 10 shows STM images of the fractured surface at various magnifications,<sup>16</sup> which reveals the nodules formed during heat treatment of the polymer precursor. At high magnification, the STM images show short-range order in the GC structure, presumably related to the edges of incompletely graphitized sheets.<sup>17</sup> Since most GC surfaces are polished, the edges will usually be terminated by surface oxides, but the oxide coverage and functional group identities can vary widely.

Hydrogen termination is widely used on silicon surfaces, since Si reacts quickly with aqueous HF to produce a Si–H surface stable in air for at least several hours.<sup>98</sup> H termination of carbon is more difficult, but also leads to a quite stable surface. A hydrogen plasma can terminate the surface of GC with C–H bonds, in addition to removing most of the surface oxides.<sup>95</sup> The surface is roughened somewhat by the reactive plasma, and the H-terminated surface has the lowest reported

reactivity toward surface oxidation in air of any disordered carbon material. As shown in Figure 11, vacuum heat-treated and H-terminated GC both start with surface oxide coverage of less than 2 atom %, but the H-terminated surface gains only 1% additional surface oxygen after four days in air, while the vacuum-treated surface increases to over 8% O/C ratio in 5 h. Although H-termination is effective for stabilizing the GC surface as well as other forms of  $sp^2$  carbon materials, it requires an expensive and cumbersome vacuum apparatus and is not widely used.

The  $H_2$  plasma used to make BDD automatically results in a H-terminated diamond surface, which reacts slowly with oxygen.<sup>30</sup> Carbon nanotubes are formed with a variety of surface terminations, depending on preparation route. While the cylindrical walls of nanotubes resemble HOPG basal plane and are relatively unreactive, the tube ends are subject to oxidation and other reactions.<sup>100–103</sup> Termination with a fullerene cage containing pentagonal and hexagonal carbon atoms yields a low reactivity and relatively stable termination. The cylindrical walls are subject to both defects and oxidation.

### 3.1.2. Surface Oxides

As noted earlier, nearly all carbon surfaces are prone to reactions with oxygen and water, and oxygen-containing functional groups will be present on carbon electrodes unless special pretreatments are used. The nature and formation of oxygen-containing functional groups on carbon have been studied extensively, and the carbonyls, phenolic OH, lactones, ethers, and carboxylates on carbon surfaces will be referred to collectively as “surface oxides” or merely “oxides”. Examples of surface oxides that form at a graphitic edge are shown schematically in Figure 12. Surface oxides on carbon electrodes have been studied by a variety of methods, notably XPS,<sup>2,3,104</sup> thermal desorption mass spectrometry,<sup>105</sup> and optical spectroscopy.<sup>2,106,107</sup> In the vast majority of electrochemical applications of carbon materials, there are oxides present whether intentional or not, and the

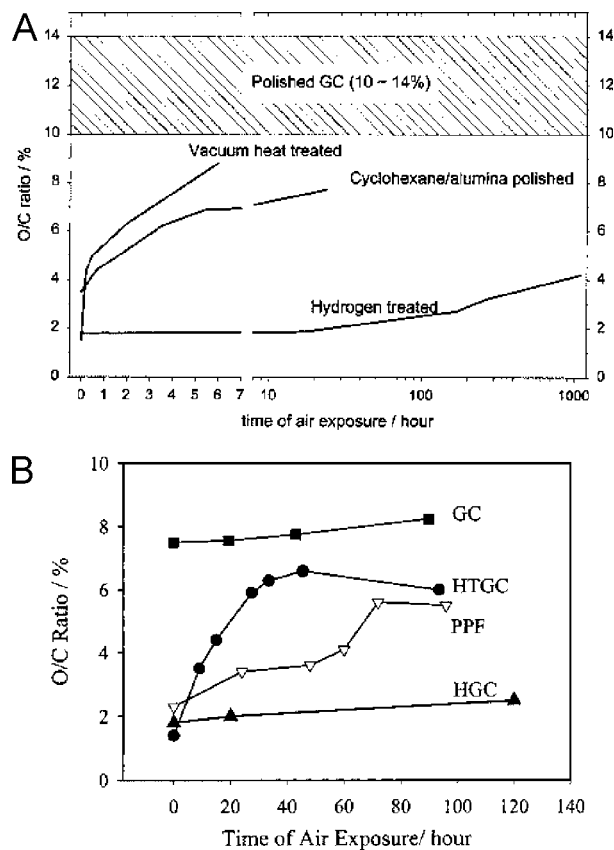


**Figure 11.** Comparisons of various carbon surfaces regarding stability toward surface oxidation in ambient air. Panel A shows the surface atomic O/C ratio determined from XPS for polished glassy carbon (GC) and GC prepared by vacuum heat treatment, polishing in cyclohexane, and a hydrogen plasma. Panel B compares H-plasma-treated GC (HGC) to pyrolyzed photoresist film (PPF) and GC heat-treated in a  $\text{H}_2/\text{N}_2$  atmosphere (HTGC). Reprinted with permission from refs 95 and 99. Copyright 1999 and 2001 American Chemical Society.

user must be cognizant of possible effects of these oxides on adsorption, electron transfer kinetics, electrocatalysis, etc. While the presence of surface oxides is unavoidable without rigorous pretreatment and handling, the distribution of functional groups is subject to manipulation. Some examples are discussed in section 3.4, but for now, suffice it to say that surface oxides are a given and in some cases may be exploited for useful electrochemical performance.

The negative surface charge resulting from some surface oxides on carbon, notably carboxylates, can have significant electrochemical effects on adsorption and electron transfer rates. The well-known Frumkin correction modifies the observed electron transfer rate to charged redox systems,<sup>52</sup> and the extent of adsorption of ionic analytes can vary strongly with surface charge.<sup>97</sup> Extreme effects of surface electrostatic charge are observed in “electrochemically pre-treated” carbon surfaces, following intentional anodization of the carbon surface to generate a variety of surface oxides, many of which are anionic.<sup>3,108–110</sup>

### 3.2. Electronic Structure and Conductivity

As noted in section 2.2, the conductivity of carbon materials has practical importance in designing electrode geometries to reduce ohmic potential losses. This issue is rarely a problem with common electrode materials such as bulk glassy carbon, but ohmic losses can be serious with

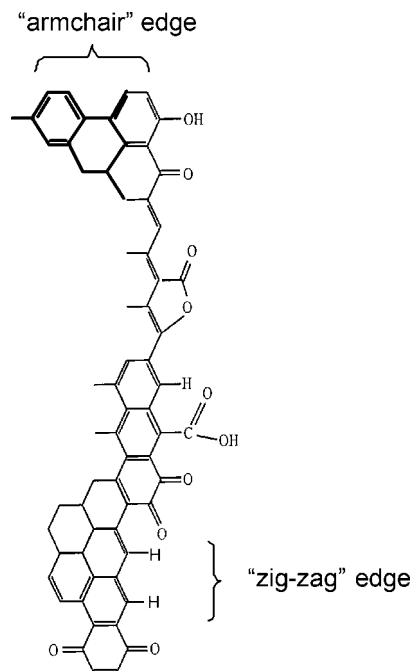


**Figure 12.** Examples of surface oxides that can occur at the edge plane surface of graphite or the graphene sheets in disordered  $\text{sp}^2$  carbon materials.

thin films of disordered carbon, such as those in carbon OTEs. A more fundamental issue is the effect of electronic DOS on electron transfer. As noted earlier in section 2.2 and Figure 2, electron transfer is fastest when there is a high density of electronic states in the electrode at the  $E^\circ$  of the redox system involved. More precisely, there should be states in the electrode with energies within the range of donor or acceptor levels in the redox system, including the distribution in such energies caused by thermal fluctuations. Metals have a high DOS over a wide energy range, including the entire electrochemical potential scale. Randin and Yeager<sup>111</sup> recognized quite early that graphite had unusually low double layer capacitance, and Gerischer et al., investigated the relationship between the capacitance and the low DOS in HOPG.<sup>49,112,113</sup> Unlike metals, carbon materials exhibit extremes of DOS, ranging from undoped diamond with a large energy gap containing no states to HOPG with its low DOS at the Fermi level (Figure 1), nanotubes with significant structure in the DOS (Figure 2), and disordered graphitic materials with a relatively even DOS distribution.

Figure 13 shows a dramatic example of the effects of basal plane orientation on electrode kinetics, for the case of cobalt trisphenanthroline on HOPG. The slightly irregular shape of the edge plane voltammogram is due to difficulty in fabricating a smooth edge plane surface; however, it is clear that the electron transfer rate is much faster at the edge plane than at the basal plane.<sup>114</sup> To avoid uncertainties about edge plane roughness, a better comparison is between HOPG basal plane and laser-activated GC, which has a smoother, reactive, and nonporous surface. For eight quasireversible one-electron redox systems, the GC rates were 1–3 orders of magnitude higher than those for HOPG basal plane, an effect attributed to the low DOS of HOPG<sup>49,113,114</sup> and its semimetal character.<sup>45</sup> For the case of  $\text{Ru}(\text{NH}_3)_6^{3+/2+}$ , Table 2 indicates that various disordered carbon materials exhibit rates in the range of 0.5 to  $>1$   $\text{cm}^2/\text{s}$ , while HOPG basal plane is 0.0014  $\text{cm}^2/\text{s}$ . Figure 14 summarizes  $k^\circ$  values for the eight redox systems on GC and HOPG, correlated with their self-

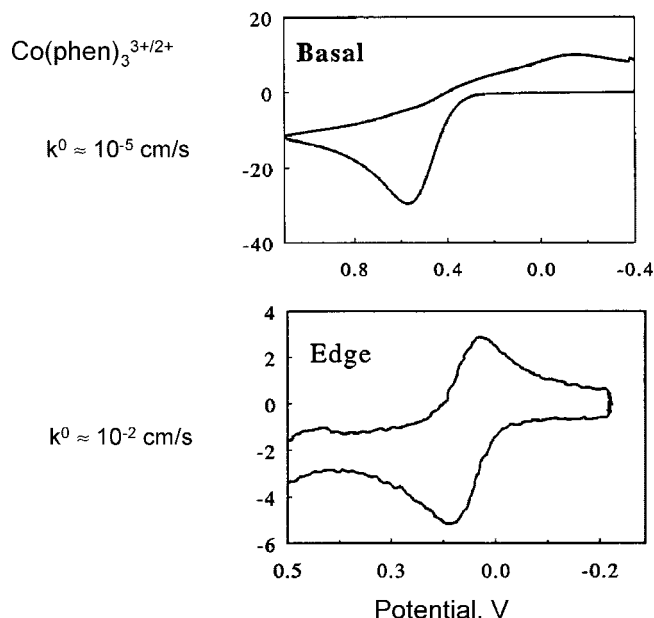


**Figure 13.** Voltammograms of  $\text{Co(phen)}_3^{3+/2+}$  in 1 M KCl, 0.2 V/s, on HOPG basal plane (upper) and HOPG edge plane (lower). Approximate rate constants determined from the peak separation are indicated, and current axis is in microamps. Reprinted with permission from ref 114. Copyright 1992 American Chemical Society.

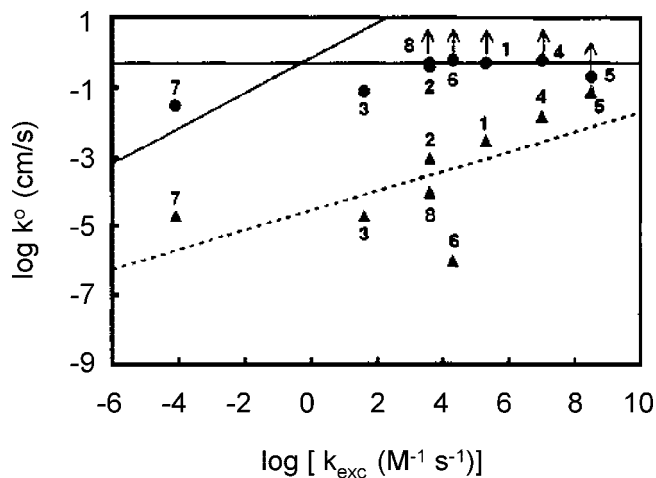


**Figure 14.** Observed rate constants on low defect HOPG basal plane ( $\blacktriangle$ ) and laser-activated glassy carbon ( $\bullet$ ). Horizontal line indicates instrumental limit for  $k^0$  determination, and dashed line is the least-squares fit to the HOPG data. Redox systems are (1)  $\text{IrCl}_6^{2-/3-}$ , (2)  $\text{Ru(NH}_3)_6^{3+/2+}$ , (3)  $\text{Co(phen)}_3^{3+/2+}$ , (4) methyl viologen, (5)  $\text{Fe(phen)}_3^{3+/2+}$ , (6)  $\text{Fe(CN)}_6^{3-/4-}$ , (7)  $\text{Co(en)}_3^{3+/2+}$ , and (8)  $\text{Ru(en)}_3^{3+/2+}$ , all in 1 M KCl. Reprinted with permission from ref 114. Copyright 1992 American Chemical Society.

exchange rates in homogeneous solution.<sup>114</sup> In addition to the consistently lower values observed on HOPG, there is a moderate correlation on HOPG with the square roots of the homogeneous rate constants, as predicted by Marcus/Levich kinetics (solid, slanted line in Figure 14). More recently, a detailed theoretical analysis of this effect was presented by Royea et al.<sup>45</sup> A natural consequence of the large reactivity difference between HOPG basal plane and the much more reactive edge plane is extreme sensitivity of the observed basal plane rates to defects. It is very easy to create step-edge defects on HOPG basal plane, and special treatment is required to reduce the defect density sufficiently to observe the true basal plane rate.<sup>114</sup> The kinetic contrast between edge

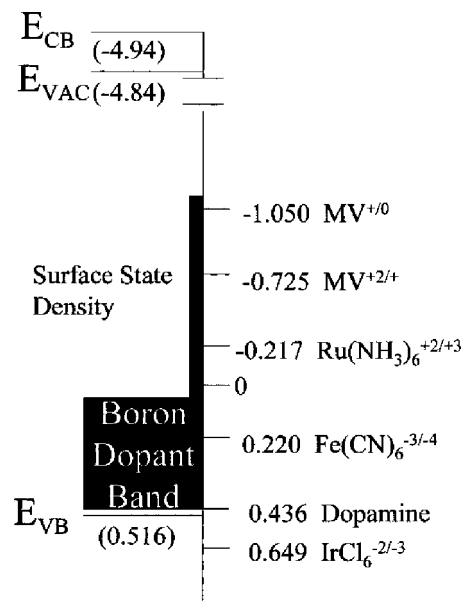


**Figure 15.** Energy states in BDD with the redox potentials of several common redox systems included. Reprinted with permission from ref 53. Copyright 2000 American Chemical Society.

and basal plane may be used to advantage, for “decoration” of adventitious step edge defects to result in metal and metal oxide “nanowires”.<sup>115–117</sup>

Undoped diamond has no electronic states within its band gap, which covers most of the electrochemical potential scale. Boron doping, however, introduces “midgap” states, which increase both conductivity and electron transfer reactivity.<sup>53</sup> For the benchmark  $\text{Ru(NH}_3)_6^{3+/2+}$  redox system, the  $k^0$  observed on BDD is 0.012 cm/s compared with 0.0014 on HOPG basal plane and 0.5–1 on  $\text{sp}^2$  hybridized disordered carbon (Table 2). Both BDD and nanocrystalline diamond have many defect states on the crystallite surfaces, many of which are also in the midgap region. In many cases, these defects include hydrogen, which significantly perturbs the local energetics of the diamond lattice. Figure 15 summarizes these effects by showing the midgap states of diamond electrode materials relative to several aqueous redox systems.<sup>53</sup> A useful conclusion related to Figure 15 is that BDD and nanocrystalline diamond contain sufficient electronic states to support reasonable electron transfer rates to at least  $-1.1$  V on the SCE potential scale,<sup>53</sup> whereas undoped diamond would not support electron transfer to any redox systems more positive than  $\sim 0.45$  V vs SCE.

As already noted in Figure 2, nanotubes have a DOS distribution related to but quite different from that of HOPG, and there should be a correlation between the DOS and electron transfer reactivity. However, the difficulty in isolating a given nanotube and characterizing its DOS makes observing such a correlation difficult. Practically speaking, most electrochemical applications of nanotubes involve ensembles of large numbers of tubes with different diameters and varying DOS distribution, so the effective DOS will be broadened by combination of many different profiles. Nevertheless, we can make a generalization about nanotubes as well as graphitic and diamond electrode materials: that the electronic DOS has magnitude and structure that is very different from that of metals and these differences can affect electrode kinetics.

### 3.3. Adsorption

Given the widespread use of  $sp^2$  hybridized carbon materials as adsorbents, there is a large body of literature on the factors governing the adsorption of molecules to carbon surfaces. A review of some will not be attempted here, except to note the main factors relevant to electrochemistry. The forces that govern adsorption to carbon depend strongly on the type of carbon, its surface chemistry, and the structure of the adsorbate, among other factors. Whether adsorption is a problem or an asset of a given carbon electrode will obviously depend on the application.

The interactions between surface and adsorbate that control adsorption include dipole–dipole interactions, induced dipoles, hydrophobic effects, and electrostatic and covalent bonds, all of which depend on the history and preparation of the carbon material. Graphitic carbon materials commonly used as adsorbents have a high microscopic surface area and many oxygen-containing functional groups. The high polarizability of graphite leads to relatively strong induced dipoles, and the permanent dipoles associated with functional groups support dipole–dipole interaction with adsorbates. The ability of carbon to form strong covalent bonds with a variety of materials has been exploited extensively for surface modification (section 5). Each of these interactions varies in magnitude depending on the carbon allotrope, the exposure of basal or edge planes at the surface, and the distribution of surface oxides. For example, adsorption to the basal plane of HOPG is relatively weak, since there are no permanent dipoles, electrostatic charges, or unsatisfied valences. However, adsorption is generally strong on edge plane graphite and on step-edge defects on the basal plane.<sup>17,94</sup> The electronic disturbance near a graphitic edge can extend onto the basal plane, creating local dipoles, which enhance adsorption relative to perfect basal plane HOPG.<sup>17</sup> A detailed scanning force microscopy study of anthraquinone adsorption on HOPG showed that anthraquinone adsorbed with various geometries on HOPG basal plane but also implied that only the adsorbate present at defect sites was electroactive.<sup>118</sup>

Figure 16 shows the results of Raman microspectroscopy used to investigate the adsorption of rhodamine 6G (R6G) on defects on HOPG basal plane.<sup>76</sup> The upper image is a photomicrograph of an intentional scratch on the basal plane surface, following adsorption of R6G from solution. Panel B is a Raman image of the same scratch, in which high intensity from the  $1180\text{ cm}^{-1}$  band of R6G is shown as yellow and green, while low  $1180$  intensity is shown as dark red. Combined with the Raman spectra at various points on the image (panels C–E), the results indicate that R6G adsorption is significantly higher on the edge plane defects than on undisturbed basal plane.

Not surprisingly, carbon electrodes are subject to unintentional or unknown adsorption of impurities during electrode preparation. Intentional or not, these adsorbates can dramatically affect the electron transfer rates and electrocatalytic activity of carbon electrodes, possibly subverting their intended electrochemical applications. There is a long history of “activation” procedures for carbon electrodes, including polishing, heat treatment, solvent treatment, laser activation, ultrasonication, and others.<sup>3,119</sup> These procedures improve electrode performance in part by removing adventitious adsorbates from the electrode surface and are discussed in somewhat more detail in section 3.6. There are many examples of electrocatalytic effects of adsorbates on carbon

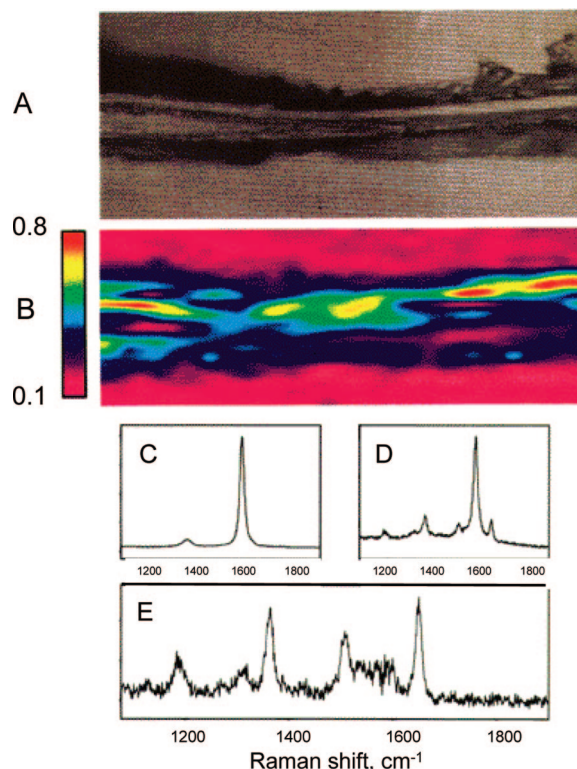


**Figure 16.** (A) Bright-field image of HOPG basal plane with an intentional defect, (B) Raman image of the same area as panel A after adsorption of R6G, constructed using the  $1180/1580$  peak area ratio from 1200 points, (C) spectrum acquired near the intentional defect before R6G exposure, (D) spectrum acquired near the intentional defect after exposure to R6G, and (E) resultant spectrum of spectrum C subtracted from spectrum D. Reprinted with permission from ref 76. Copyright 1997 American Chemical Society.

surfaces for redox reactions of redox peptides, oxygen reduction, and organic molecules, a few of which are discussed in the next section.

### 3.4. Electrocatalysis

The term “electrocatalysis” is used herein to designate a redox process that involves a specific chemical interaction with the electrode surface. Such interactions often accompany electron transfer reactions, particularly those involving organic and biological redox agents. The propensity of carbon to adsorb molecules from solution and the presence of surface oxides permit electrocatalytic reactions on carbon electrodes that are weaker or absent on metal electrodes. Furthermore, the history and preparation of carbon electrodes can have profound effects on the coverage and activity of catalytic sites; hence it is important to understand electrocatalytic effects. From the wide variety of reported electrocatalytic reactions on carbon electrodes, a few are considered here as illustrations.

As noted earlier,  $\text{Ru}(\text{NH}_3)_6^{3+/2+}$  represents the simplest case of an outer-sphere electron transfer reactions with no known chemical interactions with the surface. It is nearly unaffected by a monolayer of uncharged adsorbates and serves as the null case for electrocatalysis. The observed  $k^0$  depends on the DOS of the electrode material but in practice is uniformly high for clean electrodes with DOS similar to that of metals (Table 2). In contrast, the  $\text{Fe}^{3+/2+}$  redox reaction depends strongly on the presence of surface oxides on carbon and is inhibited significantly if they are absent or

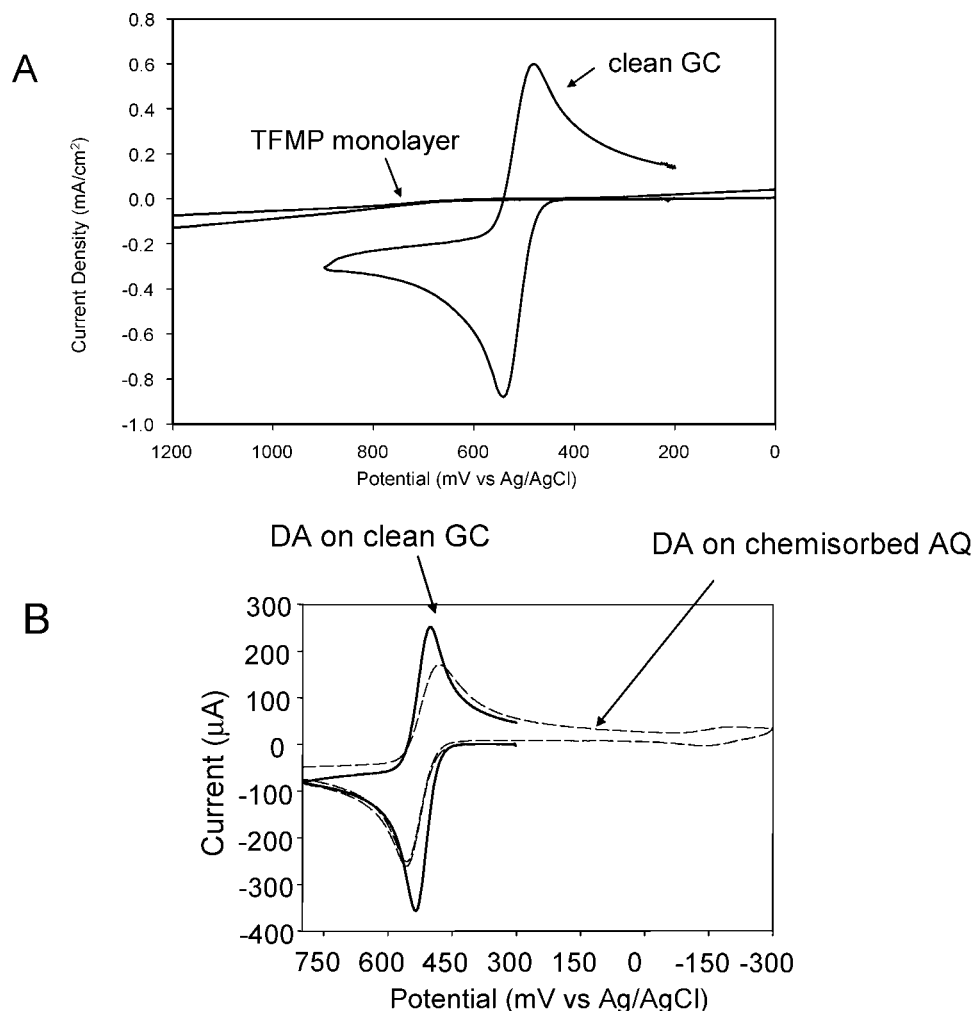


**Figure 17.** (A) Voltammetry of dopamine in 0.1 M H<sub>2</sub>SO<sub>4</sub> on clean GC and on GC modified with a monolayer of trifluorophenyl groups and (B) comparison of dopamine voltammetry on clean GC (solid line) and on a GC surface modified with chemisorbed anthraquinone (dashed line). AQ = anthraquinone, DA = dopamine, TFMP = trifluoromethylphenyl. Reprinted with permission from ref 126. Copyright 2000 American Chemical Society.

obscured by adsorbates.<sup>120–122</sup> The Fe–O bond length in hydrated Fe<sup>3+</sup> changes length upon reduction, and this process is facilitated by transient interactions with surface oxides. Fe(CN)<sub>6</sub><sup>3–/4–</sup> is also sensitive to the state of the carbon surface, although the nature of the catalytic interaction is not clear.<sup>121,122</sup> Unfortunately, Fe(CN)<sub>6</sub><sup>3–/4–</sup> is often used as an “ideal” outer-sphere redox reaction but in fact is quite complex and dependent both on the surface chemistry and interactions with cations in solution.<sup>3,123,124</sup> To use a phenomenological term, we might consider Fe<sup>3+/2+</sup> and to be “surface sensitive”, with kinetics that are influenced by an electrocatalytic interaction, while Ru(NH<sub>3</sub>)<sub>6</sub><sup>3+/2+</sup> is “surface insensitive”, with the electrode merely serving as a source or sink of electrons. An observation that clearly distinguishes Ru(NH<sub>3</sub>)<sub>6</sub><sup>3+/2+</sup> from Fe(CN)<sub>6</sub><sup>3–/4–</sup> in this respect was made with the aid of the diazonium reduction reaction described in section 5.1. A nitrophenyl modification of GC caused a significant decrease in the electron transfer rate to Fe(CN)<sub>6</sub><sup>3–/4–</sup> ( $\Delta E_p$  increased from 91 to 229 mV), but had minor effects on Ru(NH<sub>3</sub>)<sub>6</sub><sup>3+/2+</sup> (76 to 88 mV).<sup>122</sup>

The oxidation of catechol derivatives has been studied widely, due to the importance of catecholamine neurotransmitters and related compounds in biology. Dopamine (3,4-dihydroxy phenethylamine, DA) is an example of a catechol with heterogeneous electron transfer strongly dependent on electrocatalysis. As shown in Figure 17A, DA oxidation is

completely inhibited by a monolayer of triphenylmethyl phenyl groups bonded to glassy carbon.<sup>125,126</sup> This surface treatment has minor effects on Ru(NH<sub>3</sub>)<sub>6</sub><sup>3+/2+</sup>, so electrons are capable of tunneling through the monolayer.<sup>122</sup> DA oxidation is fully restored if a monolayer of anthraquinone instead of trifluoromethylphenyl covers the electrode surface, as shown in Figure 17B. The catalytic effect was attributed to the presence of hydrogen bonding sites on the surface, which assisted DA oxidation by transient bonding to the catechol hydrogen to effect “proton-assisted electron transfer”.<sup>126</sup> On a bare carbon surface lacking hydrogen bonding sites, the catechol itself can adsorb on the surface to permit “self-catalysis” by hydrogen bonding to catechols in solution undergoing oxidation.

Redox mediation is a widely studied example of electrocatalysis on carbon surfaces, in which a redox active adsorbate can act as an electron relay to molecules in solution. Of particular note is the widely used blood glucose analyzer, which is based on redox mediation between a carbon surface and NADH.<sup>127–129</sup> In some cases, a covalent chemisorption bond between the carbon surface and the electroactive species can catalyze electron transfer.<sup>130</sup> While carbon is not as broadly reactive toward chemisorption as catalytic metals such as Pt and Ru, its rich surface chemistry provides a route to build in such interactions by surface modification (section 5).

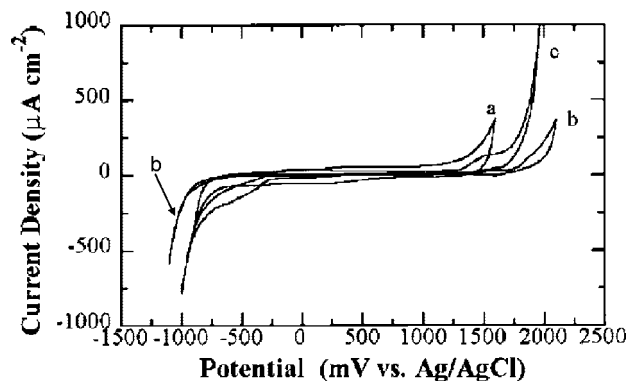


**Figure 18.** Background current for voltammetry (0.1 V/s) in 0.1 M HClO<sub>4</sub> for (a) glassy carbon, (b) moderately boron-doped microcrystalline diamond, and (c) heavily B-doped diamond. Reprinted with permission from ref 30. Copyright 2004 Marcel Dekker.

A practically important issue related to surface reactivity is the available potential range of carbon electrode materials over which background reactions contribute negligibly to the observed current. Such reactions depend strongly on the nature of the carbon electrode material as well as the preparation of the surface. The kinetics of surface oxidation and hydrogen evolution are significantly slower on carbon than on most commonly used metal electrodes, and the resulting wide potential window is one reason for the widespread use of carbon materials for electrodes. Since the onset of background current also depends strongly on solvent, pH, electrolyte composition, and current sensitivity, quantitative comparisons of different carbon materials are approximate. That said, diamond electrodes have electrochemical windows significantly wider than most graphitic materials, as demonstrated by an example shown in Figure 18. For single-crystal boron-doped diamond, positive potentials as high as +2.5 V vs NHE were accessible in water before large anodic currents occurred.<sup>131</sup> For polycrystalline diamond, a background oxidation was observed at +1.83 V on the first scan, and was attributed to irreversible oxidation of sp<sup>2</sup> impurities along grain boundaries.<sup>131</sup> Nitrogen-incorporated tetrahedral amorphous carbon and electron cyclotron deposited carbon<sup>24,132</sup> have higher potential limits than typical BDD or nanocrystalline diamond,<sup>35</sup> although this comparison will depend significantly on the origin of each sample.

Based on these examples and a host of others from the literature, it is clear that electrocatalytic reactions are very common on carbon electrodes, with the true outer-sphere redox reactions being in the minority. Obviously, the carbon electrode material and surface preparation will strongly affect the population of sites available for catalysis, and the underlying interactions are quite varied. As noted in section 3.5, the importance of identity and coverage of surface sites depends on the particular redox system involved, although some useful generalizations are available.

### 3.5. Classes of Redox Systems on Carbon Electrodes

The term “activation” has been used for several decades to describe procedures that modify the electron transfer kinetics at carbon electrodes, usually measured by the increase in  $k^0$  for a benchmark redox system. Three of the more common benchmark redox systems were Fe(CN)<sub>6</sub><sup>3-</sup>, ascorbic acid, and dopamine, all in aqueous solution, but

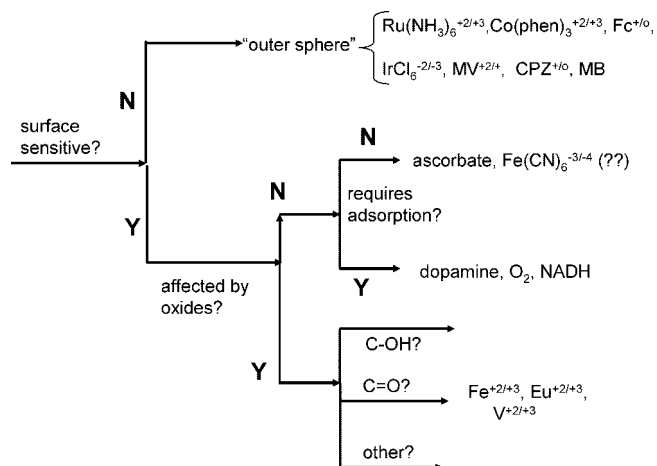


**Figure 19.** Classification of redox systems according to their kinetic sensitivity to particular surface modifications on carbon electrodes. See text and ref 121 for details. Reprinted with permission from ref 121. Copyright 1995 American Chemical Society.

others included ferrocene in acetonitrile, anthracene and anthraquinone, and dioxygen reduction. Unfortunately, the collection of activation procedures led to the inference that a “reactive” electrode will exhibit fast electron transfer kinetics for all redox systems considered, when in fact the sensitivity of  $k^0$  values to various activation procedures depends strongly on the redox system involved. This variation with electrode surface condition has been exploited to impart selectivity of carbon surfaces for particular analytes. For example, an anionic carbon surface is much more sensitive to dopamine at pH 7 (a cation) than to ascorbate (an anion) due to electrostatic repulsion of the ascorbate by the surface. Clearly any “activation” or modification of a carbon electrode surface must be considered in light of the particular redox system involved. The purpose of the present section is to classify redox systems according to the sensitivity of their electron transfer kinetics to the surface chemistry of a carbon electrode. Figure 19 presents a scheme for such a classification, based on experimental observations of a variety of carbon electrodes and mainly inorganic redox systems.<sup>122</sup> The next few sections explain the logic underlying the “tree” diagram of Figure 19, and its utility for classifying redox systems on carbon electrodes.

#### 3.5.1. Outer-Sphere Redox Systems

The first breakpoint in the tree diagram is based on “surface sensitivity”, that is, variations in  $k^0$  with the condition of the surface. Outer-sphere redox systems are generally considered to lack any electrocatalytic or adsorption step and often have low reorganization energies. Examples include Ru(NH<sub>3</sub>)<sub>6</sub><sup>3+/2+</sup>, ferrocene<sup>+0</sup>, and anthracene<sup>0/-</sup>. Figure 19 is phenomenological, in that it discriminates on the basis of an experimental observation rather than a mechanism. The “test” for surface sensitivity is the absence of a significant change in  $k^0$  when the carbon surface is purposely modified with a physi- or chemisorbed monolayer, such as a covalently bonded layer of nitrophenyl groups. An example is shown in Figure 20a, for Ru(NH<sub>3</sub>)<sub>6</sub><sup>3+/2+</sup> on GC. Adsorption of a monolayer of bis(methyl styryl)benzene has no effect on the observed peak separation or  $k^0$ , indicating that the electron transfer may occur with equal efficacy on a bare GC surface or on a surface coated with an organic molecule.<sup>121,122</sup> Obviously a significant effect would be

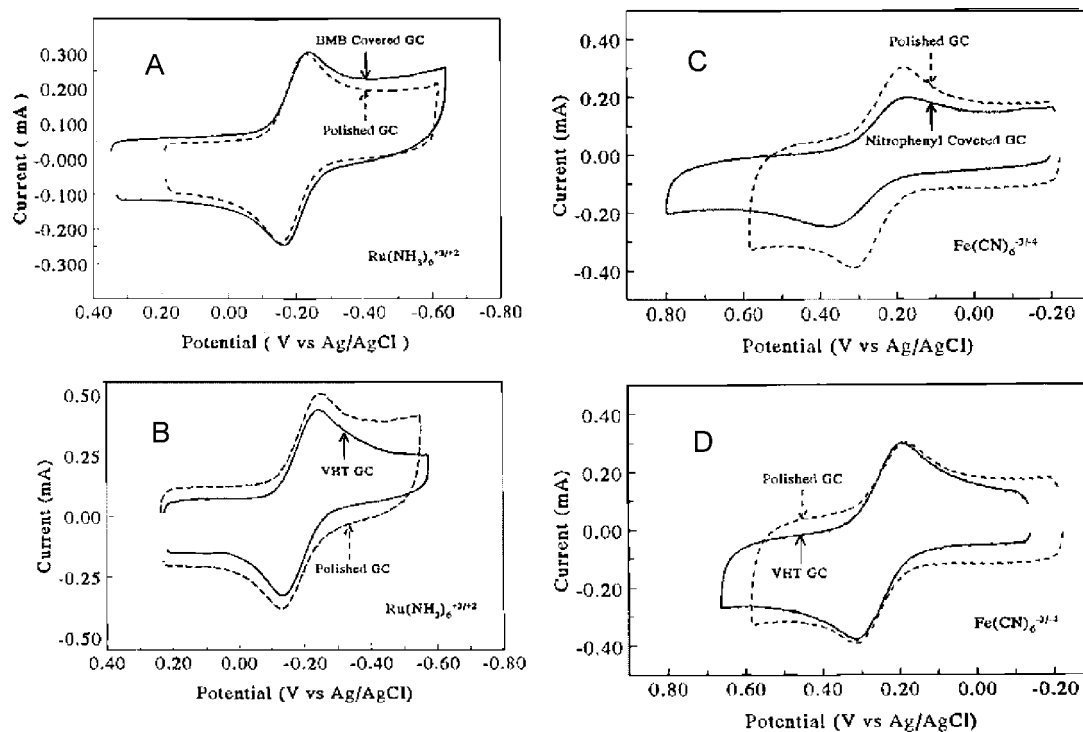


**Figure 20.** Voltammograms of  $\text{Ru}(\text{NH}_3)_6^{3+/2+}$  and  $\text{Fe}(\text{CN})_6^{3-/4-}$  on various glassy carbon electrode surfaces: (A)  $\text{Ru}(\text{NH}_3)_6^{3+/2+}$  on polished and bismethylstyrylbenzene coated GC; (B)  $\text{Ru}(\text{NH}_3)_6^{3+/2+}$  on polished and vacuum heat-treated GC; (C)  $\text{Fe}(\text{CN})_6^{3-/4-}$  on polished and nitrophenyl-modified GC, and (D)  $\text{Fe}(\text{CN})_6^{3-/4-}$  on polished and vacuum heat-treated GC. Reprinted with permission from ref 122. Copyright 1996 American Chemical Society.

expected if the  $\text{Ru}(\text{NH}_3)_6^{3+/2+}$  redox reaction depended on a surface interaction between the redox center and some site on the GC surface. It should be noted at this point that the lack of surface sensitivity, as defined here, does not rigorously establish a redox system as outer-sphere, but it does imply that significant changes in surface chemistry have no observable effect on electrode kinetics. It is also possible that the  $k^\circ$  is too fast to measure on either bare or modified electrodes, so that “surface sensitivity” was not observed.

While specific surface interactions related to electrocatalysis are clearly examples of effects that underlie “surface sensitivity”, a finer and more recent issue relates to electron tunneling. Even for outer-sphere redox reactions, a surface film will slow electron transfer because the electron must tunnel through the film between the reactant and the conducting electrode surface. The extreme case is a thick film, which totally prevents electron transfer. However, tunneling through monolayers of less than 1–2 nm thickness can be quite fast, and such monolayers are common on electrode surfaces, intentional or not. Numerous studies on electron transfer through self-assembled monolayers of alkanes and conjugated molecules have been reported, and it is well established that such monolayers slow but do not prevent electron transfer.<sup>133–138</sup> The observation that a monolayer of an organic molecule has little effect on  $\text{Ru}(\text{NH}_3)_6^{3+/2+}$  kinetics on a carbon surface (Figure 20A) indicates that electron tunneling can easily occur through a monolayer on the time scale of typical cyclic voltammetry. In the context of the “tree” of Figure 19, the test of surface sensitivity uses a monolayer thin enough for electron tunneling to be efficient on the experimental time scale employed. The tunneling rate is strongly dependent on monolayer thickness,<sup>139</sup> as expected, and can even be manipulated electrochemically by structural changes in the monolayer.<sup>140</sup> In the current context, “surface sensitive” refers to reactions that show significantly more

than the slight decrease in electron transfer kinetics expected from an organic monolayer with a thickness of less than  $\sim 1$  nm.

### 3.5.2. “Surface-Sensitive” and Electrocatalytic Redox Systems

In addition to a test based on a nonspecific organic monolayer, Figure 20B,D illustrates a second breakpoint in the classification “tree”, involving the effect of surface oxides. As will be discussed in section 3.6, polished GC carbon surfaces generally have 8–15% surface O/C ratio, while vacuum heat treatment reduces oxide coverage to a few percent. The example of dopamine oxidation cited in section 3.4 illustrates that certain redox processes have electron transfer rates that depend on the presence of surface oxides, in some cases on particular functional groups, such as carbonyl or carboxylate. Figure 20B,D shows that neither  $\text{Ru}(\text{NH}_3)_6^{3+/2+}$  nor  $\text{Fe}(\text{CN})_6^{3-/4-}$  exhibit a dependence of peak separation on oxide coverage, implying that they are not “oxide-dependent”. However,  $\text{Fe}(\text{CN})_6^{3-/4-}$  exhibits significantly slower kinetics on a surface modified with a monolayer of covalently bonded nitrophenyl groups (Figure 20C). These observations indicate that  $\text{Ru}(\text{NH}_3)_6^{3+/2+}$  is neither “surface-sensitive” nor “oxide-sensitive”, while  $\text{Fe}(\text{CN})_6^{3-/4-}$  is “surface-sensitive” but not “oxide-sensitive”. Various explanations for the dependence of  $\text{Fe}(\text{CN})_6^{3-/4-}$  on the condition of the electrode surface have been discussed.<sup>3,122–124,141</sup>

In contrast to  $\text{Ru}(\text{NH}_3)_6^{3+/2+}$  and  $\text{Fe}(\text{CN})_6^{3-/4-}$ , the  $\text{Fe}(\text{H}_2\text{O})_6^{3+/2+}$  redox system depends strongly on the presence of surface oxides on carbon electrodes.<sup>120,121</sup> The voltammetry of  $\text{Fe}^{3+/2+}$  is shown in Figures 21 and 22 for glassy carbon electrodes, and a collection of  $\Delta E_p$  values appears in Table 3. Note first that the  $\Delta E_p$  for  $\text{Fe}^{3+/2+}$  is large for carbon surfaces low in oxide coverage, notably

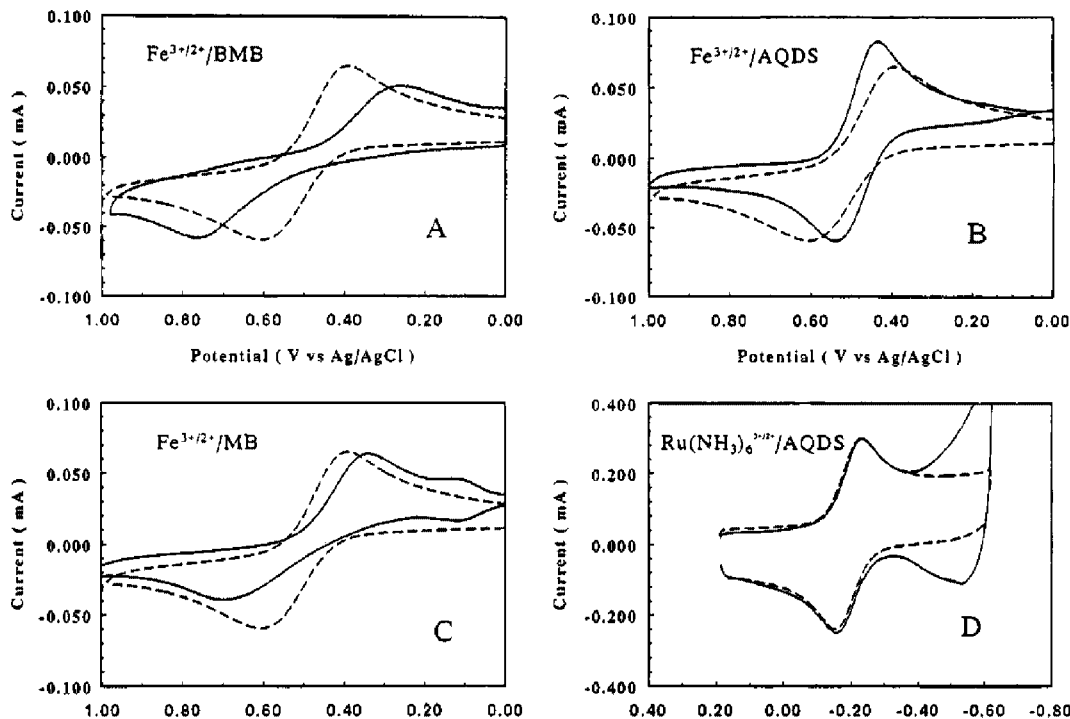


**Figure 21.** Voltammetry on polished GC before (dashed) and after (solid) adsorption of organic molecules. (A–C) Fe<sup>3+/2+</sup> with adsorption of bismethylstyrylbenzene (BMB), methylene blue (MB), and anthraquinone 2,6-disulfonate (AQDS); (D) Ru(NH<sub>3</sub>)<sub>6</sub><sup>3+/2+</sup> with AQDS. Reprinted with permission from ref 121. Copyright 1995 American Chemical Society.

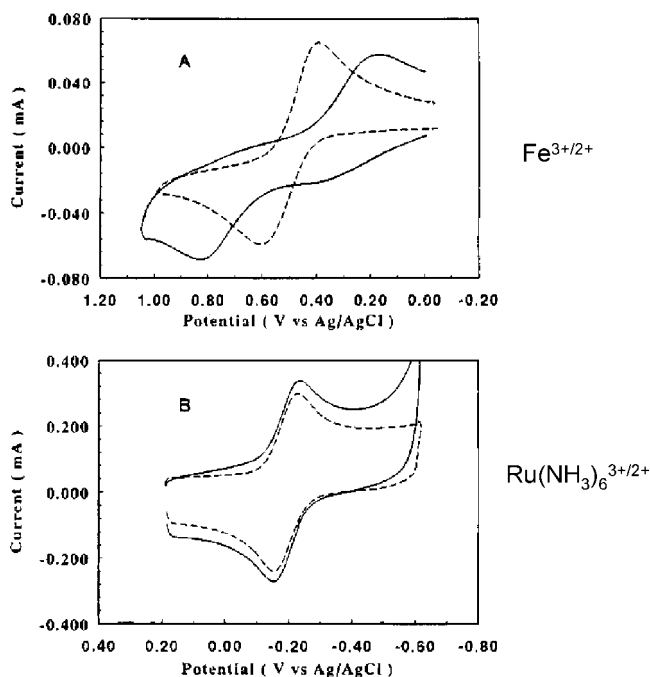


**Figure 22.** Fe<sup>3+/2+</sup> voltammetry in 0.1 M HClO<sub>4</sub> on polished GC before (dashed lines) and after (solid lines) reacting surface carbonyl groups with DNP. Reprinted with permission from ref 121. Copyright 1995 American Chemical Society.

vacuum heat treated ( $\Delta E_p = 439$  mV), and Ar<sup>+</sup> sputtered (900 mV). Electrochemical oxidation of the GC surface greatly decreases  $\Delta E_p$ , for example, from 900 to 80 mV for the Ar<sup>+</sup>-sputtered surface, indicating that surface oxides significantly accelerate electron transfer. Since a polished GC surface has significant surface oxides, it exhibits faster kinetics than the low oxide surfaces, even though it may not be as clean. However, as shown in Figure 21A,C, adsorption of a monolayer of an organic molecule on top of the polished

surface significantly increases the peak separation, presumably by obscuring oxygen-containing catalytic sites. We conclude that Fe<sup>3+/2+</sup> and other aquated transition metals like Eu<sup>3+/2+</sup> and V<sup>3+/2+</sup> have electron transfer rates that depend strongly on surface oxide level, in contrast to Ru(NH<sub>3</sub>)<sub>6</sub><sup>3+/2+</sup>, ascorbic acid, and Fe(CN)<sub>6</sub><sup>3-/4-</sup>.

The variation of electron transfer rates with surface oxide coverage implies an electrocatalytic mechanism for Fe<sup>3+/2+</sup>, and its absence with Ru(NH<sub>3</sub>)<sub>6</sub><sup>3+/2+</sup> indicates that it is more than an electrostatic effect of possible anodic functional groups. The catalysis may be probed further with reagents that react with particular oxygen-containing functional groups, and observation of the effect of these reagents on electron transfer kinetics. Two such reagents are dinitrophenylhydrazine (DNPH), which reacts with surface carbonyl groups, and dinitrobenzoylchloride (DNB), which bonds to surface hydroxyl groups. The products of the reactions of these materials with carbon surfaces are observable with Raman spectroscopy and XPS,<sup>106,107</sup> with the Raman scattering being enhanced by the resonance Raman activity of the surface adduct. As shown in Figure 22, the  $\Delta E_p$  for Fe<sup>3+/2+</sup> on polished GC increases dramatically upon DNPH treatment, while DNB had little effect on Fe<sup>3+/2+</sup> kinetics. Since DNPH binds specifically to surface carbonyl groups, the sensitivity of Fe<sup>3+/2+</sup> kinetics to DPNH treatment implies a specific surface interaction between carbonyl groups and Fe<sup>3+/2+</sup> as the electrocatalytic event. Observation of the DNPH adduct with Raman spectroscopy revealed a linear dependence of the Fe<sup>3+/2+</sup> rate with the coverage of surface carbonyl groups.<sup>121</sup> Furthermore, intentional adsorption of a molecule containing carbonyl groups accelerates Fe<sup>3+/2+</sup> electron transfer, as shown for anthraquinone in Figure 21B, but it has no effect on Ru(NH<sub>3</sub>)<sub>6</sub><sup>3+/2+</sup> (Figure 21D). An inner sphere complex of Fe<sup>3+/2+</sup> has been proposed,<sup>120,121</sup> although hydrogen bonding between the water of hydration of Fe<sup>3+/2+</sup> and a surface carbonyl is also possible.<sup>126</sup> The effect of DNPH and DNB on the kinetics of a particular redox

**Table 3. Electrode Kinetics for Fe<sup>3+/2+</sup> and for Eu<sup>3+/2+</sup> on Carbon Materials<sup>a</sup>**

electrode	$\Delta E_p$ for Fe <sup>3+/2+</sup> (mV)	$\Delta E_p$ for Eu <sup>3+/2+</sup> (mV)	atomic O/C ratio	ref
HOPG	1062	936	<<0.01	120
HOPG/ECP <sup>b</sup>	162	372		120
GC, polished in H <sub>2</sub> O	150	428	0.10–0.14	120, 122
GC, polished in cyclohexane	352		0.04	122
GC, fractured	186	509		120
GC, fractured + ECP	93	70		120
GC, polished + Ar <sup>+</sup> sputtered	908		<0.01	122
GC, polished + Ar <sup>+</sup> + ECP	80			122
GC, polished + DPNH	670			122
GC, polished + BMB	506			122
GC, polished + anthraquinone	100			122
GC, vacuum heat treatment	439		0.016	122, 409
PPF, IPA/AC	647			99
electron cyclotron resonance carbon film	587			24
boron doped nanocrystalline diamond	679			30

<sup>a</sup> 0.2 M HClO<sub>4</sub>, 0.2 V/s. <sup>b</sup> Electrochemical pretreatment by anodization.

reaction may be used as additional breakpoints in the “tree” of Figure 19.

To summarize the current section, it should come as no surprise that the extent to which surface chemistry affects electron transfer rates is a strong function of the redox reaction involved. While “activation” may be a useful term for treatments that increase electron transfer rates, it should not be assumed that all redox systems will be “activated” equally. Since electrochemical reactions are inherently heterogeneous, they will always depend to some degree on the nature of the electrode surface. If a specific surface interaction is identified as catalytic for an electrochemical reaction, then the electrode may be tailored to maximize the extent of the resulting catalysis.

### 3.6. Carbon Electrode Surface Preparation

Surface preparation is of obvious importance for any heterogeneous process like electrochemistry, and the literature on carbon electrodes is particularly rich. The three allotropes of carbon, the wide variation of surface structure and functional groups, and the propensity of carbon to adsorb adventitious impurities make the story complex, but in many cases surface preparation may be exploited to achieve selectivity or modify electrode kinetics. The extensive literature on electrode polishing, laser and electrochemical pretreatment, vacuum heat treatment, etc, was reviewed in some detail in the mid 1990s,<sup>3,119,142</sup> so the current discussion will briefly summarize the salient points from that period and emphasize recent procedures and materials. In many comparisons of preparation procedures, the  $k^\circ$  observed for Fe(CN)<sub>6</sub><sup>3-/4-</sup> in aqueous 1 M KCl is used as a benchmark of electrode “activity”. As noted in section 3.4, Fe(CN)<sub>6</sub><sup>3-/4-</sup> is far from an “ideal” outer-sphere redox system, and in fact, its kinetics depend strongly on the state of the surface. However, this sensitivity makes it a useful monitor of variations in surface condition, and it has been used for over three decades as a benchmark redox system. Preparation methods will be presented in three groups: polishing and cleaning, vacuum treatments, and activation procedures, using both Fe(CN)<sub>6</sub><sup>3-/4-</sup> and Ru(NH<sub>3</sub>)<sub>6</sub><sup>3+/2+</sup> kinetics as benchmarks of electrochemical reactivity.

#### 3.6.1. Polishing and Cleaning

Polishing has a long history for carbon materials and remains the most common preparation for carbon electrodes used in electrochemistry. Perhaps the most commonly used carbon electrode material is glassy carbon, most often polished with silicon carbide paper followed by a series of alumina slurries with successively smaller particles size, typically finishing with 0.05 μm. Past reviews should be consulted for polishing details,<sup>3,119,142</sup> but a few lessons from the past deserve repetition. First, a “course” polish with silicon carbide sandpaper results in a relatively rough but reactive surface. In the case of carbon fiber microelectrodes, the “coarsely polished” surface is adequate for many purposes, and potential contamination from polishing compounds is minimized.<sup>143</sup> Second, many commercial diamond and alumina polishing slurries contain deagglomerating agents, which can seriously affect electrode reactivity due to adsorption on the carbon surface. Good practice dictates the use of pure, dry alumina powder slurried with ultrapure water (e.g., Barnstead “nanopure”). Third, the surface oxide level can be significantly modified by polishing and by the liquid used to make the abrasive slurry. As shown in Figure 11, a water/alumina slurry yields a surface O/C atomic ratio on GC of about 10–15%, while the same surface polished with cyclohexane/alumina has an O/C ratio below 4%.<sup>95</sup> Fourth, it is good practice to sonicate after polishing, but the purity of the sonication liquid is important. Sonication may remove particles, but it may also permit adsorption of impurities from the sonication bath.<sup>144</sup> Fifth, polishing generally results in a residue of both polishing material and carbon particles, which is difficult to remove and can adversely affect electrochemical reactivity.<sup>3,144</sup> As noted in section 3.6.3.3, an effective method to remove such debris is a short anodization pulse in basic media.<sup>145</sup> As indicated by several of the entries in Table 2, variations in polishing procedure result in reported  $k^\circ$  values for Fe(CN)<sub>6</sub><sup>3-/4-</sup> in 1 M KCl from <0.001 to 0.14 cm/s. Such variations are less pronounced for outer-sphere redox systems such as Ru(NH<sub>3</sub>)<sub>6</sub><sup>3+/2+</sup>, but the Fe(CN)<sub>6</sub><sup>3-/4-</sup> results indicate the importance of surface condition to reactivity.

A more recent preparation procedure is simpler than polishing and also amenable to electrodes of any shape and size. When a carbon electrode is treated with an organic solvent containing activated carbon (AC), the much higher surface area of the AC effectively “getters” the impurities

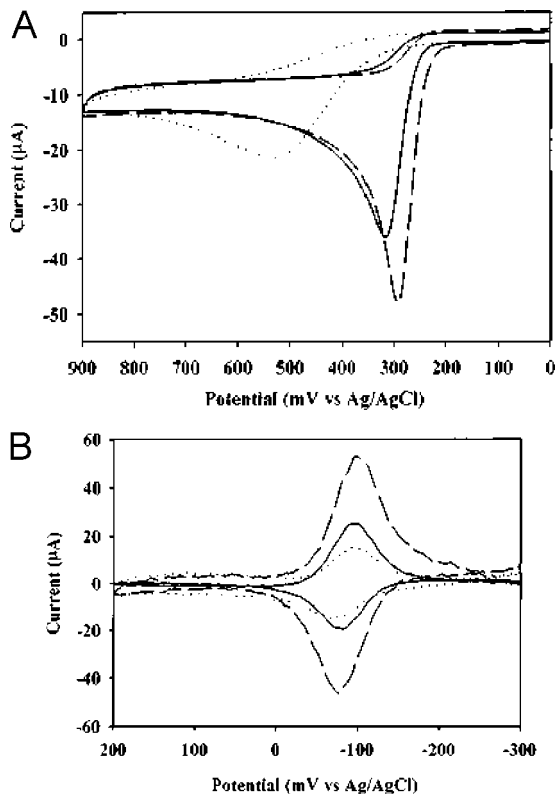


**Figure 23.** Voltammograms from GC electrodes pretreated by polishing (solid curve), isopropyl alcohol (dotted), and isopropyl alcohol in the presence of activated carbon (dashed): (A) 1 mM ascorbic acid in 0.1 M  $\text{H}_2\text{SO}_4$ ; (B) 40  $\mu\text{M}$  anthraquinone 2,6-disulfonate in 0.1 M  $\text{HClO}_4$ . Reprinted with permission from ref 146. Copyright 1999 American Chemical Society.

off the electrode surface.<sup>146</sup> Without activated carbon, organic solvents can significantly decrease the reactivity of a carbon electrode, due to adsorption of large trace organics from the solvent. A combination of AC and sonication produces a surprisingly large increase in electron transfer rates and adsorption of carbon electrodes. Figure 23A shows the effect of isopropanol/AC on the oxidation of ascorbic acid, with the solid curve being the voltammogram on a carefully polished GC electrode.

Treatment with reagent grade isopropanol (IPA) alone causes a large shift toward more positive potentials, reflecting a reduction in electron transfer rate presumably caused by adsorption of impurities in the isopropanol. Treatment with isopropanol/AC but no additional polishing shifts the peak potential to a value more negative than that on the polished surface.<sup>146</sup> A quantitative indication of the solvent/AC effect is shown in Figure 23B for the adsorption of anthraquinone 2,6-disulfonate (AQDS). The increase in AQDS adsorption after  $\text{CH}_3\text{CN}/\text{AC}$  treatment by a factor of 2 implies that about half of the polished surface was occupied by adventitious adsorbates, which prevented AQDS adsorption. For the case of dopamine oxidation in mild acid, the observed  $\Delta E_p$  was smaller for the isopropanol/AC treated GC surface than for careful polishing, and IPA/AC treatment restored the small  $\Delta E_p$  after deactivation with a surfactant solution or by exposure to ambient air for a week.<sup>146</sup> A particularly beneficial application of solvent/AC cleaning involves the exposed cylindrical sides of carbon fibers for in vivo monitoring of neurotransmitters.<sup>11,13,147</sup> Such electrodes cannot be polished and are quite fragile, but IPA/AC treatment enhances the adsorption and voltammetric response

of catecholamine neurotransmitters such as dopamine and norepinephrine.

Boron-doped diamond adsorbs most chemical species more weakly than GC or carbon fibers, due to its low polarizability and relative lack of local dipoles. The relatively large, polar impurities often present in electrochemical solvents at trace levels are less prone to adsorb on BDD compared with graphitic carbon electrodes and hence are less likely to reduce electrochemical reactivity. BDD surfaces are usually microscopically rough and not readily amenable to conventional polishing. However, BDD electrodes exhibit fast electron transfer right out of the reactor in which they are made and may be exposed to ambient air for weeks without significant decrease in electrochemical reactivity.<sup>30,53</sup> Purified IPA has also been used for cleaning BDD surfaces before electrochemical measurements.<sup>53</sup>

### 3.6.2. Vacuum and Heat Treatments

The thermodynamic stability of carbon–oxygen bonds makes most carbon materials susceptible to air oxidation, leading to the surface oxides described in section 3.2. These oxides are hard to remove and in fact can be beneficial for certain redox reactions involving adsorption or hydrogen bonding to surface oxide functional groups. Conventional polishing generally increases the level of surface oxides, as well as disordering both the oxides and the carbon microstructure. Several vacuum procedures have been developed to remove oxides from carbon surfaces, in order to study the behavior of “oxide-free” carbon. An early example was that of Mazur et al., who heated carbon fibers to 1020 °C in a  $10^{-5}$  Torr vacuum, then exposed the cooled fiber to  $\text{O}_2$  or several organic gases.<sup>148</sup> The reactions of the “oxide-free” carbon surface with olefins implied that heat treatment resulted in unsatisfied valences or “dangling bonds” on the surface, which underwent free radical addition reactions to irreversibly adsorb molecules such as allene and vinyl bromide. Vacuum heat treatment (VHT) of GC at 725 °C and  $<2 \times 10^{-6}$  Torr reduced the surface O/C ratio from 0.25 to 0.05 and resulted in a very electrochemically active surface with a  $k^\circ$  for the  $\text{Fe}(\text{CN})_6^{3-/4-}$  system of 0.14  $\text{cm/s}$ .<sup>144,146</sup>

More recent vacuum treatments are derived from chemical vapor deposition (CVD) techniques developed for fabricating diamond films, including BDD. A hydrogen plasma formed from  $\text{H}_2$  with a hot tungsten filament or microwave heating contains significant concentrations of H atoms, which react with surface oxides and etch the carbon surface. When applied to GC electrode surfaces, a hydrogen plasma roughens the surface slightly and decreases the surface O/C ratio to below 0.02.<sup>95</sup> As noted previously in section 3.1.2, the C–H termination of the GC structure resists surface oxidation by air much better than the VHT surface, with the oxide level remaining below 4% after a week in air. The unsatisfied valences on the carbon surface following VHT are more reactive to dioxygen and water than the C–H terminated surface, resulting in the behavior illustrated in Figure 5.

As described later in section 4.1, pyrolysis of an organic polymer photoresist material can be used to make an electrochemically interesting carbon surface, PPF (pyrolyzed photoresist film).<sup>99,149</sup> Heating to 1100 °C in a 5%  $\text{H}_2/\text{N}_2$  atmosphere decreased the surface O/C ratio to  $<2\%$ , which then increased to  $\sim 6\%$  after 4 days in air. The rate of increase of the O/C ratio on PPF was significantly slower than that

on GC heat treated similarly in  $\text{H}_2/\text{N}_2$ , but faster than that on H-terminated GC made in a hydrogen plasma.<sup>99</sup> We infer that pyrolysis in a hydrogen atmosphere results in a partially H-terminated surface, but the more aggressive hydrogen plasma reacts with more of the unsatisfied valences on the carbon surface.

Sputtering with high-energy ( $>500$  eV)  $\text{Ar}^+$  is commonly used in surface science to remove surface layers from samples in UHV, most commonly on metals such as Pt, Ru, etc. Sputtering of glassy carbon reduces the O/C ratio to below 1% and can result in an electrochemically active surface.<sup>122</sup> However,  $\text{Ar}^+$  sputtering damages the carbon microstructure, and there is no effective annealing procedure known for materials like GC and graphite. Given that sputtering generally requires an expensive vacuum system and  $\text{Ar}^+$  beam and also leads to a disordered material, it is not recommended for routine electrochemical applications.

### 3.6.3. Carbon Electrode Activation

The term “activation” has been used frequently to describe procedures for increasing the reactivity of carbon electrodes, often for the purpose of detecting a specific analyte. It is more frequently encountered with carbon electrodes compared with metals, since the propensity of carbon to adsorb impurities leads to electrode surfaces with decreased activity unless great care is taken to avoid adsorption. As discussed in section 3.5, the observed electron transfer kinetics for different redox systems depend on several different surface properties, so “activation” can involve more than one mechanism in terms of its effects on the electrode surface. For “outer-sphere” redox systems such as  $\text{Ru}(\text{NH}_3)_6^{3+/2+}$ , the maximum electron transfer rate is observed for a clean surface, with little or no dependence on particular surface sites or functional groups (see Table 2). The  $\text{Fe}(\text{H}_2\text{O})_6^{3+/2+}$  couple, however, exhibits kinetics strongly dependent on the presence of surface oxides, particularly carbonyl groups (Table 3). Good practice dictates that one should start with a clean electrode surface before kinetic measurements or surface modification, but beyond that, “activation” may entail formation of particular active sites on the carbon surface that “activate” redox systems to varying degrees depending on their redox mechanisms.

**3.6.3.1. Surface Cleaning.** Many “activation” procedures are in fact cleaning steps, in many cases employed to remove surface layers resulting from handling or impure materials used for polishing. Using GC as a representative carbon electrode material, we noted in section 3.2 that “fracturing” directly in the electrolyte solution of interest exposes a pristine GC surface, and should represent the cleanest possible GC electrode. Using the  $\text{Fe}(\text{CN})_6^{3-/4-}$  system as a “surface-sensitive” benchmark, we note from Table 3 that all polishing procedures result in lower observed electron transfer rates than the fractured surface, some by 2 or more orders of magnitude. Since fracturing is not practical on a routine basis for ordinary GC electrodes, solvent/AC cleaning and ultraclean polishing are reasonably successful alternatives. With carbon fibers, cutting the fiber immediately before use or the “coarse” polishing described earlier are similar to “fracturing” in terms of their effects on the carbon surface and would be expected to yield similarly clean surfaces.<sup>143,150</sup>

**3.6.3.2. Laser Activation.** It was first reported in 1984<sup>151</sup> that an energetic laser pulse irradiating a carbon electrode directly in the electrolyte of interest had dramatic effects on the electron transfer rates observed for the oxidation of

ascorbic acid and phenol. Since the initial report, the mechanism of the phenomenon has been explored in some detail,<sup>51,70,96,152–155</sup> as have electroanalytical applications in voltammetry<sup>156–161</sup> and amperometric detectors for liquid chromatography.<sup>162</sup> Laser-activated graphite, glassy carbon, and carbon fiber electrodes have been characterized with Raman, XPS, STM, and SEM to reveal changes in microstructure and surface composition.<sup>51,69,70,73,154,163</sup> As shown in Table 2, laser-activated GC and carbon fiber electrodes exhibit the highest  $k^0$  values for  $\text{Ru}(\text{NH}_3)_6^{3+/2+}$  and  $\text{Fe}(\text{CN})_6^{3-/4-}$  for carbon electrodes, as well as fast kinetics for organic systems such as ascorbic acid and dopamine. The process usually involves a 7–20 ns laser pulse from a Nd:YAG (1064 nm) or nitrogen (337 nm) laser, with peak power density in the range of 10–100 MW/cm<sup>2</sup>. The rapid thermal expansion and local heating<sup>154</sup> cause desorption of adsorbates and, at higher power density, can cause disruption of the carbon microstructure.<sup>70,164</sup> For the case of glassy carbon and carbon fiber electrodes, power densities up to 25 MW/cm<sup>2</sup> do not cause observable morphological changes on the carbon surface yet produce dramatic acceleration of electron transfer kinetics.<sup>51,154</sup> The mechanism of laser activation includes at least three effects, whose importance depends on the power density and the type of carbon electrode examined, and to a lesser extent on the laser wavelength and optical penetration depth.<sup>8</sup> Below 25 MW/cm<sup>2</sup>, the thermal transient resulting from laser light absorption desorbs impurities and produces a cleaner, more reactive electrode surface. Laser irradiation above 25 MW/cm<sup>2</sup> can disrupt the carbon microstructure, for example, by thermal stress to the graphite planes to produce a higher density of edge planes.<sup>69,70</sup> In addition, the oxide coverage of the electrode may be altered during the laser pulse, particularly if dioxygen is present in the solution.<sup>165,166</sup>

In addition to providing major increases in electron transfer rates and electrode surface reactivity, laser activation has some practical advantages for use in electrochemical and analytical applications. It may be used in situ by directing the laser through a cell wall or window, thus obviating the need for electrode removal or cell disassembly. It is fast and repeatable, thus resulting in a “renewable” carbon electrode surface amenable to pulse voltammetry.<sup>156,162</sup> Electrodes deactivated by deposition of electrolysis products (i.e., “fouling”) are easily reactivated, in situ. The laser beam may be used to microfabricate electrode surfaces by removal of an intentional film on the electrode surface to make microelectrode arrays.<sup>157</sup> Kuhr et al. used interference patterns from a 325 nm He–Cd laser to photopattern and activate glassy carbon surfaces on a micrometer scale and for photoablation of enzymes immobilized on carbon and silica surfaces.<sup>167,168</sup> Laser activation is applicable to microscopic or nonplanar electrodes not amenable to polishing, such as carbon fibers and microdisks.<sup>158–161,166</sup> While these positive aspects of laser activation have been demonstrated to be useful for many applications of carbon electrodes, the technique has not been used widely, presumably due to the requirement for a pulsed laser and the associated expense and safety concerns.

**3.6.3.3. Electrochemical Pretreatment (ECP).** Electrochemical oxidation or reduction in various media has long been used to “activate” carbon electrodes, and the many effects of ECP were reviewed in some detail in 1991.<sup>3</sup> Although most of the effects of ECP on surface structure and electrochemical activity were recognized at that time,

there has been a continuous stream of reports in recent years, including some significant new information.<sup>108–110,160,169–175</sup> A brief summary of ECP effects will be presented here, followed by some examples from the literature since 1991. As shown in Figure 18, polarization of a carbon electrode outside the electrochemical window yields significant current, which results from reactions both of the electrolyte and of the electrode itself. ECP is most commonly an oxidation for some period of time past the positive limit apparent in Figure 18, generally in the range of 1–2 V vs SCE. Depending on the duration of anodization, the carbon surface can be disrupted significantly, to the point of forming a surface film of “electrogenerated graphitic oxide” (EGO). This film has an O/C ratio above 0.2, contains many anionic sites, and is permeable to solvent and small molecules.<sup>3</sup> Carbon electrodes subjected to ECP can have dramatically different reactivity and selectivity compared with the same electrodes before ECP, particularly for charged redox systems or for those that are catalyzed by surface oxides. As shown in Table 3, the observed  $k^\circ$  for  $\text{Fe}^{3+/2+}$  is much higher on an ECP-treated GC surface, due to the generation of carbonyl groups during anodization.<sup>120</sup> ECP has also been used for decades to impart selectivity for cationic redox systems such as dopamine over anionic interferents like ascorbate, due to electrostatic interactions with the anionic EGO film.<sup>110</sup>

Examples of more recent applications of ECP for carbon electrodes include oxidation of nucleotides,<sup>160,172,175</sup> oxygen reduction,<sup>173</sup> immunoassay,<sup>174</sup> and modification of protein adsorption.<sup>176</sup> A short anodization in basic solution removed polishing debris and exposed a very clean pyrolytic carbon film, as judged by scanning probe microscopy.<sup>145,170</sup> EGO is hydrolyzed above approximately pH 10, so a surface film does not form on carbon during anodization in basic solution. As will be described in section 4.1, anodization at elevated pH can be used to microfabricate reactive sites on carbon surfaces.<sup>171</sup> Passage of a high current density through carbon fibers in an electrolyte solution has an extraordinary effect on the fiber morphology, generating a very high surface area with an apparent capacitance of  $\sim 4000 \mu\text{F}/\text{cm}^2$ , more than 100 times the typical values for GC and carbon fibers.<sup>108–110,169</sup> A combination of cation selectivity and enhanced adsorption created strong selectivity for catechols, particularly the cationic dopamine.

For the case of diamond electrodes, electrochemical pretreatment can cause significant increases in the levels of surface oxide functional groups, with attendant effects on the electron transfer kinetics for systems that interact with the surface.<sup>30,53</sup> These electrochemical effects are described in more detail in section 4.2.

### 3.7. Summary and Generalizations

Considering sections 2 and 3 together, some generalizations are useful regarding electrochemical reactivity of carbon electrodes. First, there must be sufficient electronic states in the electrode material at energies near the  $E^\circ$  of the redox system(s) of interest. The density of electronic states is determined both by the carbon microstructure and by surface states from defects and termination. A low DOS can significantly decrease the observed electron transfer rate, as is the case with lightly doped diamond or HOPG electrodes. Second, the electron transfer and adsorption reactivity of graphitic carbon electrodes is a strong function of the surface coverage of edge relative to basal plane graphite. Edge sites are more reactive to ET, adsorption, and chemical modifica-

tion, and in some cases the observed  $k^\circ$  and capacitance can be quantitatively correlated with edge plane coverage.<sup>50,51,177,178</sup> Third, redox systems differ dramatically in their sensitivity to the state of the carbon electrode surface, due to differences in their redox reaction mechanisms, ionic charge, etc.  $\text{Ru}(\text{NH}_3)_6^{3+/2+}$ , anthracene, and ferrocene are examples of nearly ideal redox systems, which are relatively insensitive to surface oxides and adsorbates, while  $\text{Fe}^{3+/2+}$  and dopamine are dependent on particular surface sites that participate in an electrocatalytic mechanism. It is unwise and often incorrect to discuss “activation” of a carbon electrode without stating the redox reaction used as the indicator of electrode reactivity. Fourth, carbon materials have more variety in both bulk and surface structure than metals, and electrode preparation is particularly important for achieving reproducible electrochemical behavior. Even the most common preparation procedures, such as polishing, significantly modify the surface structure and chemistry and can have dramatic effects on reactivity, adsorption, etc.

## 4. Advanced Carbon Electrode Materials

As noted in the Introduction, several fundamentally novel carbon materials have come into use for electrochemistry during the last 15 years. Some of these are new manifestations of materials structurally similar to glassy carbon, such as pyrolyzed photoresist, while others are completely different allotropes of carbon, such as diamond and the fullerenes. Although there is some overlap in the classification of these recently developed materials as electrode materials, they will be subdivided into microfabricated carbon, conducting diamond, fibers and nanotubes, and carbon composites. As each electrode material is discussed, the relationships between the general properties described in sections 2 and 3 and the electrochemical behavior of the material will be considered.

### 4.1. Microfabricated Carbon Thin Films

The vast majority of carbon electrodes are made from bulk materials such as graphite or glassy carbon, which are shaped and packaged to expose the electrochemically active electrode surface. “Microfabricated” is used here to mean that the electrode is formed from a gas or liquid precursor, often as a thin film and occasionally in a pattern with micrometer-scale dimensions. Pyrolysis of hydrocarbons onto metal or quartz surfaces has been used fairly extensively to make carbon films of arbitrary shape, for example, as detectors for capillary electrophoresis,<sup>179–181</sup> and on ceramic supports.<sup>182,183</sup> Reactive precursors may be employed to reduce the pyrolysis temperatures and to incorporate heteroatoms or metals.<sup>19,21,184</sup> The properties of these materials depend strongly on their thermal history, particularly maximum preparation temperature, and the presence of metal “graphitization” catalysts such as nickel and iron. They are generally less ordered than most types of graphite but exhibit moderate electron transfer rates for both catechols and  $\text{Fe}(\text{CN})_6^{3-/4-}$ .

A more recent variant of pyrolytic carbon with distinct properties for electrochemistry is pyrolyzed photoresist film (PPF),<sup>99,149,185–190</sup> although the process was reported for photolithography in 1985<sup>191,192</sup> and for microelectromechanical fabrication in 1997.<sup>193</sup> Many photoresists are based on a phenolic resin (e.g., “Novolac”) and are available commercially (e.g., AZ4330, AZ Electronic Materials, Somerville, N.J.). These materials are designed to be spin-coated

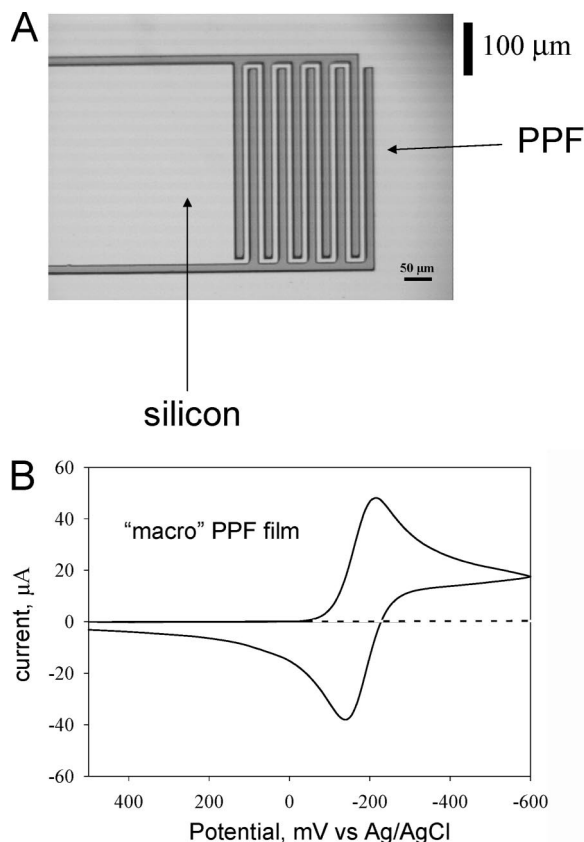


**Figure 24.** (A) Photomicrograph of pyrolyzed photoresist film pattern on silicon substrate and (B) voltammetry of  $\text{Ru}(\text{NH}_3)_6^{3+/2+}$  (1 M KCl, 0.2 V/s) on unpatterned PPF (solid line) and on uncoated Si substrate (dashed). Reprinted with permission from ref 99. Copyright 2001 American Chemical Society.

onto silicon or quartz, then patterned if desired with standard photolithographic techniques. Pyrolysis in a reducing atmosphere, typically 5%  $\text{H}_2$  in  $\text{N}_2$ , to maximum temperatures of 700–1100 °C removes nearly all of the heteroatoms and a significant fraction of the photoresist weight and yields quite pure  $\text{sp}^2$  hybridized carbon. A micrograph of a PPF pattern formed lithographically on silicon is shown in Figure 24, along with a voltammogram of  $\text{Ru}(\text{NH}_3)_6^{3+/2+}$  on a large area ( $\sim 5 \text{ mm}^2$ ) unpatterned PPF film. The resistivity of the photoresist decreases from  $> 10^{15} \Omega \cdot \text{cm}$  to  $\sim 10^{-2} \Omega \cdot \text{cm}$ , with the largest drop in resistance commencing at about 600 °C.<sup>149,186</sup> Laser pyrolysis may also be used to form patterns in the photoresist if desired.<sup>194</sup> Raman spectroscopy and TEM reveal that PPF formed at 1000–1100 °C is structurally similar to GC, with a resistivity of  $\sim 0.006 \Omega \cdot \text{cm}$ , comparable to that of GC ( $\sim 0.005 \Omega \cdot \text{cm}$ ).<sup>149</sup> AFM of the PPF surface indicates that it is very flat, with an rms roughness  $< 0.5 \text{ nm}$  and very few observable defects over areas larger than at least tens of micrometers. Although the flat surface implies some degree of plasticity during heat treatment, the photoresist does not flow during pyrolysis, and the lithographic pattern is preserved to a resolution below 1  $\mu\text{m}$ . The PPF surface structure as investigated with scanning probe microscopy is featureless down to a resolution of  $\sim 1 \text{ nm}$ ,<sup>99,195–197</sup> but its origin from a polymer implies that the surface consists of both basal and edge graphitic planes, much like GC. Finally, although PPF has a resistivity only slightly greater than GC, its usual presence as a thin film can create significant ohmic potential losses if the substrate supporting the PPF film is nonconducting.<sup>99,149</sup>

Although PPF is structurally and electronically similar to GC, it has several distinct properties of significant utility in electrochemical applications. The ability to photolithographically pattern PPF permits fabrication of microstructures such as interdigitated microelectrode arrays,<sup>186,198</sup> microcantilevers,<sup>193</sup> and even complex microstructures for batteries and micromechanical systems.<sup>199</sup> The extreme flatness of PPF is essential for applications in molecular electronics<sup>200–202</sup> and for investigations with scanning probe techniques such as AFM.<sup>195,196</sup> The PPF surface is amenable to surface modification by various routes, particularly diazonium reduction<sup>197</sup> and soft lithography,<sup>203</sup> as described in section 5.1. As noted already in Figure 11 and associated text, the surface O/C ratio of PPF is quite low, and many but not all of the surface carbons are likely to be H terminated. PPF may be formed on irregular shapes such as microelectrodes<sup>204</sup> and may also be made sufficiently thin to be optically transparent for spectroelectrochemistry.<sup>58,59,89</sup>

In terms of electrochemical reactivity for common redox systems, PPF is similar but not identical to GC. Polishing PPF would be counterproductive, so it is generally used right out of the pyrolysis oven or after solvent cleaning as described in section 3.6.1. As noted in Table 2, the  $k^\circ$  for  $\text{Ru}(\text{NH}_3)_6^{3+/2+}$  is somewhat slower than that on clean GC, with at least some of the difference due to the absence of microscopic roughness on PPF. The kinetics of  $\text{Fe}^{3+/2+}$  are much slower on PPF than on GC, due to the lack of surface oxides (Table 3). The lack of oxides and their associated surface dipoles makes PPF less prone to adsorption than GC, thus leading to slower electron transfer rates for organic systems that are catalyzed by adsorption, such as dopamine oxidation.<sup>99,126</sup> PPF may be electrochemically oxidized to increase electron transfer reactivity toward redox systems catalyzed by surface oxides.<sup>99</sup> To date, the majority of electrochemical applications of PPF have used relatively large areas, generally greater than a few micrometers. However, pyrolysis of polymer precursors can also be used to make the micromechanical structures noted earlier,<sup>193,199</sup> and block copolymer precursors can lead to carbon nanoparticles and arrays.<sup>205,206</sup>

Thin films of carbon formed in a vacuum have long been used for electron microscopy and to protect disk drive heads. Electron beam deposition of carbon for electrochemistry was first reported in the 1970s,<sup>56,87</sup> and reconsidered recently.<sup>88</sup> The initial objective was a carbon film sufficiently thin to be transparent for use with spectroelectrochemical techniques in transmission mode. A high-energy electron beam was focused onto graphite pellets in a  $\sim 10^{-6}$  Torr vacuum to generate carbon atoms and fragments, which then deposit onto a heated quartz plate. Carbon films 28 nm thick exhibited well-defined voltammograms for  $\text{Fe}(\text{CN})_6^{3-/4-}$ ; however the large peak separation of  $\sim 200 \text{ mV}$  at a scan rate of 0.01 V/s was attributed in part to significant ohmic potential error within the thin film.<sup>87</sup> The films had optical absorbances of 0.4–0.8 absorbance units in the range of 300–800 nm. The films were significantly less conductive when deposited onto a room temperature substrate. Electron beam deposition has become quite common for metals and refractory materials since these initial papers were published and is now readily available commercially. Blackstock et al. deposited carbon onto H-terminated heavily doped silicon at room temperature in order to reduce ohmic potential errors.<sup>88</sup> The carbon films were extremely flat, exhibiting an rms roughness of 0.07–0.11 nm for a 7 nm thick carbon

film on a Si substrate with a roughness of 0.06 nm. Electron transfer reactivity of carbon films formed at room temperature on silicon approached Nernstian behavior at moderate scan rates, with a  $k^\circ$  value for  $\text{Ru}(\text{NH}_3)_6^{3+/2+}$  of 0.046 cm/s (Table 2). Heat treatment in 5%  $\text{H}_2/\text{N}_2$  at 1000 °C increased the ordering of the carbon, as judged by Raman spectroscopy, and also produced changes in the voltammograms. The carbon film may be deposited through a shadow mask or a photoresist pattern, so small and complex electrodes with features down to  $\sim 1 \mu\text{m}$  may be microfabricated. Given that electron-beam deposition is expensive and cumbersome compared with many carbon electrode preparation techniques, it will likely be useful only when special properties such as a very flat surface are required.

A recent and more exotic method for carbon film formation is electron cyclotron resonance plasma sputtering.<sup>24,132,207</sup> The deposited carbon was also quite flat ( $\sim 0.07$  nm) and appeared to be amorphous, containing a significant fraction of  $\text{sp}^3$  hybridized carbon. The material had some of the properties of boron-doped diamond, particularly stability and resistance to electrode fouling. Voltammetry of several organic and biochemical redox systems was demonstrated, including nucleotides, phenols, and NADH.<sup>24,132</sup> The voltammetric detection limit reported for nonylphenol was 50 nM, with a linear range of 0.125–10  $\mu\text{M}$ .<sup>207</sup> Electron transfer rates for  $\text{Ru}(\text{NH}_3)_6^{3+/2+}$  and  $\text{Fe}(\text{CN})_6^{3-/4-}$  were comparable to those observed on GC and BDD but were significantly slower for dopamine and  $\text{Fe}^{3+/2+}$ , as shown in Tables 2 and 3. The authors concluded that the slow rates for dopamine and  $\text{Fe}^{3+/2+}$  were due to weak interactions with the carbon surface, compared with GC.<sup>24</sup>

## 4.2. Boron-Doped Diamond for Electrochemistry

The fabrication and electronic properties of BDD were discussed in section 2.1.2, and we now turn to its behavior as an electrode material. Many publications from at least five laboratories worldwide have described electrochemical applications of BDD,<sup>36,61,63,131,208–219</sup> and there are now several commercial suppliers of diamond electrodes for electrochemical use.<sup>34</sup> A comprehensive review of electrochemical applications of diamond and related materials appeared in 2004.<sup>30</sup> BDD electrodes have been made in a wide variety of shapes and sizes, including ultramicroelectrodes,<sup>215,220–222</sup> large single crystals,<sup>131,223</sup> nanocrystalline films,<sup>32,208,224,225</sup> and optically transparent electrodes.<sup>61–63</sup>

BDD and nanocrystalline diamond are not only structurally distinct from graphitic and fullerene electrode materials, but they also have some advantageous electrochemical properties.<sup>225</sup> The much greater chemical stability of BDD compared with graphitic or fullerene forms of carbon is a major advantage over the more common  $\text{sp}^2$  hybridized carbon electrode materials. In addition to providing a long lifetime, the low chemical reactivity results in a wider electrochemical potential window and the ability to carry out normally difficult reactions such as ozone generation<sup>217</sup> and the oxidation of aliphatic amines.<sup>226</sup> The significantly weaker adsorption of most solution species on BDD makes diamond electrodes more resistant to “fouling”, and they can be used after standing in ambient air for long periods without surface pretreatment. As already noted in section 2.3, diamond is sufficiently optically transparent in much of the UV–vis and infrared regions to permit spectroelectrochemistry in transmission or internal reflection modes.

Recent reports of microscopic characterization of conductivity and redox activity of both hydrogen-<sup>208</sup> and oxygen-terminated<sup>227</sup> BDD electrodes indicate that the materials are electrically heterogeneous, with both conductivity and electron transfer rates varying across the BDD surface. Conducting-tip AFM, scanning electrochemical microscopy, and cathodoluminescence permitted such heterogeneities to be observed near grain boundaries and across microcrystallite facets. Both papers noted that electron transfer reactivity for  $\text{Ru}(\text{NH}_3)_6^{3+/2+}$  was observed over the entire BDD surface but that variations in conductivity and doping level caused local variations in the electron transfer rate.<sup>208,227</sup> While such variations are usually averaged out for BDD electrodes larger than the crystallite size of a few micrometers, the user should be aware that the materials are not as electronically homogeneous as more commonly used carbon electrodes such as glassy carbon.

The electrochemical reactivity of diamond electrodes is best considered in the context of the various classes of redox systems described in section 3.5 and summarized in Figure 19. The simplest of these is the “outer-sphere” or “surface-insensitive” group, which includes  $\text{Ru}(\text{NH}_3)_6^{3+/2+}$  and  $\text{IrCl}_3^{3-/4-}$ . As shown in Figure 25B,C, these two couples show classical voltammetric waves on BDD, qualitatively similar to those observed on glassy carbon. The rate constant for  $\text{Ru}(\text{NH}_3)_6^{3+/2+}$  is somewhat slower on BDD than on GC, but higher  $k^\circ$  values have been reported on nanocrystalline, N-doped diamond (Table 2). As noted in sections 2.2 and 3.1, most diamond materials have a lower density of electronic states than graphitic carbon, and this factor may result in somewhat slower kinetics for outer-sphere systems. However, the observation that BDD exhibits reasonably fast kinetics for redox systems with  $E^\circ$  potentials spanning a wide range of the electrochemically useful scale (Figure 15) indicates that BDD does not have significant gaps in the DOS distribution.<sup>30</sup> The Swain group have reported many kinetic results for BDD under standard conditions and provide a concise comparison of several common organic and inorganic redox systems.<sup>30,53</sup>

A second class of redox systems noted in Figure 19 is “surface-sensitive” and is much more dependent on the state of the electrode surface. In the case of diamond electrodes, the surface may be affected not only by oxides and adsorbed impurities but also by nondiamond carbon, surface termination, and grain boundaries.<sup>30,53</sup> An illustrative example is shown in Figure 26 for ascorbic acid oxidation on microcrystalline BDD in 0.1 M  $\text{HClO}_4$ . Anodization of the BDD at progressively positive potentials causes a major positive shift in the observed oxidation peak potential, and the shift may be reversed by rehydrogenation of the BDD surface. Chloride oxidation to chlorine is an electrocatalytic reaction, which is very slow on BDD due to the lack of adsorption sites. The nitrogen-incorporated amorphous tetrahedral carbon variant of diamond contains such sites, and the oxidation of chloride in 2 M  $\text{HCl}$  proceeds at a potential approximately 0.5 V lower than that on BDD.<sup>35</sup> In addition, the taC:N material was very stable during  $\text{Cl}_2$  generation, despite the normally corrosive nature of chlorine evolution.

The electrochemistry of organic systems on diamond depends on the nature of surface interactions, particularly adsorption.<sup>30</sup> Methyl viologen voltammetry on BDD is quite similar to that on GC, since there is little or no adsorption or interaction with catalytic sites. However, dopamine oxidation is significantly slower on diamond than on GC, most likely because of weak adsorption.<sup>53</sup> As noted in section

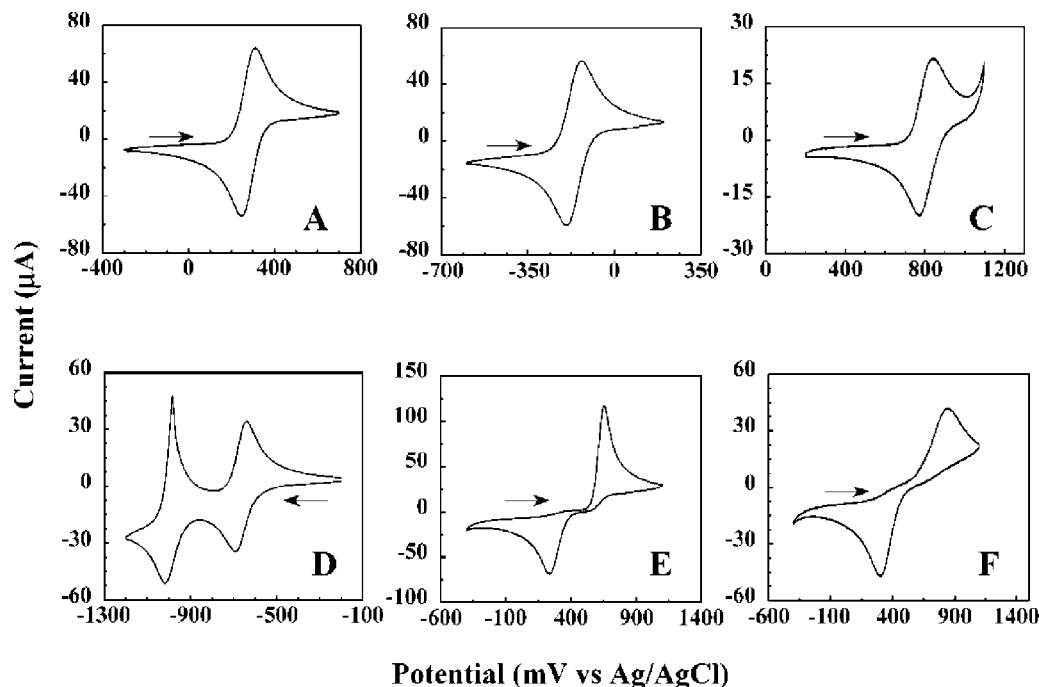


**Figure 25.** Voltammetry on boron-doped nanocrystalline diamond electrodes (0.2 cm<sup>2</sup> area, 0.1 V/s), for (A) 1.0 mM Fe(CN)<sub>6</sub><sup>3-/4-</sup>, (B) 1.0 mM Ru(NH<sub>3</sub>)<sub>6</sub><sup>3+/2+</sup>, (C) 0.25 mM IrCl<sub>6</sub><sup>2-/3-</sup>, (D) 0.50 mM methyl viologen in 1 M KCl, (E) 1.0 mM 4-*tert*-butylcatechol, and (F) 1.0 mM Fe<sup>3+/2+</sup> in 0.1 M HClO<sub>4</sub>. Reprinted with permission from ref 225. Copyright 2003 American Chemical Society.

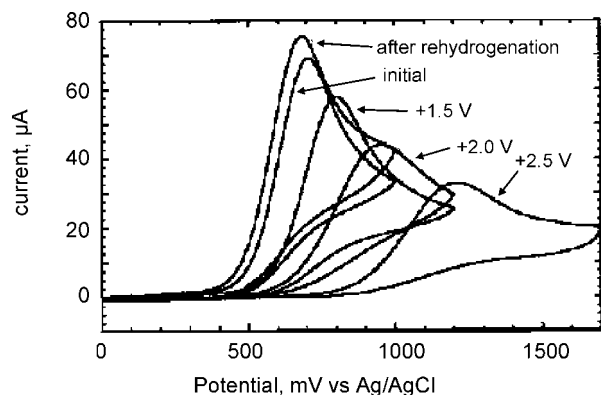


**Figure 26.** Effect of anodization on the voltammetry of ascorbic acid (1 mM in 0.1 M HClO<sub>4</sub>) on boron-doped microcrystalline diamond. BDD surface was oxidized at the indicated potentials for 5 min before each voltammogram. “Rehydrogenation” refers to exposure to a H-atom plasma. Reprinted with permission from ref 30. Copyright 2004 Marcel Dekker.

3.4, dopamine oxidation is catalyzed by hydrogen bonding of surface carbonyls to adsorbed dopamine molecules, and diamond does not provide the necessary sites in its H-terminated form. The reported observations on diamond electrodes reinforce the conclusions of section 3.5, that is, that electrode effects on redox kinetics are strongly dependent on the nature of the electron transfer mechanism. Although diamond surfaces are comparatively inactive toward adsorption and often lack catalytic sites, there have been several examples reported of complex organic and biochemical reactions on diamond materials, including cytochrome *c*,<sup>228</sup> DNA-modified diamond,<sup>224</sup> and glucose oxidation.<sup>33,213,215</sup> Additional reported analytical targets of diamond electrodes include arsenic,<sup>214,229,230</sup> dopamine and norepinephrine,<sup>219,222</sup> and polyamines.<sup>226</sup> Applications of diamond microelectrodes in biological media have been reviewed.<sup>221</sup>

In addition to the boron or nitrogen doping already discussed for diamond electrodes, several diamond compos-

ites have been studied, often to enhance the relatively weak electrocatalytic activity of diamond due to its lack of adsorption sites. Gold coating of BDD has been used for stripping voltammetry,<sup>229,230</sup> and Pt particles may be deposited on BDD to make dimensionally stable electrocatalytic surfaces.<sup>231</sup> Pt particles have also been incorporated into BDD to provide catalytic sites in a very stable conducting host.<sup>232,233</sup> Given the high stability of diamond as an electrode material, it seems likely that additional applications involving metal catalysts are likely. In addition, BDD may be chemically modified by several routes in common with sp<sup>2</sup> carbon materials, as discussed in section 5.

### 4.3. Fibers and Nanotubes

Carbon fibers have been used in electrochemistry since approximately the early 1980s, and their structures and properties relevant to electrochemical applications were reviewed in 1991.<sup>3</sup> There has been significant activity since that time due to the utility of carbon fibers for making ultramicroelectrodes and for in vivo voltammetry. Furthermore, the discovery of carbon nanotubes provided a completely new type of carbon “fiber” with distinct electrochemical properties. The discussion of carbon fibers will be divided into two sections, “conventional”, meaning nonfullerene carbon fibers, and fullerene nanotubes in their single- and multiwalled manifestations.

Although carbon fibers occur with radial, “onion”, and random orientations of the graphitic planes,<sup>3,14</sup> there does not appear to be standardization of a particular type for electrochemical applications. As with other graphitic materials, carbon fiber types differ significantly in their crystallite sizes, interplanar spacing, and disorder, but most laboratories have arrived at a useful carbon fiber source empirically. Generally, fibers used in electrochemistry are sufficiently disordered that they do not show unusual electronic properties, like HOPG or certain types of nanotubes. Fibers are encapsulated in a variety of materials, most commonly glass, often with epoxy, and then the carbon

surface is exposed by cutting the assembly.<sup>143,150</sup> The resulting carbon electrode exhibits one of the highest reported  $k^\circ$  values for  $\text{Ru}(\text{NH}_3)_6^{3+/2+}$  on carbon,<sup>150</sup> and represents a pristine surface analogous to that obtained by “fracturing” glassy carbon as discussed in section 3.6. A light polish of a glass encased carbon fiber has proven valuable for voltammetry in living organisms,<sup>143,234</sup> and various surface modifications have been investigated to improve analytical selectivity.<sup>12,147,235</sup> In some cases, a portion of the fiber walls might be exposed in addition to the fiber end to increase the electrochemically active area.<sup>11</sup> Carbon fibers and nanotubes may be “doped” with nitrogen or metals to promote electrocatalytic behavior.<sup>236–239</sup> Of particular interest is the long search for efficient electrocatalysts for oxygen reduction due to its importance to fuel cells and batteries. Incorporation of Fe, Pt, and nitrogen into carbon electrode materials provided catalytic sites for  $\text{O}_2$  reduction to both hydrogen peroxide and water.<sup>236,238,239</sup>

Several examples of thin films deposited on carbon fibers have been described, with the objective of insulating all but a small fraction of the fiber in order to decrease the active electrode area. An early example is the electropolymerization of a phenolic polymer with a thickness of  $\sim 100\text{--}300$  nm, after which a disk or elliptical electrode was exposed by cutting the fiber or by field emission.<sup>160,161,240,241</sup> A photocurable perfluoropolyether was used on both carbon and Pt fibers to make disk or conical microelectrodes, with a  $<10$   $\mu\text{m}$  thick insulating coating.<sup>242</sup> An important variation on electropolymerized films is deposition of “electrophoretic paint” based on poly(acrylic acid), followed by heat treatment to harden the coating.<sup>243–247</sup> The polymer coating shrinks slightly during heat treatment and retracts from the tip of the fiber to expose the end. Submicrometer electrode diameters were readily achieved with this approach, which was initially developed for metal electrodes.<sup>243,244</sup> A similar approach with an “inverted deposition” technique was used on  $5$   $\mu\text{m}$  diameter carbon fibers that had been electrochemically etched to generate sharp conical tips.<sup>245,246,248</sup> Figure 27 shows well-defined voltammograms for  $\text{Fe}(\text{CN})_6^{3-/4-}$  obtained with carbon fiber electrodes with apparent radii ranging from 160 to  $<1$  nm. These exceedingly small electrode radii were calculated from the limiting currents based on the assumption that the electrode acts as a microdisk, and that assumption appeared justified when supporting electrolyte was present.<sup>246</sup> However, unusual effects of both the double layer and electrode geometry have been reported for microelectrodes below  $\sim 20$  nm in diameter,<sup>244,249</sup> so the apparent electrode radii should be considered with caution. An alternative approach that permits exposure of selected regions of the carbon fiber employs photolithographic techniques to expose particular areas on a fiber that had been coated with an electrophoretic resist. After exposure of the coated fiber to light, the electrode was “developed” with standard procedures to yield reproducible active electrode areas.<sup>250</sup> “Nanogap” electrode structures consisting of two carbon fiber electrodes located  $\sim 20$  nm apart have been reported, starting with carbon fibers coated with electrophoretic “paint”.<sup>247</sup>

Many of the applications of carbon fiber electrodes have been biological, because of both their small size and their activity for a variety of biochemically important materials (neurotransmitters, nucleotides, etc.). As noted in section 5, carbon fibers are subject to chemical modification by several routes to enhance reactivity or selectivity, for example, Pt-deposition,<sup>248,251</sup> diazonium reduction,<sup>12</sup> and polypyrrole

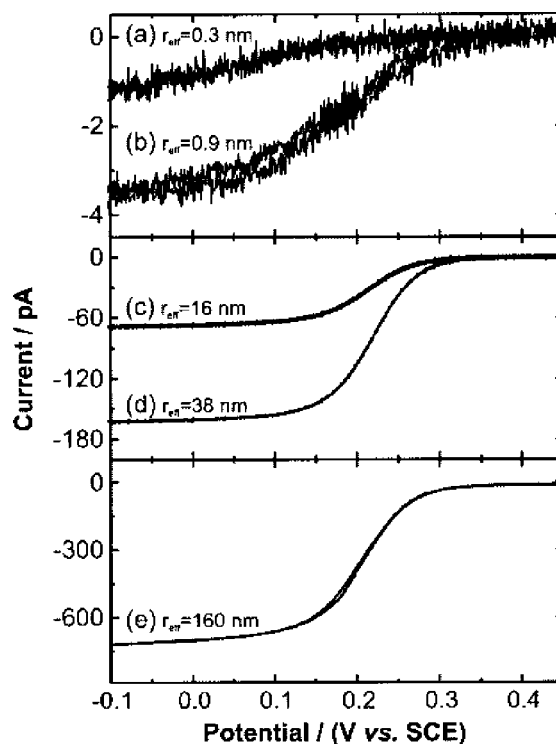


**Figure 27.** Steady-state cyclic voltammograms of reduction of 10 mM  $\text{Fe}(\text{CN})_6^{3-/4-}$  (0.5 M KCl, 10 mV/s) on carbon nanofiber electrodes. Indicated radius was calculated from the limiting current. Reprinted with permission from ref 246. Copyright 2002 American Chemical Society.

or Nafion coating.<sup>147,252,253</sup> Carbon fibers have been used to great advantage for *in vivo* monitoring of neurotransmitters in intact animals,<sup>11,13,147,254–257</sup> transmitter release and uptake by single cells,<sup>11,13,235,258–262</sup> and nucleotides.<sup>160,175,263</sup> An unusual application of carbon microelectrodes is the induction of cell–cell and cell–liposome fusion by an electric field applied at a carbon fiber.<sup>264</sup> In addition to bioanalytical applications, carbon fiber microelectrodes have been used for studying electrochemiluminescence, due to the high frequency response permitted by a low RC time constant, as well as the extended potential window compared with metal electrodes.<sup>265–267</sup>

Some generalizations about electrochemistry at “conventional” carbon fiber electrodes are available, and they are quite similar to those regarding bulk graphitic materials described in section 3.7. Most carbon fibers are sufficiently disordered that they do not display unusual electronic effects, as are observed with HOPG. The edge/basal ratio on the exposed surface determines adsorption and electrocatalytic activity, as is the case with glassy carbon and pyrolytic graphite. The potentially very small active area and total diameter of a carbon fiber electrode are of obvious importance for *in vivo* voltammetry and electron transfer kinetic measurements. Except for the case of carbon fibers embedded in a sturdy host such as glass or epoxy/glass, carbon fibers are not amenable to polishing, with the attendant risk of contamination or deactivation. Hence carbon fiber electrodes can be more active than bulk carbon materials in terms of electron transfer kinetics and electrocatalytic activity, if only because their freshly exposed surfaces have had less opportunity to adsorb impurities.

As discussed briefly in section 2.1.3, carbon nanotubes differ fundamentally from carbon fibers in their electronic properties and structures. A Scifinder search of the concept

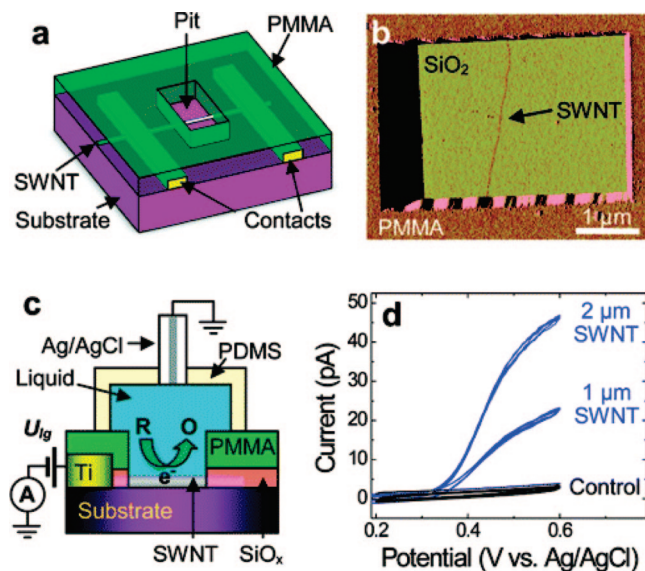


**Figure 28.** Apparatus (a–c) and response (d) for a metallic single-walled nanotube electrode in a solution of a ferrocene derivative in aqueous electrolyte. Reprinted with permission from ref 41. Copyright 2006 American Chemical Society.

“carbon nanotube electrochemistry” yielded more than 1700 citations, starting in 1999.<sup>268</sup> There is no question that nanotubes have unique conductivity and density of electronic states (Figure 2), and their small diameters and high ratio of length to diameter permit novel and unusual electrode structures. The electrochemical properties of nanotubes have been reviewed recently,<sup>37,39</sup> and those sources should be consulted for details and numerous references. In the context of alternative carbon electrode materials, several issues deserve special note. These include electronic properties, edge/basal ratio, oxide functional groups, and electrode kinetics. In addition to carbon nanotubes, “nanoscrolls” have been reported, which are formed by intercalation and fragmentation of graphite, followed by curling of the graphene fragment to form a “scroll”.<sup>269</sup>

Nanotube preparations are rarely monodisperse, and most contain a difficult to separate mixture of tubes with different lengths and diameters. Multiwalled carbon nanotubes (MWNTs) are generally considered to be metallic, with any gaps or significant variations in electronic DOS averaged out in the mixture. Roughly one-third of single-walled nanotubes (SWNTs) are metallic and the remainder semiconducting, with possibly complex DOS profiles such as that shown in Figure 2. While significant effects of the DOS of SWNTs on electron transfer properties are expected,<sup>41</sup> they have not yet been observed experimentally. An elegant study of ferrocene voltammetry at single SWNT electrodes demonstrated that steady-state diffusion to a SWNT was observable, with the expected linear dependence of current on tube length.<sup>40</sup> A metallic SWNT was suspended between two titanium contacts in a PMMA “cell”, which permitted exposure to electrolyte solution as shown in Figure 28.<sup>41</sup> A voltammogram for a 1.2 nm diameter, 2 μm long metallic SWNT is shown in Figure 29A, with a fit to Butler–Volmer kinetics, which yields a  $k^0$  for ferrocenylmethyl-trimethylammonium ion of 7.6 cm/s. The voltammograms for metallic and semiconducting SWNT electrodes were similar, perhaps because the ferrocene redox system is too fast to exhibit an observable dependence on electronic DOS. The authors point out that the very small nanotube diameter combined with its high aspect ratio permits fast mass transport to the

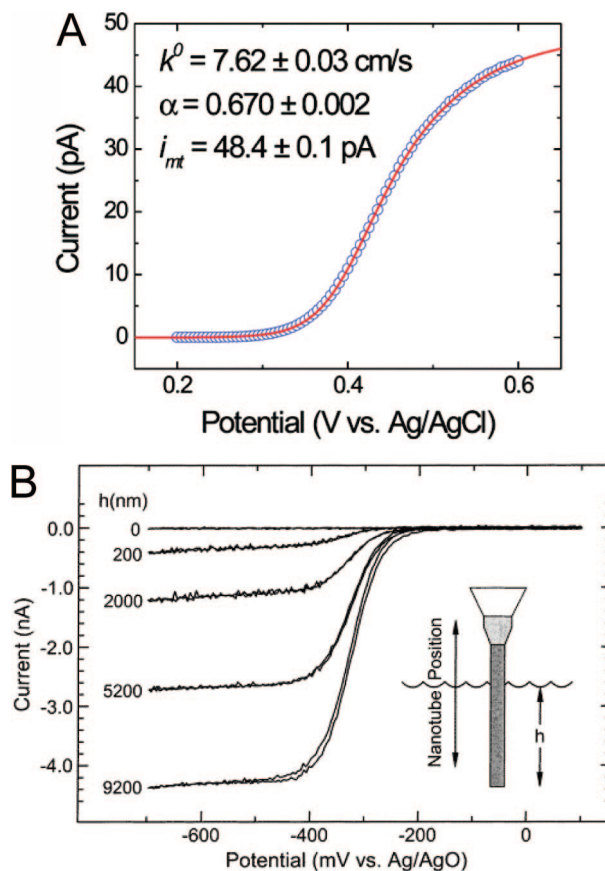


**Figure 29.** (A) Voltammogram from SWNT for ferrocene, with corresponding fit to Butler–Volmer kinetics<sup>41</sup> and (B) voltammograms at a  $\sim 100$  nm diameter MWNT electrode in 5 mM  $\text{Ru}(\text{NH}_3)_6^{3+/2+}$  in 0.1 M  $\text{K}_2\text{SO}_4$  as a function of the height ( $h$ ) of tube exposed to the solution.<sup>268</sup> Reprinted with permission from refs 41 and 268. Copyright 2006 and 1999 American Chemical Society.

electrode and correspondingly large accessible  $k^0$  values.<sup>41</sup> Although this experimental paradigm for studying electrochemistry at a SWNT is demanding, the nanotube provides a potentially valuable combination of geometry and tunable electronic properties for fundamental investigations of electron transfer kinetics.<sup>41</sup> Electrochemistry at a single, 150 nm MWNT was reported in 1999,<sup>268</sup> and a voltammogram of the reduction of  $\text{Ru}(\text{NH}_3)_6^{3+/2+}$  is shown in Figure 29B. The limiting currents were proportional to the immersion depth of the MWNT, as expected, and the mounted nanotube did not appear inordinately fragile. The MWNT could be insulated with electropolymerized phenol to yield an  $\sim 150$  nm diameter microdisk electrode after cutting.

The vast majority of investigations of electrochemistry at carbon nanotubes involve ensembles of many tubes, often in composites or as thin films. As already noted, such ensembles invariably contain a mixture of tubes of different diameters, and the collection of tubes is generally considered to be metallic in terms of electronic DOS. Most ensembles consist of randomly aligned and often tangled nanotubes, so the solution or matrix under study is presented with an average of “side” and “end” orientations. Nugent et al. reported apparently reversible electron transfer to  $\text{Fe}(\text{CN})_6^{3-/4-}$  at a bundle of MWNTs ranging in diameter from  $\sim 20$  nm to several micrometers, and the ensemble contained non-nanotube carbon residue from the tube preparation.<sup>270</sup> Alignment of nanotubes in ensembles is a difficult problem,<sup>37,39</sup> but various methods have been employed. An interesting example is a

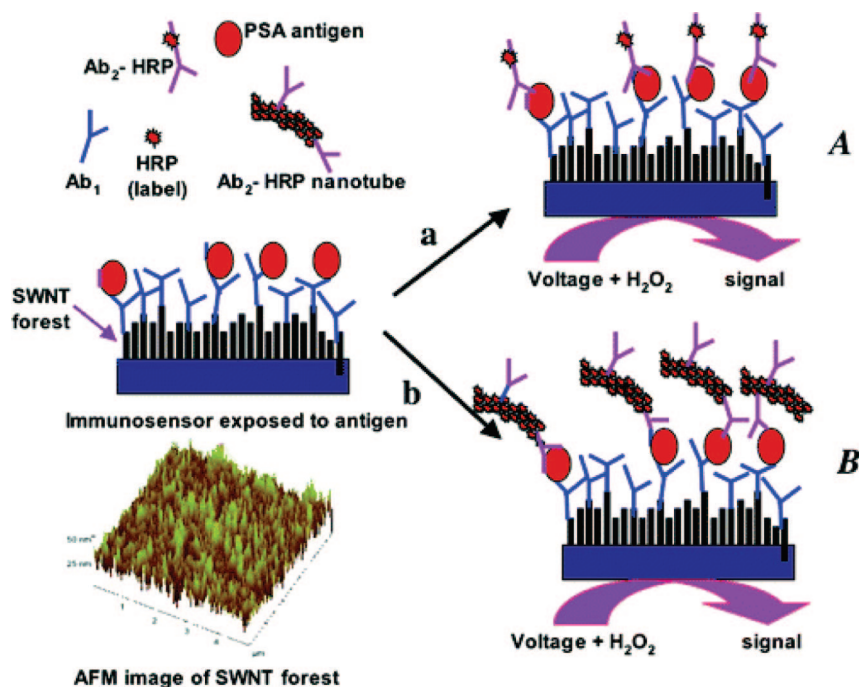


**Figure 30.** Construction of an antibody and horseradish peroxidase (HRP) on a “forest” of single-walled carbon nanotubes assembled onto an abraded pyrolytic graphite electrode. Reprinted with permission from ref 285. Copyright 2006 American Chemical Society.

two-dimensional network of nanotubes deposited on glass between two metallic contacts.<sup>271–273</sup> This arrangement permitted simultaneous monitoring of electron transfer reactivity and nanotube conductivity and also exhibited unusually high voltammetric sensitivity at the submicromolar level due to low capacitive background.<sup>273</sup>

SWNTs have been chemically “cut” with  $\text{H}_2\text{SO}_4/\text{HNO}_3$ , then modified to have thiol end groups so they could be assembled on a gold surface to make a nanotube array.<sup>274</sup> Electrochemical modification of nanotubes has been reported,<sup>100</sup> as has “site specific” binding of DNA and biotinylated biochemicals using photoresist techniques.<sup>275</sup> Arrays of nanotubes can also be “grown” on a microfabricated array of catalyst particles, then made into electrodes<sup>276</sup> or membranes<sup>277</sup> containing arrays of nanotubes suspended in either  $\text{SiO}_2$  or polystyrene. The capacitance and electron transfer kinetics for  $\text{Fe}(\text{CN})_6^{3-/4-}$  were studied on three types of SWNT and MWNT ensembles, and it was concluded that the solution could penetrate the ensemble to access a large surface area of nanotubes and non-nanotube carbon residue.<sup>278</sup> The electrochemistry of  $\text{Fe}(\text{CN})_6^{3-/4-}$  was investigated on carbon nanotubes modified with Au nanoparticles, and the response was used to determine the nanotube length.<sup>279</sup> Nitrogen-doped CNT electrodes have been shown to exhibit electrocatalytic activity toward oxygen reduction and also to efficiently oxidize catecholamines.<sup>236,237,280</sup> Arrays of nanotubes have been used for studying proteins,<sup>281</sup> DNA and nucleotides,<sup>282,283</sup> and redox enzymes,<sup>284</sup> with the latter example exploiting the ability of a nanotube to transport electrons a long distance from the electrode surface to the redox center of the enzyme. An elegant application of SWNTs to immunoassay involved formation of a “forest” of nanotubes oriented perpendicular to the basal plane surface of abraded pyrolytic graphite, as shown in Figure 30.<sup>285</sup> The antibody to prostate-specific antigen (PSA) and peroxidase retained their activity when immobilized on the top of the SWNT “forest”, providing greatly amplified response to PSA and a mass detection limit of 40 fg. Carbon fibers modified

with MWNTs exhibited unusual reactivity for ascorbate oxidation and were used for in vivo monitoring of ascorbate in rat brain.<sup>256</sup> SWNT films on GC modified with ferrocene as a redox mediator exhibited selective oxidation of dopamine over ascorbate and uric acid,<sup>286</sup> and MWNT/chitosan films on GC permitted direct oxidation of insulin.<sup>287</sup> Many electrochemical studies using nanotubes involve composites with other materials, and examples are provided in section 4.4 and Table 4.

In addition to morphology and electronic properties, the defects and oxides on carbon nanotubes have important effects on electrochemical behavior. Defects can occur in the nominally “basal plane” surface of the nanotube walls, and most preparations result in unterminated tube ends, which are prone to form oxygen-containing functional groups. It has been somewhat controversial whether the behavior of nanotube electrodes is determined by special properties of the tubes themselves or by a variable level of oxides or edge defects. For example, there are reports of high electrocatalytic activity of carbon nanotubes toward the oxidation of catecholamines,<sup>286,288,289</sup> NADH,<sup>102,290,291</sup> hydrazine,<sup>292,293</sup> and ascorbic acid,<sup>256,293–295</sup> yet at least some of these effects have been attributed to the graphitic edge plane exposed at the nanotube ends.<sup>177,178,296,297</sup> Furthermore, nanotubes are made with Fe, Ni, or Co catalysts, which are often not completely removed in the final product. As shown in Figure 31A, the electrocatalytic oxidation of hydrazine was absent when nanotubes were prepared with very low levels of trace metals, and it was concluded that hydrazine oxidation was catalyzed by metals and not nanotubes.<sup>292</sup> Also shown in Figure 31C is the effect of adding MWNTs to a HOPG basal plane surface on the voltammetry of  $\text{Fe}(\text{CN})_6^{3-/4-}$ . The apparently fast kinetics were attributed to a high fraction of edge sides on the nanotubes, and the sharp voltammetric peaks were ascribed to a thin layer effect in the porous ensemble.<sup>292</sup> The electrochemical behavior of nanotubes has also been correlated with the presence of residual iron oxides and their electrocatalytic activity.<sup>298</sup>

**Table 4. Examples of Carbon Composite Electrodes**

carbon type	host <sup>a</sup>	additive <sup>b</sup>	target analyte	reference
graphite	paraffin	enzyme, NADH	L-phenylalanine	410
graphite	mineral oil	1,2-dibromocyclohexane	vitamin B <sub>12</sub>	328
graphite	mineral oil	glucose oxidase	glucose	311
graphite	mineral oil	laccase, p-hydroxybenzoate hydroxylase	NADPH	127
graphite	nujol	chitosan, ssDNA	hepatitis B virus	314
graphite	nujol	chitosan, peroxidase	rutin	313
graphite	paraffin	chitosan, sepiolite clay	aqueous ions	312
graphite	paraffin	Zr phosphate, nitro-fluorenone	NADH	411
graphite	ionic liquid		NADH, dopamine	315
graphite	ionic liquid		dopamine, ascorbate, uric acid	317
graphite	ionic liquid	CaCO <sub>3</sub> , Nafion	hemoglobin	318
graphite	mineral oil	magnetic nanoparticles, laccase	hydroquinone	322
graphite	nujol, silicone oil	Pt nanoparticles	Cu <sup>II</sup>	319
MWNT	nujol	Nafion, thionine	dopamine, ascorbate	288
MWNT	mineral oil	ionic liquid	Fe(CN) <sub>6</sub> <sup>3-/4-</sup> , Ru(NH <sub>3</sub> ) <sub>6</sub> <sup>3+/2+</sup> , hydroquinone	316
MWNT	mineral oil	microbes, Os polymer	glucose	412, 413
MWNT	mineral oil		NADH, AA, dopamine, H <sub>2</sub> O <sub>2</sub>	294
MWNT	mineral oil	Cu particles	amino acids	325
MWNT	poly(vinyl ferrocene)		glucose	326
SWNT	mineral oil		Fe(CN) <sub>6</sub> <sup>3-/4-</sup> , ferrocene, Ru(NH <sub>3</sub> ) <sub>6</sub> <sup>3+/2+</sup>	324
SWNT	redox polymer	glucose oxidase	glucose	414
SWNT	mineral oil		nucleic acids	323
GC, MWNT		chitosan	insulin	287
GC	redox hydrogel	glucose oxidase	glucose	128

<sup>a</sup> Pasting liquid, generally inert. <sup>b</sup> Catalysts, active agents, etc.

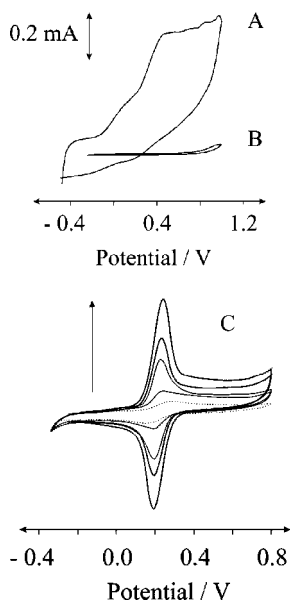


**Figure 31.** Voltammetry of hydrazine at MWNT preparations that contained metallic impurities (A) and were purified to remove metals (B). The arrow in panel C indicates the addition of increasing amounts of MWNTs to a solution of Fe(CN)<sub>6</sub><sup>3-/4-</sup>. The dotted line is the initial response from a HOPG electrode. Reprinted with permission from ref 292. Copyright 2007 American Chemical Society.

While there is little doubt that defects can play a major role in the electrochemical behavior of nanotube electrodes, there is also evidence for intrinsic nanotube reactivity in the absence of defects. Silver and palladium may be electrodeposited onto nanotubes from solution, and the resulting metal particles are randomly and nearly continuously distributed along the length of a given nanotube.<sup>299</sup> If deposition occurred only at defects, then an even distribution of metal particles would not be expected. By analogy to the basal plane of HOPG, as discussed in section 3, it is possible that the “basal plane” walls of carbon nanotubes have reduced reactivity compared with a disordered surface like GC and are relatively inactive toward adsorption. But as already

discussed, the reactivity differences between nanotubes and other carbon electrodes are likely to depend strongly on the redox system involved.

To summarize the preceding overview of carbon nanotube electrode behavior, it is clear that nanotubes have some distinct electrochemical properties, but they also introduce some additional variables, such as tube diameter and morphology, and often unknown levels of defects and surface oxides. In the context of the general discussion of section 3, some generalizations about nanotube electrodes are worthwhile. First, most nanotube electrodes studied to date consist of metallic tubes, although some interesting electronic effects occur in the few cases where the tubes are semiconducting. Second, nanotubes have a high aspect ratio compared with carbon particles, such that there is potentially both a high ratio of basal sites to edge sites and a long conduction path along the tube. However, some nanotube morphologies have much higher defect density than others, such as the “bamboo” nanotube compared with the SWNT. Since edge sites can be much more electrochemically active than basal sites, the observed reactivity of a single nanotube or a nanotube ensemble depends strongly on the defect density. The defect density and edge/basal ratio may be modified by “doping” with nitrogen, with observable electrochemical effects.<sup>280</sup> Third, nanotubes can be hydrophobic along their walls, particularly if low in defect density, and this can affect interactions with solvent or redox agents.<sup>300,301</sup> Fourth, the fact that nanotubes and their ensembles are not amenable to polishing has the indirect benefit of reducing surface contamination. It is possible that the long path for conductivity coupled with a significant coverage of edge plane defects is at least partially responsible for the reported high electrochemical reactivity of nanotubes. Fifth, nanotube preparations differ significantly in the synthetic route involved, and many include metal catalysts, non-nanotube carbon, or both, which are not completely removed in the finished product. Depending on the mechanism of a given redox reaction, the origin and purity of the nanotubes may be critical to the observed electrochemical response. Finally,

the relationship between nanotube structure, including morphology and defects, to electrochemical reactivity remains an important research goal, and there will likely be significant new insights into this area as nanotube electrode preparations are refined.

#### 4.4. Carbon Composite Electrodes

Composites of graphitic carbon with a wide variety of both active and inactive materials are very common and are generally referred to as "carbon paste". The original carbon paste electrode was introduced in 1958 by Ralph N. Adams<sup>302</sup> and represents one of the earliest applications of carbon electrodes in the modern era. A Scifinder search yielded over 3600 articles containing the concept "carbon paste electrode" and over 100 containing "nanotube paste electrode". Electrochemical applications of carbon paste electrodes have been reviewed<sup>303,304</sup> and cover a wide range of objectives in electroanalysis, pharmaceuticals, biological redox processes, and mechanistic electrochemistry. Rather than attempting a comprehensive review of the many carbon composite electrode materials, we will consider here the properties that make composites popular for electrochemistry and summarize several of the more recent variants.

The now classical carbon paste electrode is made from polycrystalline graphite powder and a water-immiscible insulating organic liquid such as Nujol or hexadecane. Alternatives to organic hydrocarbons include epoxy, Nafion, and conducting polymers.<sup>305–310</sup> The volume fraction of graphite is high enough (typically >50%) that the graphite particles are in contact to provide a conducting pathway and sufficiently low bulk resistivity. Considering carbon composites generally, their attractiveness for electrochemistry stems from both fundamental and practical advantages over conventional solid carbon electrodes such as glassy carbon. First, the paste is readily renewed without extensive polishing, so adsorbates or electrochemical products are easily removed between runs. Second, the graphite powder has randomly exposed edge and basal plane and is usually quite electrochemically reactive. Third, the fractional area of carbon exposed to the solution is generally much smaller than the geometric area of the electrode, with the remainder occupied by the insulating "host". Since the electrode capacitance is determined nearly exclusively by the exposed graphite, the background current resulting from this capacitance is much lower than expected for a given electrode area, typically by an order of magnitude or more. Fourth, radial diffusion to the closely spaced carbon particles provides efficient mass transport of electroactive species, and the current response is based on the *geometric* area rather than the exposed graphite particle area. As a result, the observed faradaic current is proportional to the total area of the electrode, while the capacitive background (or any redox reactions of the graphite surface) is proportional to the exposed area of a few percent of the total area. The ratio of faradaic to background current is therefore much higher for a carbon composite electrode than for a solid graphite electrode of the same geometric area. Fifth, carbon paste retains the wide potential window of carbon materials compared with metals, a point of particular value in early applications to organic oxidations. Finally, a paste composition permits addition of a variety of reagents to the host material, including electrocatalysts, enzymes, and chemical recognition agents. Many of the more recent carbon composites exploit this last point in order to incorporate unusual

selectivity or reactivity to the carbon composite electrode. A recent example of the merits of carbon paste is the observation that a carbon/mineral oil/enzyme composite remains active even in acidic solution, while a similar composite made with polyphenylene diamine instead of mineral oil was rapidly deactivated by acid.<sup>311</sup>

While carbon composites have the advantages of low background current and usually facile surface renewal, these positive points come with some costs. The host material may interfere with redox reactions and adsorption on the carbon particles, and carbon paste is generally less active for electrocatalytic reactions than glassy carbon. Not only can the host coat the graphite surface, the graphite area exposed to the solution is intentionally a small fraction of the geometric area, further decreasing the electrocatalytic current. The composite may not be stable in certain solvents, and there is a practical lower limit on the size of a composite electrode, significantly larger than most carbon fibers and much larger than nanotube electrodes.

Variations on carbon composite electrodes continue to be reported at a steady rate, with a noncomprehensive survey of examples appearing in Table 4. Composites of both powdered graphite and carbon nanotubes remain common, with a variety of hosts and additives. Chitosan is a poly-D-glucosamine derived from crustaceans and used in a variety of biomedical applications. Chitosan is polycationic at pH 7 and interacts with a variety of anionic peptides and hence is claimed to be beneficial for biosensors and immobilizing proteins in a composite electrode.<sup>312–314</sup> Ionic liquids such as *N*-butylpyridinium hexafluorophosphate have been incorporated into carbon composites,<sup>315–318</sup> as have catalytic<sup>318–321</sup> and magnetic<sup>322</sup> nanoparticles. Room-temperature ionic liquids were developed relatively recently, and carbon paste electrodes containing them have been shown to have some benefits. Figure 32 shows a comparison of a conventional graphite paste electrode with a graphite/ionic liquid paste for the voltammetry of dopamine, ascorbic acid, and uric acid.<sup>317</sup> There are clear differences in the apparent electrode kinetics and adsorption, which in this case permitted better resolution of the three redox systems. Composites containing single- and multiwall carbon nanotubes have been investigated with hydrocarbon,<sup>294,323–325</sup> ionic liquid,<sup>316</sup> and polymer<sup>326</sup> binders, and some interesting electrochemical behavior has been reported. Nanotube composites are apparently quite reactive compared with graphite composites for diverse redox analytes such as guanine, dopamine, hydroquinone, and ferricyanide.<sup>37,316,323,324,326–328</sup> As noted earlier, nanotube results should be viewed with some caution, due to variations in the level of edge sites and the possibility of trace metal contamination.<sup>102,178,292</sup> Electrical conductivity along the possibly long length of the nanotubes is an important difference compared with graphite powder and has been used to "wire" redox enzymes.<sup>281</sup> Nanotube composites also appear to have a large active area accessible to the solution, leading to both higher reactivity and also higher capacitance compared with conventional graphite compos-<sup>327</sup>

The huge commercial value of glucose sensors has driven development of "screen printed" and "ink jet printed" graphite electrodes, which in many cases are composites containing enzymes or other catalysts. A suspension of graphite powder in a volatile carrier is used to print patterns on an insulating surface, often in the form of a circular electrode and a carbon stripe as the electrode lead. Various

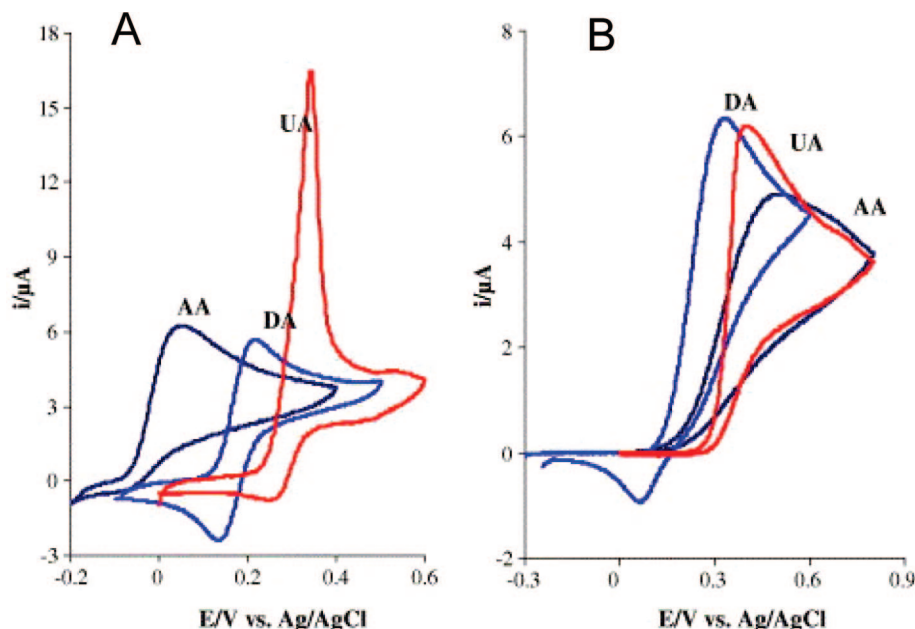


**Figure 32.** Cyclic voltammograms (PBS, pH 6.8, 50 mV/s scan rate) of dopamine (DA, 1.25 mM), ascorbic acid (AA, 1.25 mM), and uric acid (UA, 1.25 mM) at a composite carbon/ionic liquid (A) and conventional carbon paste (B) electrode. Reprinted with permission from ref 317. Copyright 2006 Elsevier Ltd.

reagents may be added to the printing solution, or printed separately on top of the carbon surface.<sup>129</sup> In commercial devices, a reference and possibly an auxiliary electrode might be printed in the same production line, resulting in automated manufacture of an electrode assembly ready for use with a drop of solution, blood, etc. Since printed electrodes may be mass produced, they are often disposable and inexpensive. Published applications of printed carbon composite electrodes include substrates for electrochemiluminescence,<sup>329,330</sup> monitoring tyrosine phosphorylation,<sup>331</sup> food analysis,<sup>332</sup> and immunoassay<sup>333</sup> and as sensors for ethanol,<sup>334</sup> nucleic acids,<sup>335</sup> and insulin.<sup>336</sup> It is not clear whether printed carbon electrodes differ from polycrystalline graphite in terms of the fundamental surface parameters affecting electron transfer, adsorption, and catalysis, but they have enormous practical value and are likely to dominate the commercial applications of carbon electrodes for electroanalysis.

## 5. Carbon Surface Modification

As already discussed in some detail, the structure and chemistry of a carbon electrode surface is vitally important to electrochemical applications, particularly those involving electrocatalysis or selectivity. Polishing, electrochemical pretreatments, and activation procedures discussed in section 3.6 could certainly be considered surface modifications, but the current section will deal with chemical reactions that lead to covalent bonds (usually) between the carbon surface and a chemical agent. Early modification procedures for carbon surfaces included adsorption of polyaromatic hydrocarbons,<sup>337,338</sup> bonding to surface carboxylate groups to form amide bonds,<sup>168,339</sup> and reactions of acid chloride reagents with surface hydroxyl groups.<sup>107</sup> Raman spectroscopy confirmed the reaction of surface carbonyl groups with dinitrophenylhydrazine to form a resonance Raman active adduct<sup>106,107</sup> and showed that the DNPH adduct was a planar molecule, oriented parallel to the graphite planes in HOPG.<sup>340,341</sup> A recent example of modification by physisorption involved the adsorption of pyrene modified DNA on the basal plane of HOPG.<sup>342</sup> Although these modifications often result in

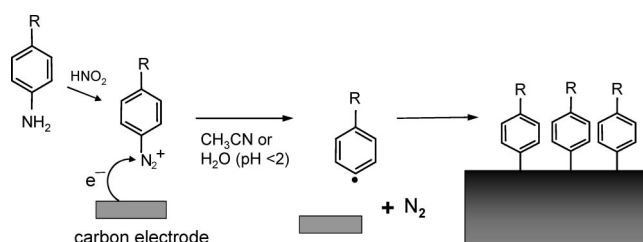


**Figure 33.** Modification of carbon surfaces by reduction of aryl diazonium reagents made by the reaction of an aromatic amine with nitrous acid. For details, see refs 197 and 346.

strong surface/adsorbate bonds, they are generally low in surface coverage (<10%) and often unstable toward acidic or basic media. Starting in the early 1990s, significant new approaches to surface modification were reported by several laboratories, based on radical and photochemical reactions with mainly sp<sup>2</sup> hybridized carbon surfaces. The most commonly used reaction was electrochemical reduction of phenyl diazonium reagents to produce a phenyl radical, which then formed a covalent bond with the carbon surface.<sup>343</sup> Oxidation of primary amines to a radical, which then bonded to the carbon, was reported in 1990.<sup>344,345</sup> As will be described below, these reactions and more recent related processes can lead to high coverage and very stable surface modifications, which have significantly broadened the utility of carbon electrodes.

### 5.1. Diazonium Ion Reduction

The electrochemical reduction of phenyl diazonium ions at a carbon electrode to form a covalently modified surface was first reported by Delamar et al. in 1992<sup>343</sup> and was recently reviewed.<sup>346</sup> The process is shown schematically in Figure 33 for the case of a generic aromatic amine. The reaction of a wide range of phenyl amines with NaNO<sub>2</sub> at low temperature leads to phenyl diazonium reagents, usually isolated as a tetrafluoroborate salt. Such reagents are stable for months at low temperature, and several examples can be purchased commercially. Electrochemical reduction by one

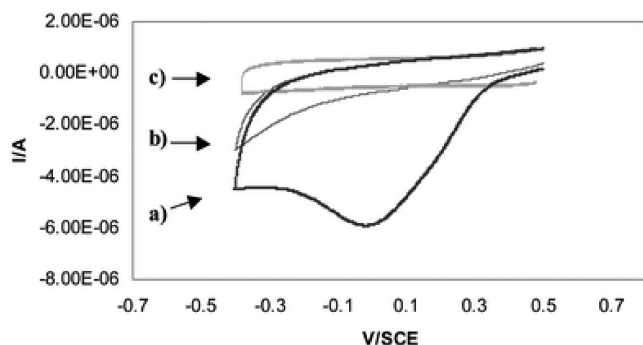


**Figure 34.** Voltammetric reduction of the diazonium ion  ${}^+\text{N}_2\text{C}_6\text{H}_4\text{NO}_2$  in 0.1 M TBABF<sub>4</sub> in acetonitrile on a GC electrode. Curves a, b, and c are the first, second, and third scans, respectively. From ref 346 (Copyright 2005). Reproduced by permission of The Royal Society of Chemistry.

electron on carbon electrodes forms a phenyl radical and  $\text{N}_2$ ; then the phenyl radical reacts with the carbon surface by coupling to an unsatisfied valence or adding to a double bond. It is likely that a short-lived neutral phenyl- $\text{N}_2$  species exists as an intermediate, but it rapidly and irreversibly dissociates to the much more stable  $\text{N}_2$  and phenyl radical.<sup>347</sup> The fact that the reduction of aryl diazonium ions is chemically strongly irreversible provides additional driving force for radical formation, such that surface modification can occur even without an applied potential.<sup>348,349</sup> As shown for the case of nitrophenyl diazonium ion in Figure 34, the voltammetry of a phenyl diazonium reagent typically exhibits a broad, chemically irreversible reduction peak in the region of 0 V vs SCE, with the peak potential depending on the substituents on the phenyl ring.<sup>346</sup> The low reduction potential of the diazonium ion has been attributed to the strong electron-withdrawing effect of the  $\text{N}_2^+$  group, with electron-withdrawing R-groups shifting the peak even more positive. The second and subsequent voltammetric scans generally have much smaller peak currents, because the electrode is by then covered with an organic layer, which partially inhibits further reduction. The current efficiency for surface attachment, that is, the fraction of electrogenerated phenyl radicals that bond to the surface, is generally less than 100%, with values of 56% reported for a HOPG surface and 84% for GC.

Diazonium ion reduction has several features that make it attractive for surface modification. Since the reactive radical is made electrochemically, it is generated precisely where it is most likely to react with the electrode surface. Second, uncovered regions of the electrode surface are more likely to reduce diazonium ions than modified regions, since the electron does not have to traverse an organic layer by tunneling or hopping. Thus film formation is “self-patching” with the result being relatively even surface coverage.<sup>197</sup> The C–C bond that is formed between the phenyl radical and the carbon surface is strong and is stable to at least 500 °C in vacuum.<sup>347,350</sup> The phenyl–phenyl coupling that results from diazonium modification of  $\text{sp}^2$  carbon surfaces is symmetric and should exhibit relatively strong electronic coupling between the carbon surface and the modification layer.<sup>140,200,202</sup> In some cases, surface modification of carbon materials is spontaneous,<sup>348,349,351,352</sup> although generally yielding lower surface coverage than the electrochemical route. In addition to chemical modification of  $\text{sp}^2$  carbon surfaces, diazonium reduction has also been used successfully on boron-doped diamond,<sup>68</sup> carbon nanotubes,<sup>353–355</sup> silicon,<sup>349,356</sup> GaAs,<sup>349</sup> coinage metals,<sup>357–361</sup> stainless steel,<sup>362</sup> and

iron.<sup>358,359</sup> Diazonium reactions with metals vary significantly from those with carbon, and only the latter case will be discussed here in any detail.

Molecular layers formed on graphitic and diamond surfaces by diazonium reduction have been characterized by a variety of techniques, including Raman spectroscopy,<sup>68,76,341,348,363–365</sup> FTIR spectroscopy,<sup>366,367</sup> secondary ion mass spectrometry,<sup>368</sup> XPS,<sup>68,200,347,363,369</sup> ellipsometry,<sup>349,370</sup> and scanning probe techniques.<sup>189,195–197,371</sup> A common electrochemical probe of the modification layer is the reduction of a redox active substituent, notably the surface nitro group resulting from reduction of nitrophenyl diazonium ion.<sup>363,372,373</sup> Several of these methods have been used to determine surface coverage, with often significant variation in the apparent degree of phenyl modification and the occurrence of pinholes. The predicted coverage for a close-packed monolayer is  $\sim 12 \times 10^{-10}$  mol/cm<sup>2</sup>, based on the geometric size of a phenyl ring and minimal spacing between molecules on a flat surface.<sup>363</sup> Quantitative estimates of coverage are generally lower than this value, in the region of  $4 \times 10^{-10}$  mol/cm<sup>2</sup>, and the discrepancy has been the subject of significant discussion.<sup>189,372–374</sup>

The variations in apparent coverage turned out to be an early indication of the complexity of organic films formed by diazonium reduction. Several years after the introduction of the reaction, it became apparent that multilayers were possible due to the aggressive reactions of electrogenerated radicals.<sup>366</sup> Since all diazonium reagents used for carbon surface modification to date are aromatic, electron tunneling through a monolayer is fairly efficient, thus permitting the generation of a second equivalent of radicals.<sup>140,197</sup> Alternatively, a radical generated at an unmodified carbon surface can attack an adjacent surface-bound molecule instead of the carbon surface itself. A proposed mechanism for multilayer formation is shown in Figure 35, and both SIMS<sup>368</sup> and FTIR<sup>366</sup> evidence have been presented in support of this or similar reactions. Note that the film resulting from the mechanism shown remains conjugated, although alternative mechanisms can result in termination of the chain reaction. Multilayer films as thick as 20 nm have been observed,<sup>366</sup> implying that the multilayer film has significant electronic conductivity.<sup>140,197</sup> Experience with a wide variety of diazonium reagents and carbon surfaces indicates that the tendency to form multilayers and the thickness of the modification layer depend on the nature of the surface, the particular diazonium reagent employed, and the deposition conditions, including scan rate and potential range, diazonium ion concentration, and number of deposition scans.<sup>189,197,372</sup>

The propensity for diazonium-generated radicals to form multilayers can be appreciated by considering the kinetics of the surface reaction. Newly electrogenerated phenyl radicals can react with the carbon surface or with each other, depending on concentration and relative reaction rates. If radical bonding to the surface is fast relative to attack of molecules already bonded to the surface, then a monolayer will form, possibly completely, before a second layer of molecules begins to form. In contrast, if the rate of radical attack on surface molecules is faster than bonding to the carbon surface, “mushrooms” will form rather than “wheat fields”. On HOPG, for example, diazonium reduction resulted in nucleation of bonded molecules at edge plane defects and tall clusters of molecules were observed along edge sites by AFM.<sup>371</sup> Theoretical calculations predict that phenyl bonding is much stronger at graphitic edge planes than on pristine

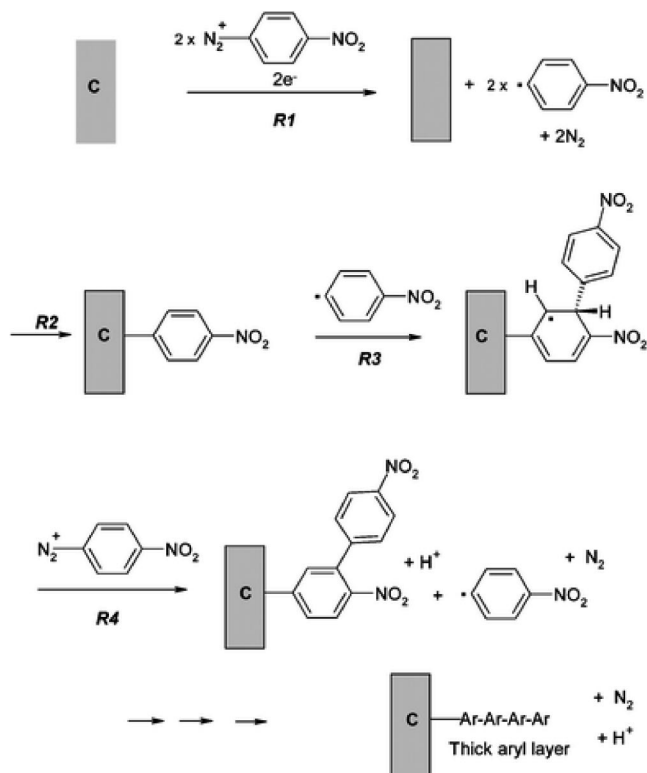


**Figure 35.** Proposed mechanism for the formation of multilayers during diazonium reduction at carbon electrode surfaces. From ref 346 (Copyright 2005). Reproduced by permission of The Royal Society of Chemistry.

basal plane.<sup>375</sup> Spatially resolved Raman spectroscopy of nitroazobenzene-modified HOPG revealed a much higher coverage of NAB molecules at defects on HOPG than on apparently defect-free basal plane.<sup>76</sup> Glassy carbon and PPF have a much higher density of edge plane than HOPG and therefore many more sites for radical bonding. Figure 36 shows a progression of AFM images acquired from modified PPF with scans to increasingly negative potentials in a solution of biphenyl 4-diazonium reagent.<sup>197</sup>

For scans from +0.4 to 0 or -0.2 V, coverage is incomplete and the variation in film thickness is large (~40%). The scan to -0.4 V shows even coverage and low roughness, while a scan to -0.6 V exhibits high points, which indicate beginning of formation of a second layer of biphenyl molecules. The squares apparent in Figure 36 are intentional “scratches” cut into the modification layer using contact mode AFM with a force gentle enough to avoid damaging the carbon surface. The depth of this scratch was determined statistically with several line profiles to provide a direct determination of film thickness. The conditions of the diazonium reduction were tuned for each molecule to produce monolayers, although the AFM thicknesses were systematically about 0.2 nm larger than that predicted for a perpendicular monolayer.<sup>197</sup> An FTIR investigation of molecular layers formed with the same procedure revealed an average tilt angle of ~35° relative to the surface normal.<sup>367</sup> Additional evidence for complete coverage of GC and PPF surfaces by monolayers resulting from diazonium reduction is the complete absence of electrochemical reactivity for the oxidation of catechols, which rely on adsorption to the carbon surface for electrocatalysis<sup>126,140</sup> (Figure 17A) and the ability to vapor deposit metals on top of molecular layers without contact between the metal and the carbon substrate.<sup>200,376</sup>

Although careful control of deposition conditions can result in monolayers from diazonium reduction, monolayers are by no means assured. If the reaction between the radical and the surface is slow, then molecule–molecule coupling reactions make multilayers possible and even likely. In order to form the 5–20 nm thick films reported for such multilayers, it must be possible for solvent and diazonium reagents to enter the film<sup>189,203,366,374</sup> or for the film to become electronically conductive.<sup>140,197,377</sup> Solvent has been observed in multilayer films, as have swelling and shrinking with changes in environment.<sup>189</sup> Unlike Au/thiol self-assembled monolayers, diazonium reduction is not inherently self-limiting, due to the possibility of further radical formation after deposition of initial monolayer. Fortunately, it is possible to control film thickness with suitable deposition conditions, but good practice dictates an independent verification of film thickness, for example, by AFM or ellipsometry.

The high coverage and strong surface bond resulting from diazonium modification of carbon surfaces has proven useful for a variety of applications. The surface modification may be patterned at the microscale using “soft” lithography with polydimethylsiloxane molds<sup>203</sup> or at the nanoscale using scanning probe lithography.<sup>196</sup> High coverage of the modification layer can completely inhibit electron transfer for reactions requiring adsorption to the carbon surface, such as catechol oxidation<sup>126,140</sup> or can significantly modify the mechanism of electrocatalytic reactions such as dioxygen reduction.<sup>130</sup> Modified electrodes can exhibit “conductance switching”, in which the observed electron transfer rate can be increased dramatically by a redox process within the modification layer.<sup>140</sup> For example, the  $k^{\circ}$  observed for ferrocene on a GC electrode modified by reduction of biphenyl diazonium ion increased by a factor of 45 when the biphenyl layer was electrochemically reduced to a more conducting quinoid form. Carbon fiber electrodes modified with phenyl sulfonate groups by diazonium reduction show increased selectivity and sensitivity for catecholamine neurotransmitters during *in vivo* voltammetry,<sup>12</sup> while modification of GC with anthraquinone groups leads to enhanced electrocatalytic oxidation of dopamine,<sup>126</sup> as already noted above.

Dioxygen reduction at GC and carbon nanotube electrodes may be catalyzed significantly by bonding quinone species to the electrode surface using diazonium reduction.<sup>173,378–380</sup> Large biological molecules such as horseradish peroxidase may be immobilized on carbon electrodes after first reacting the protein with a phenyl diazonium reagent containing a *para* carboxylic acid group.<sup>381</sup> The utility of diazonium ion bonding to carbon surfaces may be broadened to a wider range of reagents by a two-step modification in which a “primer” is first attached to the surface by diazonium reduction and then a second reagent is attached to the primer, usually in a second step. Examples include attachment of epichlorohydrin to surface-bound aminophenyl groups<sup>347</sup> and nucleophilic substitution of surface benzyl chloride.<sup>382</sup>

The strong surface bond resulting from diazonium reduction on carbon is particularly important for making “molecular junctions” consisting of a layer of molecules oriented between two conductors.<sup>200,383</sup> A significant difficulty with making such junctions has been the deposition of a metal “top contact” on a modified electrode surface without the metal penetrating to the substrate and creating short circuits. Au/thiol monolayers are prone to this problem due to the

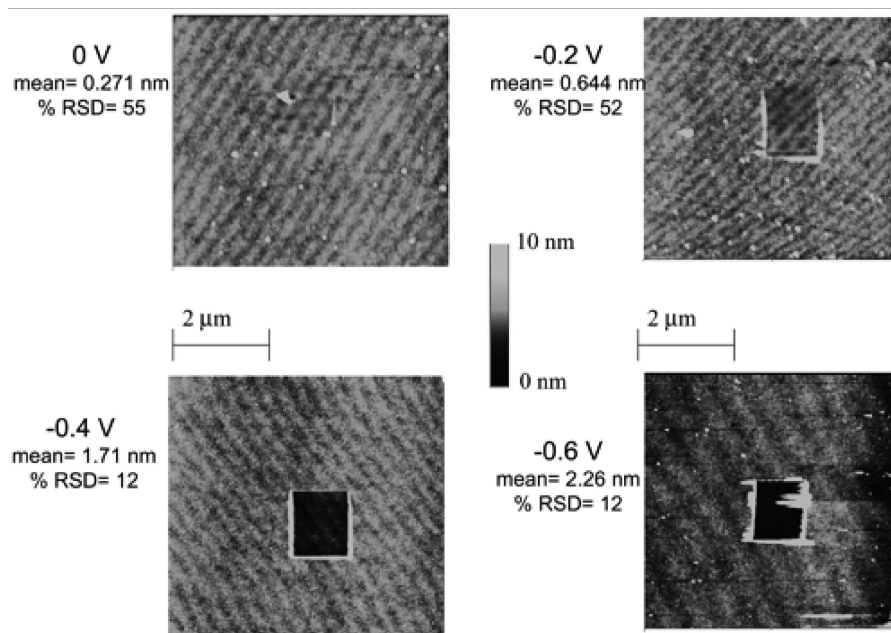


**Figure 36.** Tapping mode AFM images for a biphenyl-modified PPF surface following a contact mode “scratch”. Single derivatization scans from +0.4 to 0, -0.2, -0.4, and -0.6 V vs  $\text{Ag}/\text{Ag}^+$  were used to modify the PPF surface, as indicated. Also shown are the mean thickness (mean) and relative standard deviation (%RSD) determined statistically as described in the ref 197. Reprinted with permission from ref 197 Copyright 2003 American Chemical Society.

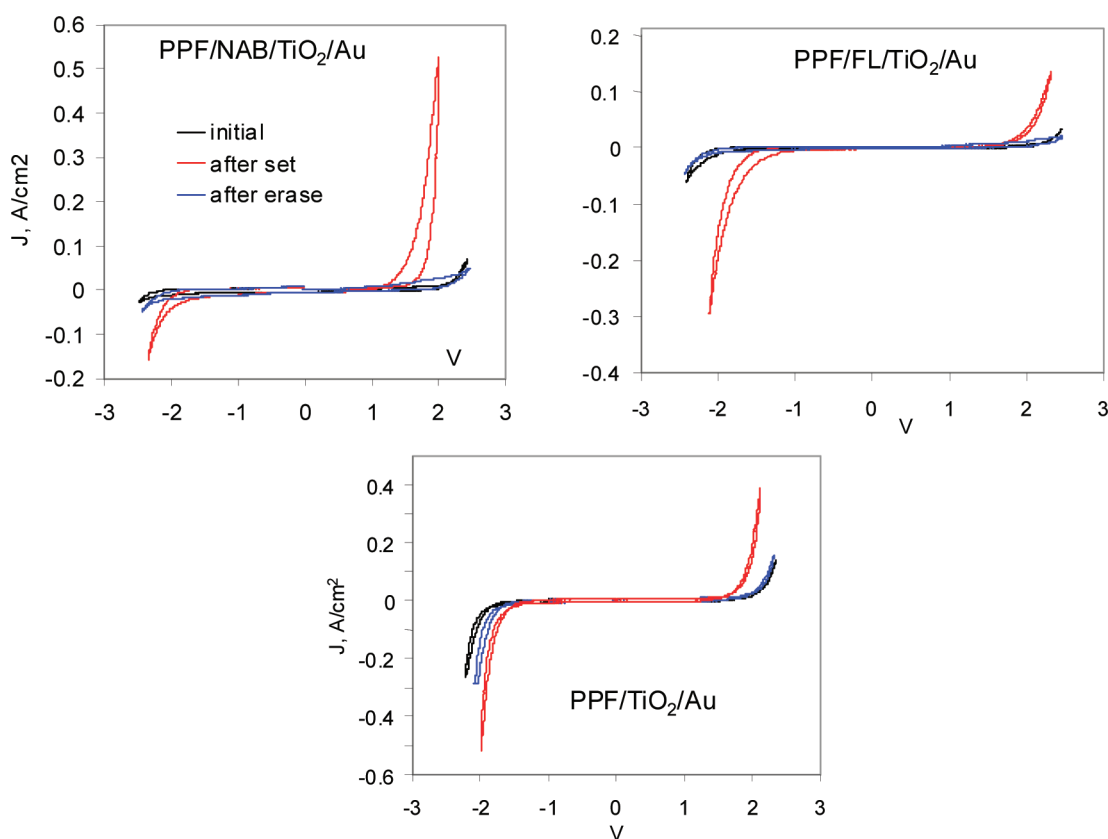


**Figure 37.** Current/voltage curves of molecular junctions made from nitroazobenzene (NAB) and fluorene (FL) monolayers with  $\text{TiO}_2$  between PPF and Au conducting “contacts”. Black curves are the initial scans at 1000 V/s, red are after a +3 V, 100 ms pulse (PPF relative to Au), and blue after a -3 V, 100 ms pulse. Adapted in part from ref 200 (Copyright 2006) by permission of the PCCP Owner Societies.

relatively weak surface bond and associated mobility of the monolayer.<sup>384–386</sup> The strong C–C bond from diazonium reduction ( $\sim 4$  eV compared with  $\sim 1.6$  eV for Au–S) permits vapor deposition of metals or metal oxides on modified carbon surfaces without observable short circuits. An ex-

ample of the behavior of a molecular junction made by vapor deposition of  $\text{TiO}_2$  and Au onto PPF surfaces modified by diazonium reduction of fluorene and nitroazobenzene reagents is shown in Figure 37.<sup>387</sup> The molecular and oxide layers total 10–15 nm in thickness, and there is no intentional

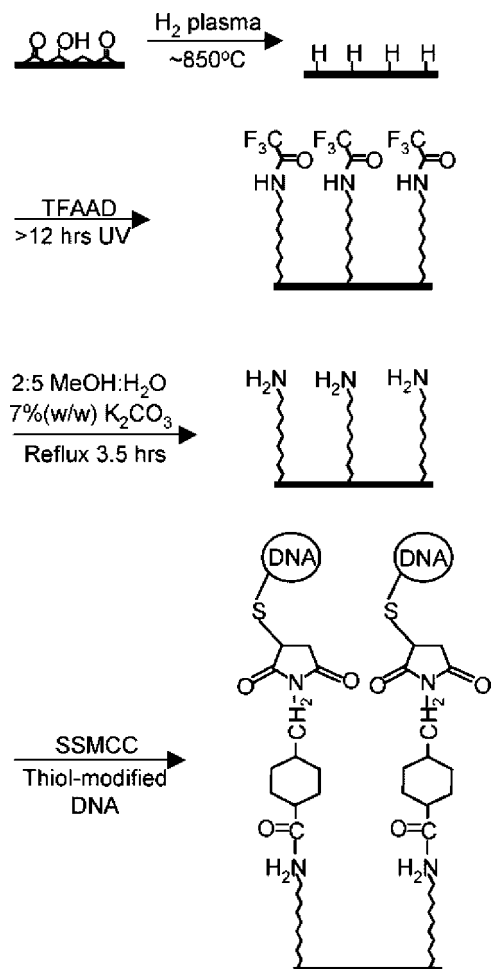


**Figure 38.** Photochemical route to covalent modification of diamond surfaces. TFAAD is trifluoroacetamide-protected 10-aminodec-1-ene; SSMCC is sulfosuccinimidyl-4-(*N*-maleimidomethyl) cyclohexane-1-carboxylate. Reprinted with permission from ref 397. Copyright 2003 American Chemical Society.

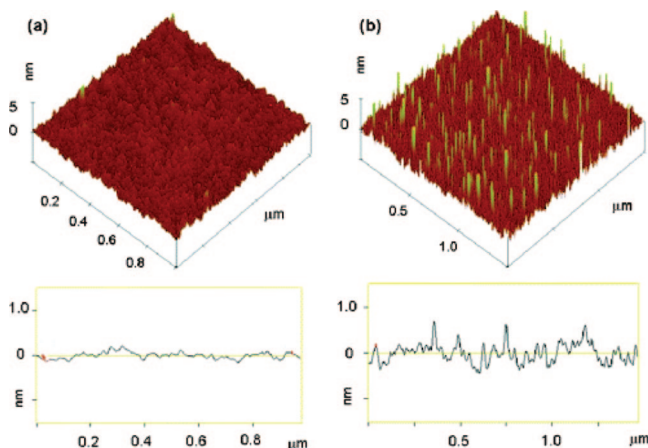


**Figure 39.** AFM images of PPF before (left) and after (right) UV irradiation in the presence of 1-decene, along with line profiles across the imaged surfaces. Reprinted with permission from ref 190. Copyright 2007 American Chemical Society.

solvent or electrolyte present. These molecular junctions exhibit “memory”, in that they can switch between metastable low and high conductance states in response to “set” and “erase” voltage pulses. The local temperature rise of the device during metal deposition is significant, and the good thermal stability of a C–C surface bond is important to successful fabrication. The mechanisms and utility of these

effects in molecular electronics have been described in some detail.<sup>200,201,364,387</sup>

Formation of C–C bonds between diamond surfaces and phenyl radicals generated by diazonium reduction has been reported<sup>68</sup> for the boron-doped diamond electrodes described in section 4.2. XPS and Raman spectroscopy of BDD modified with nitrophenyl, trifluoromethyl, and nitroazobenzene diazonium reagents revealed high coverage and stable modification layers. The modification reaction had a lower current efficiency than typically observed for graphitic carbon surfaces, presumably because 1 equiv of electrogenerated radical was required to abstract a hydrogen atom from the H-terminated BDD surface. After that, a second radical could couple with the surface radical to form the final C–C bond. Figure 4D shows a Raman spectrum of BDD before and after covalent modification of the diamond surface by reduction of nitroazobenzene diazonium ion.

Some significant variations on diazonium reduction have been reported recently, based on reactions of reactive precursors with carbon surfaces to result in a covalently bonded organic layer. These include the reduction of aryl and alkynyl iodonium salts,<sup>388</sup> reduction of diaryl iodonium salts,<sup>389</sup> and reduction of diazonium reagents that contain disulfides.<sup>390</sup> In the latter case, a multilayer of disulfide reagents was cleaved to yield a monolayer of a thiophenolate, thus providing a reliable route to a monolayer modification. A different example of radical mediated carbon surface modification is reduction of triaryl and alkyldiphenyl sulfonium ions, which leads to a carbon surface modified with aryl groups or with a mixture of covalently bonded alkyl and aryl groups.<sup>391</sup>

## 5.2. Thermal and Photochemical Modifications

Cycloaddition and photochemical reactions developed for modifying silicon surfaces<sup>98</sup> have been applied to graphitic carbon and diamond surfaces,<sup>392–394</sup> although the applications have not been as extensive as those of diazonium reduction. In ultrahigh vacuum (UHV), clean diamond surfaces form surface “dimers”, which can react at room temperature with olefins to form C–C surface bonds. The product of the cycloaddition reaction is a four-membered ring with two C–C bonds to the diamond surface.<sup>395</sup> Diels–Alder type (4 + 2) cycloadditions have been reported on diamond, as well as the (2 + 2) route, again under UHV conditions.<sup>396</sup> A photochemical route to modification of diamond with DNA is shown in Figure 38, involving formation of a surface amine with trifluoroacetamide-protected 10-aminodec-1-ene (TFAAD) followed by coupling to DNA through a cross-linker sulfosuccinimidyl-4-(*N*-maleimidomethyl) cyclohexane-1-carboxylate (SSMCC).<sup>397,398</sup> A simpler modification of diamond with alkanes was achieved by UV treatment of H-terminated BDD in the presence of 1-decene, and the electrical properties of the modified surface were investigated.<sup>399</sup> The stability of both GC and BDD electrodes modified by covalent monolayers was found to be superior to alternative bonding schemes such as silane and Au/thiol reactions in biosensor applications due to the thermal and hydrolytic stability of the C–C bond.<sup>224,398</sup>

A photochemical route to bonding alkenes and alkynes to polished GC and as-prepared PPF has been reported, involving illumination of the surface in the presence of a range of alkenes and one alkyne with 254 nm light.<sup>190</sup> The reaction could be conducted in air without extensive electrode pretreatment. AFM images of a PPF surface before and after

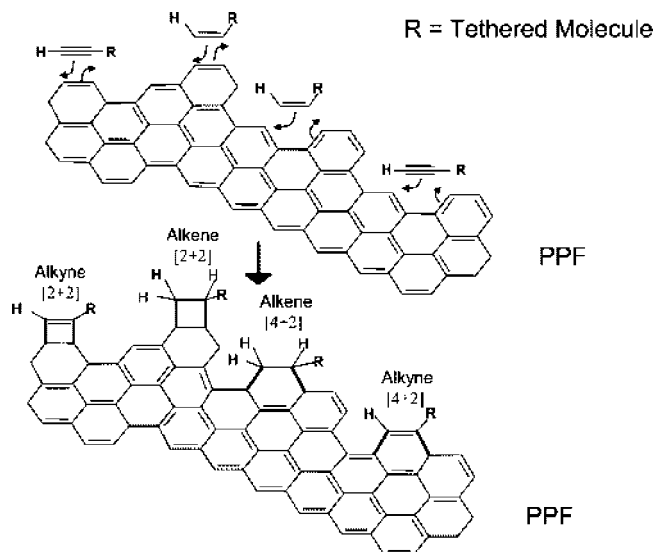


**Figure 40.** Mechanism proposed for thermal attachment of alkene and alkyne reagents to PPF. Reprinted with permission from ref 400. Copyright 2005 American Chemical Society.

modification are shown in Figure 39, indicating that the coverage of the surface is not complete for the conditions employed. Based on the voltammetric peak area for oxidation of a PPF surface modified similarly with ferrocene-alkyne, the coverage in that case was 16% of a densely packed monolayer. Alkene and alkyne derivatives of porphyrin and ferrocene can also be attached to graphitic carbon surfaces by heat treatment, in which a solution of the reagent reacts with a hot (175–400 °C) carbon surface in argon.<sup>400</sup> FTIR was used to determine that the tilt angle of the attached porphyrin center was 37°–45° relative to the surface normal. The modified surfaces were stable to sonication in tetrahydrofuran, treatment with aqueous acid or base, and extensive potential cycling in propylene carbonate electrolyte. Surface coverage was generally less than a complete monolayer, ranging from  $0.2 \times 10^{-10}$  to  $3 \times 10^{-10}$  mol/cm<sup>2</sup>, determined voltammetrically for the porphyrin modification. Although the detailed geometry of the surface bonding was not determined from the FTIR spectra due to interference from the carbon substrate, the tilt angle was statistically different for alkene compared with alkyne modification. A proposed modification scheme<sup>400</sup> based on Diels–Alder and (2 + 2) cycloaddition chemistry is shown in Figure 40.

### 5.3. Amine and Carboxylate Oxidation

Covalent bonding to graphitic carbon surfaces by oxidation of amines was reported initially in the early 1990s for carbon fiber<sup>344</sup> and glassy carbon electrodes<sup>345</sup> and has been studied in additional detail more recently.<sup>203,361,373,401,402</sup> Electrochemical oxidation of aliphatic primary amines yields an amine radical, which can then bond to an unsatisfied valence or double bond on the carbon electrode surface. An example is shown in Figure 41 for the oxidation of three aliphatic amines on glassy carbon in acetonitrile electrolyte.<sup>402</sup>

Electrolysis in a solution of a primary amine leads to complete inhibition of the voltammetric oxidation peak, while similar treatment in a secondary or tertiary amine results in only minor changes to the voltammetry. A mechanistic investigation supported by FTIR and XPS characterization of the modified carbon surfaces concluded that the reactive surface binding agent is the neutral, deprotonated amine

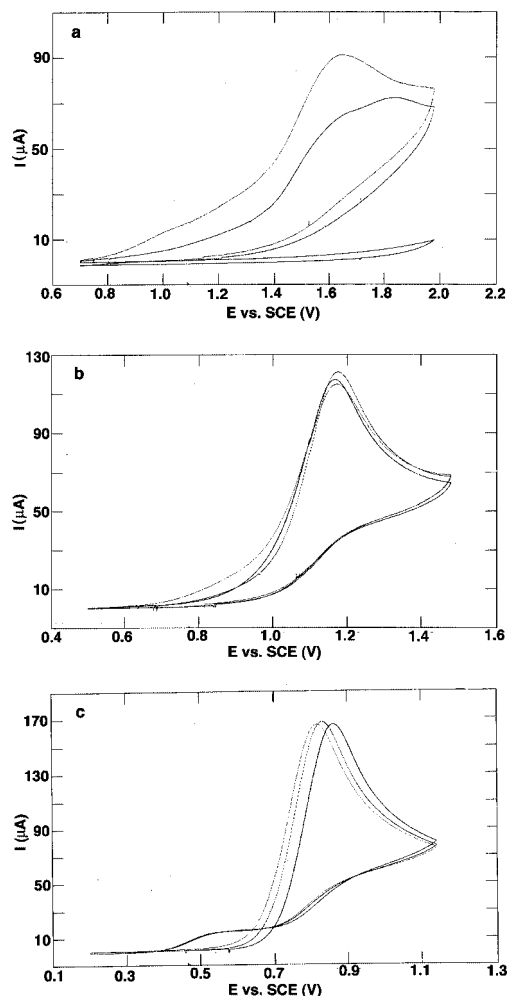


**Figure 41.** Cyclic voltammetry during the course of electrolytic oxidation of (a) *n*-butylamine, (b) di-*n*-butylamine, and (c) tri-*n*-butylamine in a 5.0 mM solution of the amine in acetonitrile electrolyte. Reprinted with permission from ref 402. Copyright 2004 American Chemical Society.

radical.<sup>402</sup> Both the earlier<sup>345</sup> and later<sup>402</sup> studies concluded that surface binding is much more efficient for primary amines than for secondary amines and that binding is essentially absent for tertiary amines. Coverage was assessed by voltammetry of surface-bound nitrophenyl groups following oxidation of nitrobenzylamine on GC to be in the range of  $(3\text{--}6) \times 10^{-10}$  mol/cm<sup>2</sup>. While this is close to that expected for monolayer coverage, there was evidence for pinholes from the electrochemical activity of modified GC surfaces.<sup>402</sup> Amine oxidation was also used to immobilize Au nanoparticles on carbon surfaces<sup>361</sup> and for detailed studies of the “blocking” properties of modification layers on carbon electrodes.<sup>373</sup> In a somewhat surprising recent report, spontaneous adsorption of primary amines to a GC surface was described, forming nearly monolayer coverage that resisted removal by sonication.<sup>401</sup> XPS and FTIR were used to observe surface bound nitrogen, and the surfaces were characterized electrochemically.<sup>401</sup>

A distinct modification reaction that is also mediated by a primary carbon radical is based on the oxidation of carboxylates.<sup>374</sup> After carboxylate oxidation and subsequent loss of CO<sub>2</sub>, the primary radical may bond to the carbon surface. The voltammetry shown in Figure 42 illustrates the oxidation of naphthyl-methyl carboxylate at +1 to 1.1 V vs Ag<sup>+</sup>/Ag on either GC or PPF, with the second voltammetric

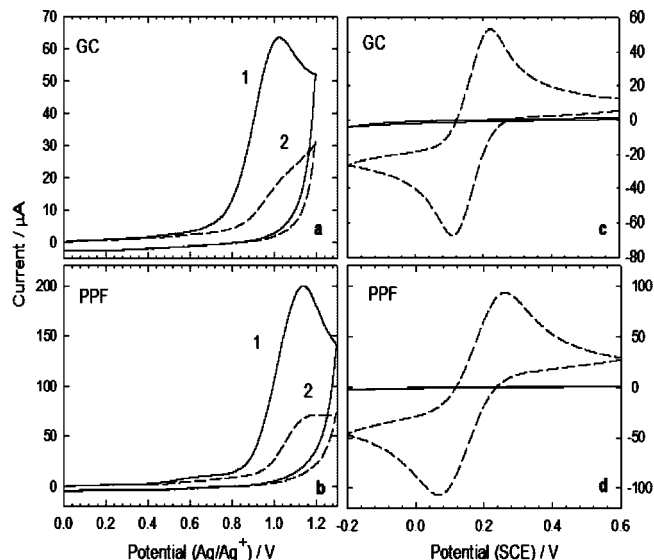


**Figure 42.** Cyclic voltammetry at GC (a, c) and PPF (b, d) surfaces, 0.2 V/s: (a, b) first scan (solid line) and second scan (dashed) with stirring between scans of 5.2 mM naphthylmethyl-carboxylate in 0.1 M TBABF<sub>4</sub>/CH<sub>3</sub>CN solution; (c, d) scans of 3.1 mM Fe(CN)<sub>6</sub><sup>3-</sup> in aqueous 0.2 M KCl at bare (dashed) and naphthylmethyl-modified (solid) surfaces. Reprinted with permission from ref 374. Copyright 2005 American Chemical Society.

scan much smaller due to formation of the modification layer. The naphthyl-methyl film bonded to the surface completely inhibited electron transfer to a Fe(CN)<sub>6</sub><sup>3-/4-</sup> redox system, and it was concluded that the modification reaction formed multilayers under the conditions employed.<sup>374</sup>

#### 5.4. Modification by “Click” Chemistry

A recent and potentially versatile carbon surface modification is based on “click” cycloaddition chemistry to a surface-

bound azide group.<sup>403</sup> Cu(I)-catalyzed cycloaddition of alkynes to azides yields a stable triazole ring, and the reaction has been used in a variety of applications, including linking electroactive alkynes with azide groups in self-assembled monolayers on Au electrodes.<sup>404–406</sup> For graphitic carbon electrodes,<sup>407</sup> the azide may be covalently attached to the surface by addition of iodine azide, IN<sub>3</sub>, across a double bond on a graphitic edge plane, as shown in Figure 43.

XPS analysis of the azide-modified PPF surface revealed the presence of a surface bound azide group (shown in Figure 43B) with a coverage of  $\sim 1 \times 10^{-10}$  mol/cm<sup>2</sup>. Reaction of the azide-modified surface with ethynylferrocene in the presence of a Cu(I) catalyst resulted in the appearance of the surface voltammetric wave for ferrocene oxidation, shown in the inset of Figure 43, as well as changes to the N<sub>1s</sub> XPS bands (395–406 eV). The coverage of ferrocene determined voltammetrically was less than that of a typical monolayer. The use of “click” chemistry for carbon surface modification has the attraction of using a reaction with a single reagent to bond a “primer” to the surface, followed by coupling to a possibly wide range of alkynes to yield functionalized surfaces.

#### 6. Synopsis and Outlook

Despite at least 100 years of active use of carbon materials in electrochemistry, there is no shortage of new materials, properties, and applications. The advent of fullerenes and conducting diamond by themselves represent major new avenues for research and development of carbon electrodes, but these innovations are accompanied by microfabricated carbon films and devices, aggressive covalent surface modifications, and a variety of new carbon composites for mechanistic and analytical electrochemistry. The continued growth of applications for carbon materials in electrochemistry is assured by the properties that attracted the initial users

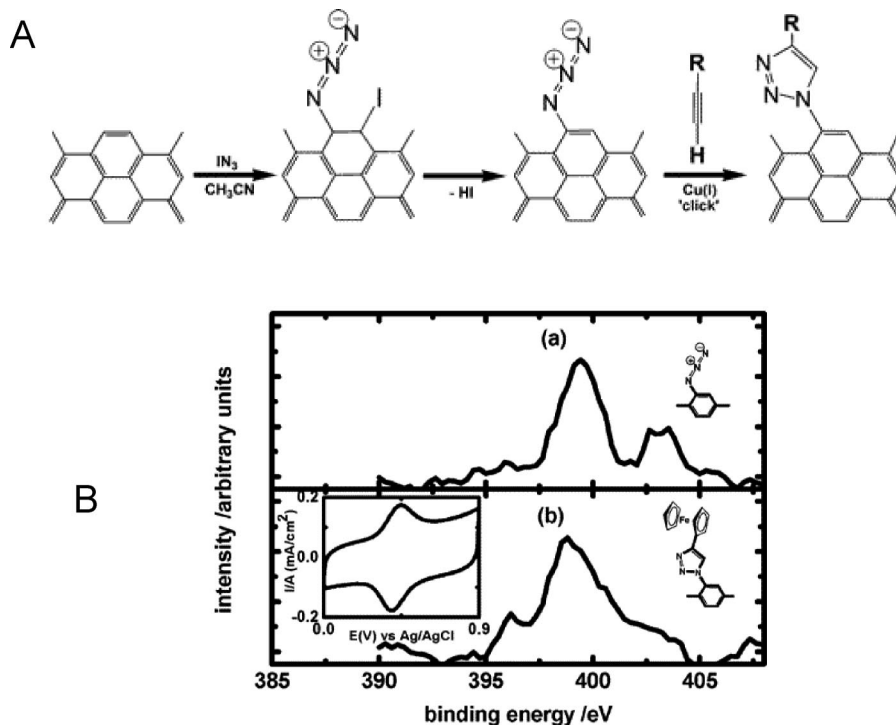


**Figure 43.** (A) Proposed reaction sequence for treatment of carbon surfaces with iodine azide followed by a terminal alkyne and (B) XPS spectra of a PPF surface before (a) and after (b) reaction of the azide-modified surface with a ferrocene alkyne. Inset in panel b is the surface voltammetry of the ferrocene modified surface. Reprinted with permission from ref 407. Copyright 2007 American Chemical Society.

of carbon electrodes long ago: the availability of different conducting allotropes, the strong covalent bonds within carbon materials and to a variety of surface modifiers, the good thermal and electrochemical stability, and the possibility of a wide range of carbon microstructures of varying hardness, cost, and reactivity. The obvious point that  $sp^2$  and  $sp^3$  hybridized carbon materials differ fundamentally from metals in their structure, reactivity, and electronic properties still deserves emphasis, because those differences enable many of the major applications of carbon materials in electrochemistry.

It is generally risky to attempt to predict future results of scientific research, but some consideration of probable upcoming developments in carbon electrochemistry is stimulated by the preceding review. Carbon nanotubes and conducting diamond both hold significant promise, the former for unusual electrode architectures enabled by nanotube conductivity and aspect ratio and the latter by the hardness and stability of diamond. Just as the dimensionally stable anode revolutionized industrial electrochemistry, the stability of diamond may find significant applications where stability is paramount. The large length to diameter ratio of carbon nanotubes, combined with their high conductivity enable new electrode architectures for “wired” composites which enhance electrical communication between a bulk conductor and an enzyme or redox-active electrode modifier. In the author’s opinion, there is still work to be done on the preparation of monodisperse CNT materials and on determining and controlling the structural parameters that underlie their behavior. Applications requiring ordered arrays of CNTs with low defects will depend additionally on growth and fabrication innovations.

Another promising area for future advances in carbon electrochemistry is micro- or nanostructuring of thin films and their surfaces. With electron beam and nanoimprint lithography permitting design and microfabrication of carbon thin films at the 10–100 nm level and the variety of surface modifications discussed in section 5, there is a wealth of opportunities for nanoscale electrochemical devices based on carbon materials. These may include interdigitated arrays, nanogaps, ultramicroelectrodes, and microfluidic channels and detectors. When the dimensions of an electrode approach the nanometer scale of nanotubes and modern lithographic structures, mass transport is much more efficient, thus permitting the study of very fast electrode kinetics and enhancing the response of many electroanalytical sensors. Furthermore, when the electrode dimension approaches the double layer thickness, interesting and unusual kinetic and electrostatic effects occur. It is likely that carbon nanotubes and other nanostructured electrodes will be key players in the investigation of such phenomena. Even when the many advances in carbon materials for electrochemistry of the past ~15 years are considered, it is clear there remains plenty of “mileage” in carbon materials for both fundamental and applied research and development in electrochemistry.

## 7. Acknowledgments

Most of the work cited from the author’s laboratory was supported by the National Science Foundation (USA), the Air Force Office of Scientific Research (USA), and ZettaCore (Denver, USA). Work performed in Canada was supported by the Natural Science and Engineering Research Council, the National Research Council, and the Alberta Ingenuity Fund.

## 8. References

- (1) Walker, P. L.; Radovic, L. R. *Chemistry and Physics of Carbon*; Dekker: New York.
- (2) Kinoshita, K. *Carbon, Electrochemical and Physicochemical Properties*; John Wiley and Sons: New York, 1988.
- (3) McCreery, R. L. In *Electroanalytical Chemistry*; Bard, A. J., Ed.; Dekker, New York, 1991; Vol 17.
- (4) Leon y Leon, C. A.; Radovic, L. R. In *Chemistry and Physics of Carbon*; Thrower, P. A., Ed.; Dekker: New York, 1994; Vol 24.
- (5) Wu, J.; Pisula, W.; Mullen, K. *Chem. Rev.* **2007**, *107*, 718–747.
- (6) Moore, A. In *Chemistry and Physics of Carbon*; Thrower, P. A., Ed., 1981; Vol 17.
- (7) Matthews, M. J.; Pimenta, M. A.; Dresselhaus, G.; Dresselhaus, M. S.; Endo, M. *Phys. Rev. B* **1999**, *59*, R6585–R6588.
- (8) Speck, J. S.; Steinbeck, J.; Dresselhaus, G. *J. Mater. Res.* **1990**, *5*, 980–988.
- (9) Al-Jishi, R.; Dresselhaus, G. *Phys. Rev. B* **1982**, *26*, 4523–4538.
- (10) Wang, Y.; Alsmeyer, D. C.; McCreery, R. L. *Chem. Mater.* **1990**, *2*, 557–563.
- (11) Wightman, R. M. *Science* **2006**, *311*, 1570–1574.
- (12) Hermans, A.; Seipel, A. T.; Miller, C. E.; Wightman, R. M. *Langmuir* **2006**, *22*, 1964–1969.
- (13) Heien, M. L. A. V.; Johnson, M. A.; Wightman, R. M. *Anal. Chem.* **2004**, *76*, 5697–5704.
- (14) Dresselhaus, M. S. *Graphite Fibers and Filaments*; Springer-Verlag: New York, 1988.
- (15) Jenkins, G. M.; Kawamura, K. *Polymeric Carbons, Carbon Fibre, Glass and Char*; University Press: Cambridge, England, 1976.
- (16) McDermott, M. T.; McDermott, C. A.; McCreery, R. L. *Anal. Chem.* **1993**, *65*, 937.
- (17) McDermott, C. A.; McCreery, R. L. *Langmuir* **1994**, *10*, 4307.
- (18) Howard, H. D.; Pocard, N. L.; Alsmeyer, D.; Schueller, O. J. A.; Spontak, R. J.; Huston, M. E.; Huang, W.; McCreery, R. L.; Neenan, T.; Callstrom, M. *Chem. Mater.* **1993**, *5*, 1727.
- (19) Hutton, H. D.; Huang, W.; Alsmeyer, D.; Kometani, J.; McCreery, R. L.; Neenan, T.; Callstrom, M. R. *Chem. Mater.* **1993**, *5*, 1110.
- (20) Hutton, H. D.; Alsmeyer, D. C.; McCreery, R. L.; Neenan, T. X.; Callstrom, M. *Polym. Mater. Sci. Eng.* **1992**, *67*, 237.
- (21) Callstrom, M.; Neenan, T.; McCreery, R. L.; Alsmeyer, D. J. *Am. Chem. Soc.* **1990**, *112*, 4954.
- (22) Kim, H.-G.; Ahn, S.-H.; Kim, J.-G.; Park, S. J.; Lee, K.-R. *Thin Solid Films* **2005**, *475*, 291.
- (23) Godet, C.; Conway, N. M. J.; Bouere, J. E.; Bouamra, K.; Grosman, A.; Ortega, C. *J. Appl. Phys.* **2002**, *91*, 4154–4162.
- (24) Jia, J.; Kato, D.; Kurita, R.; Sato, Y.; Maruyama, K.; Suzuki, K.; Hirono, S.; Ando, T.; Niwa, O. *Anal. Chem.* **2007**, *79*, 98–105.
- (25) Zhou, M.; Ding, J.; Guo, L.-p.; Shang, Q.-k. *Anal. Chem.* **2007**, *79*, 5328–5335.
- (26) Li, H.-Q.; Luo, J.-Y.; Zhou, X.-F.; Yu, C.-Z.; Xia, Y.-Y. *J. Electrochem. Soc.* **2007**, *154*, A731.
- (27) Raghuvver, V.; Manthiram, A. *J. Electrochem. Soc.* **2005**, *152*, A1504.
- (28) Santiago, E. I.; Varanda, L. C.; Villullas, H. M. *J. Phys. Chem. C* **2007**, *111*, 3146–3151.
- (29) Fang, B.; Kim, J. H.; Lee, C.; Yu, J. S. *J. Phys. Chem. C* **2008**, *112*, 639–645.
- (30) Swain, G. M. In *Electroanalytical Chemistry*; Bard, A. J., Rubinstein, I., Eds.; Dekker: New York, 2004; Vol. 22.
- (31) Gruen, D. M. *Annu. Rev. Mater. Sci.* **1999**, *29*, 211.
- (32) Pleskov, Y.; Krotova, M.; Ralchenko, V.; Saveliev, A.; Bozhko, A. *Russ. J. Electrochem.* **2007**, *43*, 827.
- (33) Zhao, W.; Xu, J.-J.; Qiu, Q.-Q.; Chen, H.-Y. *Biosens. Bioelectron.* **2006**, *22*, 649.
- (34) Fischer, A. E.; Show, Y.; Swain, G. M. *Anal. Chem.* **2004**, *76*, 2553–2560.
- (35) Yoo, K.; Miller, B.; Kalish, R.; Shi, X. *Electrochem. Solid-State Lett.* **1999**, *2*, 233.
- (36) Lee, J.-J.; Miller, B.; Shi, X.; Kalish, R.; Wheeler, K. A. *J. Electrochem. Soc.* **2001**, *148*, C183.
- (37) Wildgoose, G. G.; Banks, C. E.; Leventis, H. C.; Compton, R. G. *Electrochim. Acta* **2006**, *152*, 187–214.
- (38) Valcarcel, M.; Cardenas, S.; Simonet, B. M. *Anal. Chem.* **2007**, *79*, 4788–4797.
- (39) Gooding, J. J. *Electrochim. Acta* **2005**, *50*, 3049.
- (40) Heller, I.; Kong, J.; Heering, H.; Williams, K.; Lemay, S. G.; Dekker, C. *Nano Lett.* **2005**, *5*, 137–142.
- (41) Heller, I.; Kong, J.; Williams, K. A.; Dekker, C.; Lemay, S. G. *J. Am. Chem. Soc.* **2006**, *128*, 7353–7359.
- (42) Goldsmith, B. R.; Coroneus, J. G.; Khalap, V. R.; Kane, A. A.; Weiss, G. A.; Collins, P. G. *Science* **2007**, *315*, 77–81.
- (43) Kokko, K.; Ojala, E.; Mansikka, K. *Phys. Status Solidi B* **1989**, *153*, 235.

- (44) Iwasita, T.; Schmickler, W. *Ber. Bunsen-Ges.* **1985**, *89*, 138–42.
- (45) Royea, W. J.; Hamann, T. W.; Brunschwig, B. S.; Lewis, N. S. *J. Phys. Chem. B* **2006**, *110*, 19433–19442.
- (46) Dresselhaus, M. S.; Dresselhaus, G.; Fischer, J. E. *Phys. Rev. B* **1977**, *15*, 3180.
- (47) Spain, I. L. In *Chemistry and Physics of Carbon*; Thrower, P. L., Ed.; Dekker: New York, 1981; Vol 16.
- (48) Koivusaari, K. J.; Rantala, T. T.; Leppavuori, S. *Diamond Relat. Mater.* **2000**, *9*, 736.
- (49) Gerischer, H.; McIntyre, R.; Scherson, D.; Storck, W. *J. Phys. Chem.* **1987**, *91*, 1930.
- (50) Rice, R. J.; McCreery, R. L. *Anal. Chem.* **1989**, *61*, 1637.
- (51) Rice, R. J.; Pontikos, N.; McCreery, R. L. *J. Am. Chem. Soc.* **1990**, *112*, 4617.
- (52) Bard, A. J.; Faulkner, L. R. *Electrochemical Methods*; 2nd ed.; Wiley: New York, 2001.
- (53) Granger, M. C.; Witek, M.; Xu, J.; Wang, J.; Hupert, M.; Hanks, A.; Koppang, M. D.; Butler, J. E.; Lucazeau, G.; Mermoux, M.; Strojek, J. W.; Swain, G. M. *Anal. Chem.* **2000**, *72*, 3793–3804.
- (54) Taft, E. A.; Philipp, H. R. *Phys. Rev.* **1965**, *138*, A197–A201.
- (55) Williams, M. W.; Arakawa, E. T. *J. Appl. Phys.* **1972**, *43*, 3460–3463.
- (56) Mattson, J. S.; Smith, C. A. *Anal. Chem.* **1975**, *47*, 1122–1125.
- (57) Anjo, D. M.; Brown, S.; Wang, L. *Anal. Chem.* **1993**, *65*, 317–319.
- (58) Donner, S.; Li, H. W.; Yeung, E. S.; Porter, M. D. *Anal. Chem.* **2006**, *78*, 2816–2822.
- (59) Tian, H.; Bergren, A. J.; McCreery, R. L. *Appl. Spectrosc.* **2007**, *61*, 1246–1253.
- (60) Obratsov, A. N.; Pavlovsky, I. Y.; Izumi, T.; Okushi, H.; Watanabe, H. *Appl. Phys. A: Mater. Sci. Process.* **1997**, *65*, 505.
- (61) Stotter, J.; Show, Y.; Wang, S.; Swain, G. *Chem. Mater.* **2005**, *17*, 4880–4888.
- (62) Stotter, J.; Zak, J.; Behler, Z.; Show, Y.; Swain, G. M. *Anal. Chem.* **2002**, *74*, 5924–5930.
- (63) Martin, H. B.; Morrison, P. W. *Electrochem. Solid-State Lett.* **2001**, *4*, E17.
- (64) Tuinstra, F.; Koenig, J. L. *J. Chem. Phys.* **1970**, *53*, 1126.
- (65) Negri, F.; Castiglioni, C.; Tommasini, M.; Zerbi, G. *J. Phys. Chem. A* **2002**, *106*, 3306–3317.
- (66) Chieu, T. C.; Dresselhaus, M. S.; Endo, M. *Phys. Rev. B* **1982**, *26*, 5867–5877.
- (67) Nemanich, R. J.; Solin, S. A. *Phys. Rev. B* **1979**, *20*, 392–401.
- (68) Kuo, T.-C.; McCreery, R. L.; Swain, G. M. *Electrochem. Solid State Lett.* **1999**, *2*, 288–291.
- (69) Bowling, R.; Packard, R. T.; McCreery, R. L. *J. Electrochem. Soc.* **1988**, *135*, 1605.
- (70) Bowling, R.; Packard, R. T.; McCreery, R. L. *J. Am. Chem. Soc.* **1989**, *111*, 1217.
- (71) Bowling, R.; Packard, R. T.; McCreery, R. L. *Langmuir* **1989**, *5*, 683.
- (72) Alsmeyer, Y.-W.; McCreery, R. L. *Anal. Chem.* **1991**, *63*, 1289.
- (73) Alsmeyer, Y. W.; McCreery, R. L. *Langmuir* **1991**, *7*, 2370.
- (74) Alsmeyer, D.; McCreery, R. L. *Anal. Chem.* **1992**, *64*, 1528.
- (75) Kudin, K. N.; Ozbas, B.; Schniepp, H. C.; Prud'homme, R. K.; Aksay, I. A.; Car, R. *Nano Lett.* **2008**, *8*, 36–41.
- (76) Ray, K. G.; McCreery, R. L. *Anal. Chem.* **1997**, *69*, 4680–4687.
- (77) Fischer, A. E.; Lowe, M. A.; Swain, G. M. *J. Electrochem. Soc.* **2007**, *154*, K61.
- (78) Dresselhaus, M. S.; Dresselhaus, G.; Jorio, A. *J. Phys. Chem. C* **2007**, *111*, 17887–17893.
- (79) Heller, D. A.; Barone, P. W.; Swanson, J. P.; Mayrhofer, R. M.; Strano, M. S. *J. Phys. Chem. B* **2004**, *108*, 6905–6909.
- (80) Oron-Carl, M.; Henrich, F.; Kappes, M. M.; Lohneysen, H. v.; Krupke, R. *Nano Lett.* **2005**, *5*, 1761–1767.
- (81) Kim, U. J.; Furtado, C. A.; Liu, X.; Chen, G.; Eklund, P. C. *J. Am. Chem. Soc.* **2005**, *127*, 15437–15445.
- (82) Rafailov, P.; Stoll, M.; Thomsen, C. *J. Phys. Chem B* **2004**, *108*, 19241–19245.
- (83) Anglaret, E.; Dragin, F.; Penicaud, A.; Martel, R. *J. Phys. Chem. B* **2006**, *110*, 3949–3954.
- (84) Mattia, D.; Rossi, M. P.; Kim, B. M.; Korneva, G.; Bau, H. H.; Gogotsi, Y. *J. Phys. Chem. B* **2006**, *110*, 9850–9855.
- (85) Zhang, L.; Jia, Z.; Huang, L.; O'Brien, S.; Yu, Z. *J. Phys. Chem. C* **2007**, *111*, 11240–11245.
- (86) Zhou, J.; Booker, C.; Li, R.; Zhou, X.; Sham, T. K.; Sun, X.; Ding, Z. *J. Am. Chem. Soc.* **2007**, *129*, 744–745.
- (87) DeAngelis, T. P.; Hurst, R. W.; Yacynych, A. M.; Mark, H. B., Jr.; Heineman, W. R.; Mattson, J. S. *Anal. Chem.* **1977**, *49*, 1395–1398.
- (88) Blackstock, J. J.; Rostami, A. A.; Nowak, A. M.; McCreery, R. L.; Freeman, M.; McDermott, M. T. *Anal. Chem.* **2004**, *76*, 2544–2552.
- (89) Liang, H.; Tian, H.; McCreery, R. L. *Appl. Spectrosc.* **2007**, *61*, 613.
- (90) Watcharotone, S.; Dikin, D. A.; Stankovich, S.; Piner, R.; Jung, I.; Dommett, G. H. B.; Evmenenko, G.; Wu, S. E.; Chen, S. F.; Liu, C. P.; Nguyen, S. T.; Ruoff, R. S. *Nano Lett.* **2007**, *7*, 1888–1892.
- (91) Sun, P.; Mirkin, M. V. *Anal. Chem.* **2006**, *78*, 6526–6534.
- (92) Birkin, P. R.; Silva-Martinez, S. *Anal. Chem.* **1997**, *69*, 2055–2062.
- (93) Chang, H.; Bard, A. J. *Langmuir* **1991**, *7*, 1143–1153.
- (94) McDermott, M. T.; Kneten, K.; McCreery, R. L. *J. Phys. Chem.* **1992**, *96*, 3124.
- (95) Kuo, T.-C.; McCreery, R. L. *Anal. Chem.* **1999**, *71*, 1553–1560.
- (96) Rice, R.; Allred, C.; McCreery, R. L. *J. Electroanal. Chem.* **1989**, *263*, 163.
- (97) Allred, C.; McCreery, R. L. *Anal. Chem.* **1992**, *64*, 444.
- (98) Buriak, J. M. *Chem. Rev.* **2002**, *102*, 1271–1308.
- (99) Ranganathan, S.; McCreery, R. L. *Anal. Chem.* **2001**, *73*, 893–900.
- (100) Ye, X. R.; Chen, L. H.; Wang, C.; Aubuchon, J. F.; Chen, I. C.; Gapin, A. I.; Talbot, J. B.; Jin, S. *J. Phys. Chem. B* **2006**, *110*, 12938–12942.
- (101) Osswald, S.; Flahaut, E.; Gogotsi, Y. *Chem. Mater.* **2006**, *18*, 1525–1533.
- (102) Banks, C. E.; Compton, R. G. *The Analyst* **2005**, *130*, 1232–1239.
- (103) Fang, H. T.; Liu, C.-G.; Liu, C.; Li, F.; Liu, M.; Cheng, H. M. *Chem. Mater.* **2004**, *16*, 5744–5750.
- (104) Langley, L. A.; Villanueva, D. E.; Fairbrother, D. H. *Chem. Mater.* **2006**, *18*, 169–178.
- (105) Fagan, D. T.; Kuwana, T. *Anal. Chem.* **1989**, *61*, 1017–1023.
- (106) Fryling, M.; Zhao, J.; McCreery, R. L. *Anal. Chem.* **1995**, *67*, 967.
- (107) Ray, K. G.; McCreery, R. L. *J. Electroanal. Chem.* **1999**, *469*, 150–158.
- (108) Gotch, A. J.; Kelly, R. S.; Kuwana, T. *J. Phys. Chem. B* **2003**, *107*, 935–941.
- (109) Weiss, D. J.; Kelly, R. S.; Cumaranutunge, M.; Kuwana, T. *Anal. Chem.* **1999**, *71*, 3712–3720.
- (110) Kelly, R. S.; Weiss, D. J.; Chong, S. H.; Kuwana, T. *Anal. Chem.* **1999**, *71*, 413–418.
- (111) Randin, J.-P.; Yeager, E. *J. Electroanal. Chem.* **1972**, *36*, 257–276.
- (112) Gerischer, H. *J. Phys. Chem.* **1985**, *89*, 4249–4251.
- (113) McIntyre, R.; Scherson, D.; Storck, W.; Gerischer, H. *Electrochim. Acta* **1987**, *32*, 51–53.
- (114) Kneten, K.; McCreery, R. L. *Anal. Chem.* **1992**, *64*, 2518.
- (115) Murray, B. J.; Newberg, J. T.; Walter, E. C.; Li, Q.; Hemminger, J. C.; Penner, R. M. *Anal. Chem.* **2005**, *77*, 5205–5214.
- (116) Walter, E. C.; Murray, B. J.; Favier, F.; Kaltenpoth, G.; Grunze, M.; Penner, R. M. *J. Phys. Chem. B* **2002**, *106*, 11407–11411.
- (117) Li, Q.; Olson, J. B.; Penner, R. M. *Chem. Mater.* **2004**, *16*, 3402–3405.
- (118) Ta, T. C.; Kanda, V.; McDermott, M. T. *J. Phys. Chem. B* **1999**, *103*, 1295–1302.
- (119) McCreery, R. L.; Cline, K. K.; McDermott, C. A.; McDermott, M. T. *Colloids Surf.* **1994**, *93*, 211.
- (120) McDermott, C. A.; Kneten, K.; McCreery, R. L. *J. Electrochem. Soc.* **1993**, *140*, 2593.
- (121) Chen, P.; Fryling, M.; McCreery, R. L. *Anal. Chem.* **1995**, *67*, 3115.
- (122) Chen, P.; McCreery, R. L. *Anal. Chem.* **1996**, *68*, 3958.
- (123) Peter, L. M.; Durr, W.; Bindra, P.; Gerischer, H. *J. Electroanal. Chem.* **1976**, *71*, 31.
- (124) Huang, W.; McCreery, R. L. *J. Electroanal. Chem.* **1992**, *1*, 326.
- (125) DuVall, S.; McCreery, R. L. *Anal. Chem.* **1999**, *71*, 4594–4602.
- (126) DuVall, S.; McCreery, R. L. *J. Am. Chem. Soc.* **2000**, *122*, 6759–6764.
- (127) Huang, T.; Warsinke, A.; Koroljova-Skorobogatko, O. V.; Makower, A.; Kuwana, T.; Scheller, F. W. *Electroanalysis* **1999**, *11*, 295–300.
- (128) Mao, F.; Mano, N.; Heller, A. *J. Am. Chem. Soc.* **2003**, *125*, 4951–4957.
- (129) Newman, J. D.; White, S. F.; Tothill, I. E.; Turner, A. P. F. *Anal. Chem.* **1995**, *67*, 4594–4599.
- (130) Yang, H.-H.; McCreery, R. L. *J. Electrochem. Soc.* **2000**, *147*, 3420–3428.
- (131) Martin, H. B.; Argoitia, A.; Angus, J. C.; Landau, U. *J. Electrochem. Soc.* **1999**, *146*, 2959.
- (132) Niwa, O.; Jia, J.; Sato, Y.; Kato, D.; Kurita, R.; Maruyama, K.; Suzuki, K.; Hirono, S. *J. Am. Chem. Soc.* **2006**, *128*, 7144–7145.
- (133) Devaraj, N. K.; Decreau, R. A.; Ebina, W.; Collman, J. P.; Chidsey, C. E. D. *J. Phys. Chem. B* **2006**, *110*, 15955–15962.
- (134) Smalley, J. F.; Finkea, H. O.; Chidsey, C. E. D.; Linford, M. R.; Creager, S. E.; Ferraris, J. P.; Chalfant, K.; Zawodzinski, T.; Feldberg, S. W.; Newton, M. D. *J. Am. Chem. Soc.* **2003**, *125*, 2004–2013.
- (135) Finklea, H. O. In *Electroanalytical Chemistry*; Bard, A. J., Ed.; Dekker: New York, 1996; Vol 19.
- (136) French, M.; Creager, S. *Langmuir* **1998**, *14*, 2129–2133.
- (137) Creager, S.; Yu, C. J.; Bamdad, C.; O'Connor, S.; MacLean, T.; Lam, E.; Chong, Y.; Olsen, G. T.; Luo, J.; Gozin, M.; Kayyem, J. F. *J. Am. Chem. Soc.* **1999**, *121*, 1059–1064.

- (138) Roth, K. M.; Yasseri, A. A.; Liu, Z. M.; Dabke, R. B.; Malinovsky, V.; Schweikart, K. H.; Yu, L. H.; Tiznado, H.; Zaera, F.; Lindsey, J. S.; Kuhr, W. G.; Bocian, D. F. *J. Am. Chem. Soc.* **2003**, *125*, 505–517.
- (139) Yang, H.-H.; McCreery, R. L. *Anal. Chem.* **1999**, *71*, 4081–4087.
- (140) Solak, A. O.; Eichorst, L. R.; Clark, W. J.; McCreery, R. L. *Anal. Chem.* **2003**, *75*, 296–305.
- (141) Kawiak, J.; Kulesza, P. J.; Galus, Z. *J. Electroanal. Chem.* **1987**, *226*, 305.
- (142) McCreery, R. L.; Cline, K. K. In *Laboratory Techniques in Electroanalytical Chemistry*; Kissinger, P. T., Heineman, W. R., Eds.; Dekker: New York, 1996.
- (143) Kawagoe, K. T.; Zimmerman, J. B.; Wightman, R. M. *J. Neurosci. Methods* **1993**, *48*, 225.
- (144) Hu, I. F.; Karweik, D. H.; Kuwana, T. *J. Electroanal. Chem.* **1985**, *188*, 59.
- (145) Kiema, G. K.; Aktay, M.; McDermott, M. T. *J. Electroanal. Chem.* **2003**, *540*, 7.
- (146) Ranganathan, S.; Kuo, T.-C.; McCreery, R. L. *Anal. Chem.* **1999**, *71*, 3574–3580.
- (147) Runnels, P. L.; Joseph, J. D.; Logman, M. J.; Wightman, R. M. *Anal. Chem.* **1999**, *71*, 2782–2789.
- (148) Mazur, S.; Matusinovic, T.; Cammann, K. *J. Am. Chem. Soc.* **1977**, *99*, 3888–3891.
- (149) Ranganathan, S.; McCreery, R. L.; Majji, S. M.; Madou, M. *J. Electrochem. Soc.* **2000**, *147*, 277–282.
- (150) Hsueh, C. C.; Brajter-Toth, A. *Anal. Chem.* **1993**, *65*, 1570–1575.
- (151) Hershenhart, E.; McCreery, R. L.; Knight, R. D. *Anal. Chem.* **1984**, *56*, 2256.
- (152) Poon, M.; McCreery, R. L. *Anal. Chem.* **1986**, *58*, 2745.
- (153) Poon, M.; McCreery, R. L. *Anal. Chem.* **1988**, *60*, 1725.
- (154) Rice, R.; McCreery, R. L. *J. Electroanal. Chem.* **1991**, *310*, 127.
- (155) Robinson, R. S.; Sternitzke, K. D.; McCreery, R. L. *J. Vac. Sci. Technol. B* **1991**, *9*, 960.
- (156) Poon, M.; McCreery, R. L. *Anal. Chem.* **1987**, *59*, 1615.
- (157) Sternitzke, K. D.; McCreery, R. L. *Anal. Chem.* **1990**, *62*, 1339.
- (158) Strein, T. G.; Ewing, A. G. *Anal. Chem.* **1994**, *66*, 3864–3872.
- (159) Strein, T. G.; Ewing, A. G. *Anal. Chem.* **1991**, *63*, 194–198.
- (160) Chen, T. K.; Strein, T. G.; Abe, T.; Ewing, A. G. *Electroanalysis* **1994**, *6*, 746–751.
- (161) Farrell; Patrick, C.; Kinley; Patrick, R.; Weiss; David, J.; Strein; Timothy, G. *Electroanalysis* **2003**, *15*, 813–820.
- (162) Sternitzke, K. D.; McCreery, R. L.; Bruntlett, C.; Kissinger, P. T. *Anal. Chem.* **1989**, *61*, 1989.
- (163) Treado, P. J.; Govil, A.; Morris, M. D.; Sternitzke, K. D.; McCreery, R. L. *Appl. Spectrosc.* **1990**, *44*, 1270.
- (164) Braunstein, G.; Steinbeck, J.; Dresselhaus, M. S.; Dresselhaus, G.; Elman, B. S.; Venkatesan, T.; Wilkens, B.; Jacobson, D. C. *Mater. Res. Symp.* **1986**, 233–243.
- (165) Jaworski, R. K.; McCreery, R. L. *J. Electrochem. Soc.* **1993**, *140*, 1360.
- (166) Jaworski, R. K.; McCreery, R. L. *J. Electroanal. Chem.* **1994**, *369*, 175.
- (167) Rosenwald, S. E.; Nowall, W. B.; Dontha, N.; Kuhr, W. G. *Anal. Chem.* **2000**, *72*, 4914–4920.
- (168) Brooks, S. A.; Ambrose, W. P.; Kuhr, W. G. *Anal. Chem.* **1999**, *71*, 2558–2563.
- (169) Kelly, R. S.; Coleman, B. D.; Huang, T.; Inkaew, P.; Kuwana, T. *Anal. Chem.* **2002**, *74*, 6364–6369.
- (170) Kiema, G. K.; Fitzpatrick, G.; McDermott, M. T. *Anal. Chem.* **1999**, *71*, 4306–4312.
- (171) Kiema, G. K.; Ssenyange, S.; McDermott, M. T. *J. Electrochem. Soc.* **2004**, *151*, C142.
- (172) Wang, H.-S.; Ju, H.-X.; Chen, H.-Y. *Anal. Chim. Acta* **2002**, *461*, 243.
- (173) Vaik, K.; Schiffrin, D. J.; Tammeveski, K. *Electrochem. Commun.* **2004**, *6*, 1.
- (174) Akram, M.; Stuart; Margaret, C.; Wong; Danny, K. Y. *Electroanalysis* **2006**, *18*, 237–246.
- (175) El-Nour, K. A.; Brajter-Toth, A. *The Analyst* **2003**, *128*, 1056–1061.
- (176) Downard, A. J.; Roddick, A. D. *Electroanalysis* **1994**, *6*, 409–414.
- (177) Moore, R. R.; Banks, C. E.; Compton, R. G. *Anal. Chem.* **2004**, *76*, 2677–2682.
- (178) Banks, C. E.; Davies, T. J.; Wildgoose, G. G.; Compton, R. G. *Chem. Commun.* **2005**, 829–841.
- (179) Saraceno, R. A.; Engstrom, C. E.; Rose, M.; Ewing, A. G. *Anal. Chem.* **1989**, *61*, 560–565.
- (180) Kim, Y.-T.; Scarnulis, D. M.; Ewing, A. G. *Anal. Chem.* **1986**, *58*, 1782–1786.
- (181) Wallingford, R. A.; Ewing, A. G. *Anal. Chem.* **1988**, *60*, 258–263.
- (182) Clark, J. K.; Schilling, W. A.; Wijayawardhana, C. A.; Melaragno, P. R. *Anal. Chem.* **1994**, *66*, 3528–3532.
- (183) McFadden, C. F.; Melaragno, P. R.; Davis, J. A. *Anal. Chem.* **1990**, *62*, 742–746.
- (184) Pocard, N. L.; Alsmeyer, D.; McCreery, R. L.; Neenan, T.; Callstrom, M. *J. Am. Chem. Soc.* **1992**, *114*, 769.
- (185) Kostecki, R.; Schnyder, B.; Alliat, D.; Song, X.; Kinoshita, K.; Kotz, R. *Thin Solid Films* **2001**, *396*, 36–43.
- (186) Kostecki, R.; Song, X.; Kinoshita, K. *Electrochem. Solid-State Lett.* **1999**, *2*, 465.
- (187) Fischer; David, J.; Vandaveer; Walter, R.; Ryan, I. V.; Grigsby, J.; Lunte; Susan, M. *Electroanalysis* **2005**, *17*, 1153–1159.
- (188) Galobardes, F.; Wang, C.; Madou, M. *Diamond Relat. Mater.* **2006**, *15*, 1930.
- (189) Brooksby, P. A.; Downard, A. J. *J. Phys. Chem. B* **2005**, *109*, 8791–8798.
- (190) Yu, S. S. C.; Downard, A. J. *Langmuir* **2007**, *23*, 4662–4668.
- (191) Lyons, A. M. *J. Non-Cryst. Solids* **1985**, *70*, 99.
- (192) Lyons, A. M.; Hale, L. P.; Wilkins, J. C. W. *J. Vac. Sci. Technol. B* **1985**, *3*, 447.
- (193) Schueller, O. J. A.; Brittain, S. T.; Marzolin, C.; Whitesides, G. M. *Chem. Mater.* **1997**, *9*, 1399–1406.
- (194) Kostecki, R.; Song, X.; Kinoshita, K. *Electrochem. Solid-State Lett.* **2002**, *5*, E29.
- (195) Brooksby, P. A.; Downard, A. J. *Langmuir* **2004**, *20*, 5038–5045.
- (196) Brooksby, P. A.; Downard, A. J. *Langmuir* **2005**, *21*, 1672–1675.
- (197) Anariba, F.; DuVall, S. H.; McCreery, R. L. *Anal. Chem.* **2003**, *75*, 3837–3844.
- (198) Kostecki, R.; Song, X. Y.; Kinoshita, K. *J. Electrochem. Soc.* **2000**, *147*, 1878.
- (199) Wang, C.; Madou, M. *Biosens. Bioelectron.* **2005**, *20*, 2181.
- (200) McCreery, R.; Wu, J.; Kalakodimi, R. *J. Phys. Chem. Chem. Phys.* **2006**, *8*, 2572–2590.
- (201) Nowak, A.; McCreery, R. *J. Am. Chem. Soc.* **2004**, *126*, 16621–16631.
- (202) McCreery, R. L.; Dieringer, J.; Solak, A. O.; Snyder, B.; Nowak, A.; McGovern, W. R.; DuVall, S. *J. Am. Chem. Soc.* **2003**, *125*, 10748–10758.
- (203) Downard, A. J.; Garrett, D. J.; Tan, E. S. Q. *Langmuir* **2006**, *22*, 10739–10746.
- (204) Hermans, A.; Wightman, R. M. *Langmuir* **2006**, *22*, 10348–10353.
- (205) Tang, C.; Qi, K.; Wooley, K. L.; Matyjaszewski, K.; Kowalewski, T. *Angew. Chem., Int. Ed.* **2004**, *43*, 2783–2787.
- (206) Kowalewski, T.; Tsarevsky, N. V.; Matyjaszewski, K. *J. Am. Chem. Soc.* **2002**, *124*, 10632–10633.
- (207) You, T.; Niwa, O.; Tomita, M.; Ichino, T.; Hirono, S. *J. Electrochem. Soc.* **2002**, *149*, E479.
- (208) Wang, S.; Swain, G. M. *J. Phys. Chem. C* **2007**, *111*, 3986–3995.
- (209) Lowe, M. A.; Fischer, A. E.; Swain, G. M. *J. Electrochem. Soc.* **2006**, *153*, B506.
- (210) Farrell, J.; Martin, F. J.; Martin, H. B.; O'Grady, W. E.; Natishan, P. *J. Electrochem. Soc.* **2005**, *152*, E14.
- (211) Pleskov, Y. V. *Russ. J. Electrochem.* **2002**, *38*, 1275.
- (212) Pleskov, Y. V.; Evstefeeva, Y. E.; Krotova, M. D.; Varnin, V. P.; Teremetskaya, I. G. *J. Electroanal. Chem.* **2006**, *595*, 168.
- (213) Ivandini, T. A.; Sato, R.; Makide, Y.; Fujishima, A.; Einaga, Y. *Diamond Relat. Mater.* **2004**, *13*, 2003.
- (214) Ivandini, T. A.; Sato, R.; Makide, Y.; Fujishima, A.; Einaga, Y. *Anal. Chem.* **2006**, *78*, 6291–6298.
- (215) Watanabe, T.; Ivandini, T. A.; Makide, Y.; Fujishima, A.; Einaga, Y. *Anal. Chem.* **2006**, *78*, 7857–7860.
- (216) Yamaguchi, Y.; Yamanaka, Y.; Miyamoto, M.; Fujishima, A.; Honda, K. *J. Electrochem. Soc.* **2006**, *153*, J123.
- (217) Arihara, K.; Terashima, C.; Fujishima, A. *J. Electrochem. Soc.* **2007**, *154*, E71.
- (218) Cai, Y.; Anderson, A. B.; Angus, J. C.; Kostadinov, L. N. *J. Electrochem. Soc.* **2007**, *154*, F36.
- (219) Sopchak, D.; Miller, B.; Kalish, R.; Avyigal, Y.; Shi, X. *Electroanalysis* **2002**, *14*, 473–478.
- (220) Cvacka, J.; Quaiserova, V.; Park, J.; Show, Y.; Muck, A.; Swain, G. M. *Anal. Chem.* **2003**, *75*, 2678–2687.
- (221) Park, J.; Show, Y.; Quaiserova, V.; Galligan, J. J.; Fink, G. D.; Swain, G. M. *J. Electroanal. Chem.* **2005**, *583*, 56.
- (222) Park, J.; Galligan, J. J.; Fink, G. D.; Swain, G. M. *Anal. Chem.* **2006**, *78*, 6756–6764.
- (223) Rezek, B.; Shin, D.; Nakamura, T.; Nebel, C. E. *J. Am. Chem. Soc.* **2006**, *128*, 3884–3885.
- (224) Yang, W.; Auciello, O.; Butler, J. E.; Cai, W.; Carlisle, J.; Gerbi, J.; Gruen, D.; Knickerbocker, T.; Lasseter, T.; John, N.; Russell, J.; Smith, L. M.; Hamers, R. J. *Nat. Mater.* **2002**, *1*, 253–257.
- (225) Show, Y.; Witek, M. A.; Sonthalia, P.; Swain, G. M. *Chem. Mater.* **2003**, *15*, 879–888.
- (226) Koppang, M. D.; Witek, M.; Blau, J.; Swain, G. M. *Anal. Chem.* **1999**, *71*, 1188–1195.

- (227) Wilson, N. R.; Clewes, S. L.; Newton, M. E.; Unwin, P. R.; Macpherson, J. V. *J. Phys. Chem. B* **2006**, *110*, 5639–5646.
- (228) Haymond, S.; Babcock, G. T.; Swain, G. M. *J. Am. Chem. Soc.* **2002**, *124*, 10634–10635.
- (229) Song, Y.; Swain, G. M. *Anal. Chem.* **2007**, *79*, 2412–2420.
- (230) Song, Y.; Swain, G. M. *Anal. Chim. Acta* **2007**, *593*, 7.
- (231) Bennett, J. A.; Show, Y.; Wang, S.; Swain, G. M. *J. Electrochem. Soc.* **2005**, *152*, E184.
- (232) Wang, J.; Swain, G. M.; Tachibana, T.; Kobashi, K. *Electrochem. Solid-State Lett.* **2000**, *3*, 286.
- (233) Wang, J.; Swain, G. M. *J. Electrochem. Soc.* **2003**, *150*, E24.
- (234) Schrock, D. S.; Wipf, D. O.; Baur, J. E. *Anal. Chem.* **2007**, *79*, 4931–4941.
- (235) Ewing, A. G.; Strein, T. G.; Lau, Y. Y. *Acc. Chem. Res.* **1992**, *25*, 440–447.
- (236) Maldonado, S.; Stevenson, K. J. *J. Phys. Chem. B* **2005**, *109*, 4707–4716.
- (237) Maldonado, S.; Morin, S.; Stevenson, K. J. *Carbon* **2006**, *44*, 1429.
- (238) Vijayaraghavan, G.; Stevenson, K. J. *Langmuir* **2007**, *23*, 5279–5282.
- (239) Maldonado, S.; Stevenson, K. J. *J. Phys. Chem. B* **2004**, *108*, 11375–11383.
- (240) Strein, T. G.; Ewing, A. G. *Anal. Chem.* **1992**, *64*, 1368–1373.
- (241) El-Giar; EmadE-Deen, M.; Wipf; David, O. *Electroanalysis* **2006**, *18*, 2281–2289.
- (242) Liu, B.; Rolland, J. P.; DeSimone, J. M.; Bard, A. J. *Anal. Chem.* **2005**, *77*, 3013–3017.
- (243) Slevin, C. J.; Gray, N. J.; Macpherson, J. V.; Webb, M. A.; Unwin, P. R. *Electrochem. Commun.* **1999**, *1*, 282.
- (244) Conyers, J. L.; White, H. S. *Anal. Chem.* **2000**, *72*, 4441–4446.
- (245) Chen, S.; Kucernak, A. *Electrochem. Commun.* **2002**, *4*, 80.
- (246) Chen, S.; Kucernak, A. *J. Phys. Chem. B* **2002**, *106*, 9396–9404.
- (247) Tel-Vered, R.; Walsh, D. A.; Mehrgardi, M. A.; Bard, A. J. *Anal. Chem.* **2006**, *78*, 6959–6966.
- (248) Chen, S.; Kucernak, A. *J. Phys. Chem. B* **2003**, *107*, 8392–8402.
- (249) Oldham, K. *Anal. Chem.* **1992**, *64*, 646–651.
- (250) Lambie, B. A.; Orwar, O.; Weber, S. G. *Anal. Chem.* **2006**, *78*, 5165–5171.
- (251) Wu, Z.; Chen, L.; Shen, G.; Yu, R. *Sens. Actuators, B* **2006**, *119*, 295.
- (252) Pihel, K.; Walker, Q. D.; Wightman, R. M. *Anal. Chem.* **1996**, *68*, 2084–2089.
- (253) Kawagoe, K. T.; Garris, P. A.; Wightman, R. M. *J. Electroanal. Chem.* **1993**, *259*, 193–207.
- (254) Zimmerman, J. B.; Wightman, R. M. *Anal. Chem.* **1991**, *63*, 24–28.
- (255) Peters, J. L.; Kulagina, N. V.; Hua, Y.; Michael, A. C. In *Encyclopedia of Electrochemistry*; Bard, A., Stratmann, M., Eds.; Wiley-VCH: Weinheim, Germany, 2002; Vol 9.
- (256) Zhang, M.; Liu, K.; Xiang, L.; Lin, Y.; Su, L.; Mao, L. *Anal. Chem.* **2007**, *79*, 6559–6565.
- (257) Clark, R. A.; Zerby, R. A.; Ewing, A. G. In *Electroanalytical Chemistry*; Bard, A., Ed.; Dekker: New York, 1998; Vol 20.
- (258) Wang, W.; Xiong, Y.; Du, F.-Y.; Huang, W.-H.; Wu, W.-Z.; Wang, Z.-L.; Cheng, J.-K.; Yang, Y.-F. *The Analyst* **2007**, *132*, 515–518.
- (259) Verchier, Y.; Lardy, B.; Nguyen, M. V. C.; Morel, F.; Arbault, S.; Amatore, C. *Biochem. Biophys. Res. Commun.* **2007**, *361*, 493.
- (260) Amatore, C.; Arbault, S.; Bouret, Y.; Guille, M.; Lemaître, F.; Verchier, Y. *ChemBioChem* **2006**, *7*, 1998–2003.
- (261) Troyer, K. P.; Wightman, R. M. *Anal. Chem.* **2002**, *74*, 5370–5375.
- (262) Amatore, C.; Arbault, S.; Bruce, D.; Oliveira, P. d.; Erard, M.; Vuillaume, M. *Faraday Discuss.* **2000**, *116*, 319–333.
- (263) El-Nour, K. A.; Brajter-Toth, A. *Electroanalysis* **2000**, *12*, 805–810.
- (264) Stromberg, A.; Ryttsen, F.; Chiu, D. T.; Davidson, M.; Eriksson, P. S.; Wilson, C. F.; Orwar, O.; Zare, R. N. *Proc. Natl. Acad. Sci. U.S.A.* **2000**, *97*, 7–11.
- (265) Gross, E. M.; Pastore, P.; Wightman, R. M. *J. Phys. Chem. B* **2001**, *105*, 8732–8738.
- (266) Badocco, D.; Zanon, F.; Pastore, P. *Electrochim. Acta* **2006**, *51*, 6442.
- (267) Maus, R. G.; Wightman, R. M. *Anal. Chem.* **2001**, *73*, 3993–3998.
- (268) Campbell, J. K.; Sun, L.; Crooks, R. M. *J. Am. Chem. Soc.* **1999**, *121*, 3779–3780.
- (269) Viculis, L. M.; Mack, J. J.; Kaner, R. B. *Science* **2003**, *299*, 1361.
- (270) Nugent, J. M.; Santhanam, K. S. V.; Rubio, A.; Ajayan, P. M. *Nano Lett.* **2001**, *1*, 87–91.
- (271) Dumitrescu, I.; Wilson, N. R.; Macpherson, J. V. *J. Phys. Chem. C* **2007**, *111*, 12944–12953.
- (272) Wilson, N. R.; Guille, M.; Dumitrescu, I.; Fernandez, V. R.; Rudd, N. C.; Williams, C. G.; Unwin, P. R.; Macpherson, J. V. *Anal. Chem.* **2006**, *78*, 7006–7015.
- (273) Bertonecello, P.; Edgeworth, J. P.; Macpherson, J. V.; Unwin, P. R. *J. Am. Chem. Soc.* **2007**, *129*, 10982–10983.
- (274) Liu, Z.; Shen, Z.; Zhu, T.; Hou, S.; Ying, L.; Shi, Z.; Gu, Z. *Langmuir* **2000**, *16*, 3569–3573.
- (275) McKnight, T. E.; Peeraphatdit, C.; Jones, S. W.; Fowlkes, J. D.; Fletcher, B. L.; Klein, K. L.; Melechko, A. V.; Doktycz, M. J.; Simpson, M. L. *Chem. Mater.* **2006**, *18*, 3203–3211.
- (276) Li, J.; Ng, H. T.; Cassell, A.; Fan, W.; Chen, H.; Ye, Q.; Koehne, J.; Han, J.; Meyyappan, M. *Nano Lett.* **2003**, *3*, 597–602.
- (277) Hinds, B. J.; Chopra, N.; Rantell, T.; Andrews, R.; Gavalas, V.; Bachas, L. G. *Science* **2004**, *303*, 62–65.
- (278) Li, J.; Cassell, A.; Delzeit, L.; Han, J.; Meyyappan, M. *J. Phys. Chem. B* **2002**, *106*, 9299–9305.
- (279) Streeter, I.; Xiao, L.; Wildgoose, G. G.; Compton, R. G. *J. Phys. Chem. C* **2008**, *112*, 1933–1937.
- (280) Maldonado, S.; Morin, S.; Stevenson, K. J. *The Analyst* **2006**, *131*, 262–267.
- (281) Gooding, J. J.; Wibowo, R.; Liu, J. Q.; Yang, W.; Losic, D.; Orbons, S.; Mearns, F. J.; Shapter, J. G.; Hibbert, D. B. *J. Am. Chem. Soc.* **2003**, *125*, 9006–9007.
- (282) Erdem, A.; Papakonstantinou, P.; Murphy, H. *Anal. Chem.* **2006**, *78*, 6656–6659.
- (283) Tuukkanen, S.; Toppari, J. J.; Kuzyk, A.; Hirviniemi, L.; Hytonen, V. P.; Ihalainen, T.; Torma, P. *Nano Lett.* **2006**, *6*, 1339–1343.
- (284) Patolsky, F.; Weizmann, Y.; Willner, I. *Angew. Chem., Int. Ed.* **2004**, *43*, 2113–2117.
- (285) Yu, X.; Munge, B.; Patel, V.; Jensen, G.; Bhirde, A.; Gong, J. D.; Kim, S. N.; Gillespie, J.; Gutkind, J. S.; Papadimitrakopoulos, F.; Rusling, J. F. *J. Am. Chem. Soc.* **2006**, *128*, 11199–11205.
- (286) Jiao, S.; Li, M.; Wang, C.; Chen, D.; Fang, B. *Electrochim. Acta* **2007**, *52*, 5939.
- (287) Zhang, M.; Mullens, C.; Gorski, W. *Anal. Chem.* **2005**, *77*, 6396–6401.
- (288) Shahrokhian, S.; Zare-Mehrjardi, H. R. *Electrochim. Acta* **2007**, *52*, 6310.
- (289) Pumera, M.; Merkoçi, A.; Alegret, S. *Electrophoresis* **2007**, *28*, 1274–1280.
- (290) Lawrence; Nathan, S.; Deo; Randhir, P.; Wang, J. *Electroanalysis* **2005**, *17*, 65–72.
- (291) Zeng, J.; Gao, X.; Wei, W.; Zhai, X.; Yin, J.; Wu, L.; Liu, X.; Liu, K.; Gong, S. *Sens. Actuators, B* **2007**, *120*, 595.
- (292) Jones, C. P.; Jurkschat, K.; Crossley, A.; Compton, R. G.; Riehl, B. L.; Banks, C. E. *Langmuir* **2007**, *23*, 9501–9504.
- (293) Wang, J.; Chen, G.; Chatrathi, M. P.; Musameh, M. *Anal. Chem.* **2004**, *76*, 298–302.
- (294) Rivas, G. A.; Rubianes, M. D.; Pedano, M. L.; Ferreyra, N. F.; Luque, G. L.; Rodríguez, M. C.; Miscoria, S. A. *Electroanalysis* **2007**, *19*, 823–831.
- (295) Punbusayakul, N.; Talapatra, S.; Ci, L.; Surareungchai, W.; Ajayan, P. M. *Electrochem. Solid-State Lett.* **2007**, *10*, F13.
- (296) Banks, C. E.; Crossley, A.; Salter, C.; Wilkins, S. J.; Compton, R. G. *Angew. Chem., Int. Ed.* **2006**, *45*, 2533–2537.
- (297) Banks, C. E.; Moore, R. R.; Davies, T. J.; Compton, R. G. *Chem. Commun.* **2004**, 1804–1805.
- (298) Kruusma, J.; Mould, N.; Jurkschat, K.; Crossley, A.; Banks, C. E. *Electrochem. Commun.* **2007**, *9*, 2330–2333.
- (299) Day, T. M.; Unwin, P. R.; Wilson, N. R.; Macpherson, J. V. *J. Am. Chem. Soc.* **2005**, *127*, 10639–10647.
- (300) Kaempgen, M.; Roth, S. *Synth. Met.* **2005**, *152*, 353.
- (301) Li, J.; Xu, Y.; Wei, H.; Huo, T.; Wang, E. *Anal. Chem.* **2007**, *79*, 5439–5443.
- (302) Adams, R. N. *Anal. Chem.* **1958**, *30*, 1576–1576.
- (303) Kalcher, K.; Kauffmann, J. M.; Wang, J.; Svancara, I.; Wytras, K.; Neuhold, C.; Yang, Z. *Electroanalysis* **1995**, *7*, 5–22.
- (304) Svancara, I.; Wytras, K.; Barek, J.; Zima, J. *Crit. Rev. Anal. Chem.* **2001**, *31*, 311–345.
- (305) Zhang, X.; Wang, J.; Wang, Z.; Wang, S. *Synth. Met.* **2005**, *155*, 95–99.
- (306) Wu, A.; Venancio, E. C.; MacDiarmid, A. G. *Synth. Met.* **2007**, *157*, 303–310.
- (307) Rusling, J. F.; Zhou, L.; Munge, B.; Yang, J.; Estavillo, C.; Schenkman, J. B. *Faraday Discuss.* **2000**, *116*, 77–87.
- (308) Sebkova, S.; Navratil, T.; Kopanica, M. *Anal. Lett.* **2005**, *38*, 1747–1758.
- (309) Biljana, S.; Banks, Craig, E.; Crossley, A.; Compton, R. G. *Electroanalysis* **2006**, *18*, 1757–1762.
- (310) Ambrosi, A.; Castaneda, M. T.; Killard, A. J.; Smyth, M. R.; Alegret, S.; Merkoci, A. *Anal. Chem.* **2007**, *79*, 5232–5240.
- (311) Wang, J.; Musameh, M.; Mo, J. W. *Anal. Chem.* **2006**, *78*, 7044–7047.
- (312) Darder, M.; Lopez-Blanco, M.; Aranda, P.; Aznar, A. J.; Bravo, J.; Ruiz-Hitzky, E. *Chem. Mater.* **2006**, *18*, 1602–1610.
- (313) Zwirnes de Oliveira, I. R. W.; Fernandes, S. C.; Vieira, I. C. J. *Pharm. Biomed. Anal.* **2006**, *41*, 366.
- (314) Mandong, G.; Yanqing, L.; Hongxia, G.; Xiaojin, W.; Lifang, F. *Bioelectrochemistry* **2007**, *70*, 245.

- (315) Maleki, N.; Safavi, A.; Tajabadi, F. *Anal. Chem.* **2006**, *78*, 3820–3826.
- (316) Kachoosangi; Roohollah, T.; Wildgoose; Gregory, G.; Compton, R. G. *Electroanalysis* **2007**, *19*, 1483–1489.
- (317) Safavi, A.; Maleki, N.; Moradlou, O.; Tajabadi, F. *Anal. Biochem.* **2006**, *359*, 224.
- (318) Sun, W.; Gao, R.; Jiao, K. J. *Phys. Chem. B* **2007**, *111*, 4560–4567.
- (319) Yoon, J.-H.; Muthuraman, G.; Yang, J.; Shim, Y.-B.; Won, M.-S. *Electroanalysis* **2007**, *19*, 1160–1166.
- (320) Nie, L.; Guo, H.; He, Q.; Chen, J.; Miao, Y. *J. Nanosci. Nanotechnol.* **2007**, *7*, 560–564.
- (321) Wildgoose, G. G.; Banks, C. E.; Compton, R. G. *Small* **2006**, *2*, 182–193.
- (322) Zhang, Y.; Zeng, G.-M.; Tang, L.; Huang, D.-L.; Jiang, X.-Y.; Chen, Y.-N. *Biosens. Bioelectron.* **2007**, *22*, 2121.
- (323) Valentini, F.; Amine, A.; Orlanducci, S.; Terranova, M. L.; Palleschi, G. *Anal. Chem.* **2003**, *75*, 5413–5421.
- (324) Antiochia, R.; Lavagnini, I.; Magno, F.; Valentini, F.; Palleschi, G. *Electroanalysis* **2004**, *16*, 1451–1458.
- (325) Arribas, A. S.; Bermejo, E.; Chicharro, M.; Zapardiel, A.; Luque, G. L.; Ferreyra, N. F.; Rivas, G. A. *Anal. Chim. Acta* **2006**, *577*, 183.
- (326) Slijukic, B.; Banks, C. E.; Salter, C.; Crossley, A.; Compton, R. G. *The Analyst* **2006**, *131*, 670–677.
- (327) Wang, J.; Kawde, A.-N.; Musameh, M. *The Analyst* **2003**, *128*, 912–916.
- (328) Tomcik, P.; Banks, C. E.; Davies, T. J.; Compton, R. G. *Anal. Chem.* **2004**, *76*, 161–165.
- (329) Corgier, B. P.; Marquette, C. A.; Blum, L. J. *Anal. Chim. Acta* **2005**, *538*, 1.
- (330) Corgier, B. P.; Li, F.; Blum, L. J.; Marquette, C. A. *Langmuir* **2007**, *23*, 8619–8623.
- (331) Kerman, K.; Vestergaard, M.; Tamiya, E. *Anal. Chem.* **2007**, *79*, 6881–6885.
- (332) Prodromidis; Mamas, I.; Karayannis; Miltiades, I. *Electroanalysis* **2002**, *14*, 241–261.
- (333) Crew, A.; Alford, C.; Cowell, D. C. C.; Hart, J. P. *Electrochim. Acta* **2007**, *52*, 5232.
- (334) Azevedo, A. M.; Prazeres, D. M. F.; Cabral, J. M. S.; Fonseca, L. P. *Biosens. Bioelectron.* **2005**, *21*, 235.
- (335) Dequaire, M.; Heller, A. *Anal. Chem.* **2002**, *74*, 4370–4377.
- (336) Wang, J.; Mo, J.-W.; Erdem, A. *Electroanalysis* **2002**, *14*, 1365–1368.
- (337) Jaegfeldt, H.; Kuwana, T.; Johansson, G. *J. Am. Chem. Soc.* **1983**, *105*, 1805–1814.
- (338) Murray, R. W. In *Electroanalytical Chemistry*; Bard, A., Ed.; Dekker: New York, 1983; Vol 13.
- (339) Pantano, P.; K, W. *Anal. Chem.* **1993**, *65*, 623–630.
- (340) Zhao, J.; McCreery, R. L. *Langmuir* **1995**, *11*, 4036.
- (341) Liu, Y.-C.; McCreery, R. L. *Anal. Chem.* **1997**, *69*, 2091.
- (342) Gorodetsky, A. A.; Barton, J. K. *Langmuir* **2006**, *22*, 7917–7922.
- (343) Delamar, M.; Hitmi, R.; Pinson, J.; Saveant, J. M. *J. Am. Chem. Soc.* **1992**, *114*, 5883–5884.
- (344) Barbier, B.; Pinson, J.; Desarmot, G.; Sanchez, M. *J. Electrochem. Soc.* **1990**, *137*, 1757.
- (345) Deinhammer, R. S.; Ho, M.; Anderegg, J. W.; Porter, M. D. *Langmuir* **1994**, *10*, 1306–1313.
- (346) Pinson, J.; Podvorica, F. *Chem. Soc. Rev.* **2005**, *34*, 429–439.
- (347) Allongue, P.; Delamar, M.; Desbat, B.; Fagebaume, O.; Hitmi, R.; Pinson, J.; Saveant, J. M. *J. Am. Chem. Soc.* **1997**, *119*, 201–207.
- (348) Itoh, T.; McCreery, R. L. *J. Am. Chem. Soc.* **2002**, *124*, 10894–10902.
- (349) Stewart, M. P.; Maya, F.; Kosynkin, D. V.; Dirk, S. M.; Stapleton, J. J.; McGuinness, C. L.; Allara, D. L.; Tour, J. M. *J. Am. Chem. Soc.* **2004**, *126*, 370–378.
- (350) Kuo, T.-C. Ph.D. Thesis, The Ohio State University, 1999.
- (351) Price, B. K.; Hudson, J. L.; Tour, J. M. *J. Am. Chem. Soc.* **2005**, *127*, 14867–14870.
- (352) Adenier, A.; Cabet-Deliry, E.; Chaussé, A.; Griveau, S.; Mercier, F.; Pinson, J.; Vautrin-UI, C. *Chem. Mater.* **2005**, *17*, 491–501.
- (353) Strano, M. S.; Dyke, C. A.; Usrey, M. L.; Barone, P. W.; Allen, M. J.; Shan, H.; Kittrell, C.; Hauge, R. H.; Tour, J. M.; Smalley, R. E. *Science* **2003**, *301*, 1519–1522.
- (354) Cheng, F.; Adronov, A. *Chem. Mater.* **2006**, *18*, 5389–5391.
- (355) Dyke, C. A.; Tour, J. M. *J. Am. Chem. Soc.* **2003**, *125*, 1156–1157.
- (356) de Villeneuve, C. H.; Pinson, J.; Bernard, M. C.; Allongue, P. *J. Phys. Chem. B* **1997**, *101*, 2415–2420.
- (357) Hurley, B. L.; McCreery, R. L. *J. Electrochem. Soc.* **2004**, *151*, B252.
- (358) Bernard, M.-C.; Chausse, A.; Cabet-Deliry, E.; Chehimi, M. M.; Pinson, J.; Podvorica, F.; Vautrin-UI, C. *Chem. Mater.* **2003**, *15*, 3450–3462.
- (359) Chausse, A.; Chehimi, M. M.; Karsi, N.; Pinson, J.; Podvorica, F.; Vautrin-UI, C. *Chem. Mater.* **2002**, *14*, 392–400.
- (360) Paulik, M. G.; Brooksby, P. A.; Abell, A. D.; Downard, A. J. *J. Phys. Chem. C* **2007**, *111*, 7808–7815.
- (361) Downard, A. J.; Tan, E. S. Q.; Yu, S. S. C. *New J. Chem.* **2006**, *30*, 1283–1288.
- (362) Deniau, G.; Azoulay, L.; Bougerolles, L.; Palacin, S. *Chem. Mater.* **2006**, *18*, 5421–5428.
- (363) Liu, Y.-C.; McCreery, R. L. *J. Am. Chem. Soc.* **1995**, *117*, 11254.
- (364) Kalakodimi, R. P.; Nowak, A.; McCreery, R. L. *Chem. Mater.* **2005**, *17*, 4939–4948.
- (365) Nowak, A. M.; McCreery, R. L. *Anal. Chem.* **2004**, *76*, 1089–1097.
- (366) Kariuki, J. K.; McDermott, M. T. *Langmuir* **2001**, *17*, 5947–5951.
- (367) Anariba, F.; Viswanathan, U.; Bocian, D. F.; McCreery, R. L. *Anal. Chem.* **2006**, *78*, 3104–3112.
- (368) Combellas, C.; Kanoufi, F.; Pinson, J.; Podvorica, F. *Langmuir* **2005**, *21*, 280–286.
- (369) Saby, C.; Ortiz, B.; Champagne, G. Y.; Belanger, D. *Langmuir* **1997**, *13*, 6805–6813.
- (370) Rappich, J.; Merson, A.; Roodenko, K.; Ditttrich, T.; Gensch, M.; Hinrichs, K.; Shapira, Y. *J. Phys. Chem. B* **2006**, *110*, 1332–1337.
- (371) Kariuki, J. K.; McDermott, M. T. *Langmuir* **1999**, *15*, 6534–6540.
- (372) Downard, A. J. *Langmuir* **2000**, *16*, 9680–9682.
- (373) Cruickshank, A. C.; Tan, E. S. Q.; Brooksby, P. A.; Downard, A. J. *Electrochem. Commun.* **2007**, *9*, 1456.
- (374) Brooksby, P. A.; Downard, A. J.; Yu, S. S. C. *Langmuir* **2005**, *21*, 11304–11311.
- (375) Jiang, D. e.; Sumpster, B. G.; Dai, S. J. *Phys. Chem. B* **2006**, *110*, 23628–23632.
- (376) Anariba, F.; Steach, J.; McCreery, R. *J. Phys. Chem. B* **2005**, *109*, 11163–11172.
- (377) McCreery, R. *Electrochem. Soc. Interface* **2004**, *13*, 46–51.
- (378) Vaik, K.; Sarapuu, A.; Tammeveski, K.; Mirkhalaf, F.; Schiffrin, D. J. *J. Electroanal. Chem.* **2004**, *564*, 159.
- (379) Mirkhalaf, F.; Tammeveski, K.; Schiffrin, D. J. *Phys. Chem. Chem. Phys.* **2004**, *6*, 1321–1327.
- (380) Alexeyeva, N.; Laaksonen, T.; Kontturi, K.; Mirkhalaf, F.; Schiffrin, D. J.; Tammeveski, K. *Electrochem. Commun.* **2006**, *8*, 1475.
- (381) Poljsky, R.; Harper, J. C.; Dirk, S. M.; Arango, D. C.; Wheeler, D. R.; Brozik, S. M. *Langmuir* **2007**, *23*, 364–366.
- (382) Holm, A. H.; Moller, R.; Vase, K. H.; Dong, M.; Norrman, K.; Besenbacher, F.; Pedersen, S. U.; Daasbjerg, K. *New J. Chem.* **2005**, *29*, 659–666.
- (383) McCreery, R. *Chem. Mater.* **2004**, *16*, 4477–4496.
- (384) Fisher, G. L.; Hooper, A.; Opila, R. L.; Jung, D. R.; Allara, D. L.; Winograd, N. *J. Electron Spectrosc. Relat. Phenom.* **1999**, *98–99*, 139–148.
- (385) Fisher, G. L.; Hooper, A. E.; Opila, R. L.; Jung, D. R.; Allara, D. L.; Winograd, N. *J. Phys. Chem. B* **2000**, *104*, 3267–3273.
- (386) Haynie, B. C.; Walker, A. V.; Tighe, T. B.; Allara, D. L.; Winograd, N. *Appl. Surf. Sci.* **2003**, *203–204*, 433–436.
- (387) Wu, J.; Mobley, K.; McCreery, R. *J. Chem. Phys.* **2007**, *126*, 24704.
- (388) Vase, K. H.; Holm, A. H.; Pedersen, S. U.; Daasbjerg, K. *Langmuir* **2005**, *21*, 8085–8089.
- (389) Vase, K. H.; Holm, A. H.; Norrman, K.; Pedersen, S. U.; Daasbjerg, K. *Langmuir* **2007**, *23*, 3786–3793.
- (390) Nielsen, L. T.; Vase, K. H.; Dong, M.; Besenbacher, F.; Pedersen, S. U.; Daasbjerg, K. *J. Am. Chem. Soc.* **2007**, *129*, 1888–1889.
- (391) Vase, K. H.; Holm, A. H.; Norrman, K.; Pedersen, S. U.; Daasbjerg, K. *Langmuir* **2008**, *24*, 182–188.
- (392) Buriak, J. M. *Angew. Chem., Int. Ed.* **2001**, *40*, 532–534.
- (393) Hamers, R. J.; Coulter, S. K.; Ellison, M. D.; Hovis, J. S.; Padowitz, D. F.; Schwartz, M. P.; Greenleaf, C. M.; Russell, J. N., Jr. *Acc. Chem. Res.* **2000**, *33*, 617–624.
- (394) Nichols, B. M.; Metz, K. M.; Tse, K. Y.; Butler, J. E.; Russell, J. N.; Hamers, R. J. *J. Phys. Chem. B* **2006**, *110*, 16535–16543.
- (395) Hovis, J. S.; Coulter, S. K.; Hamers, R. J.; D'Evelyn, M. P.; Russell, J. N.; Butler, J. E. *J. Am. Chem. Soc.* **2000**, *122*, 732–733.
- (396) Wang, G. T.; Bent, S. F.; Russell, J. N.; Butler, J. E.; D'Evelyn, M. P. *J. Am. Chem. Soc.* **2000**, *122*, 744–745.
- (397) Knickerbocker, T.; Strother, T.; Schwartz, M. P.; Russell, J. N., Jr.; Butler, J.; Smith, L. M.; Hamers, R. J. *Langmuir* **2003**, *19*, 1938–1942.
- (398) Lasseter, T.; Clare, B.; Abbott, N.; Hamers, R. J. *J. Am. Chem. Soc.* **2004**, *126*, 10220–10221.
- (399) Tse, K.-Y.; Nichols, B. M.; Yang, W.; Butler, J. E.; Russell, J. N., Jr.; Hamers, R. J. *J. Phys. Chem. B* **2005**, *109*, 8523–8532.
- (400) Ssenyange, S.; Anariba, F.; Bocian, D. F.; McCreery, R. L. *Langmuir* **2005**, *21*, 11105–11112.
- (401) Gallardo, I.; Pinson, J.; Vila, N. *J. Phys. Chem. B* **2006**, *110*, 19521–19529.
- (402) Adenier, A.; Chehimi, M. M.; Gallardo, I.; Pinson, J.; Vila, N. *Langmuir* **2004**, *20*, 8243–8253.
- (403) Tornøe, C. W.; Christensen, C.; Meldal, M. *J. Org. Chem.* **2002**, *67*, 3057–3064.

- (404) Devaraj, N. K.; Dinolfo, P. H.; Chidsey, C. E. D.; Collman, J. P. *J. Am. Chem. Soc.* **2006**, *128*, 1794–1795.
- (405) Collman, J. P.; Devaraj, N. K.; Eberspacher, T. P. A.; Chidsey, C. E. D. *Langmuir* **2006**, *22*, 2457–2464.
- (406) Collman, J. P.; Devaraj, N. K.; Chidsey, C. E. D. *Langmuir* **2004**, *20*, 1051–1053.
- (407) Devadoss, A.; Chidsey, C. E. D. *J. Am. Chem. Soc.* **2007**, *129*, 5370–5371.
- (408) Beriet, C.; Pletcher, D. *J. Electroanal. Chem.* **1994**, *375*, 213.
- (409) Fagan, D. T.; Hu, I.; Kuwana, T. *Anal. Chem.* **1985**, *57*, 2759–63.
- (410) Huang, T.; Warsinke, A.; Kuwana, T.; Scheller, F. W. *Anal. Chem.* **1998**, *70*, 991–997.
- (411) Munteanu, F. D.; Mano, N.; Kuhn, A.; Gorton, L. *J. Electroanal. Chem.* **2004**, *564*, 167.
- (412) Timur, S.; Anik, U.; Odaci, D.; Gorton, L. *Electrochem. Commun.* **2007**, *9*, 1810.
- (413) Antiochia, R.; Gorton, L. *Biosens. Bioelectron.* **2007**, *22*, 2611.
- (414) Joshi, P. P.; Merchant, S. A.; Wang, Y.; Schmidtke, D. W. *Anal. Chem.* **2005**, *77*, 3183–3188.

CR068076M